1-1-2013

Toward Directing Cell Fate: Carbon Nanotubes As Modulators of Extracellular and Transporters of Intracellular Cues

Qingsu Cheng
University of South Carolina - Columbia

TOWARD DIRECTING CELL FATE: CARBON NANOTUBES AS MODULATORS OF EXTRACELLULAR AND TRANSPORTERS OF INTRACELLULAR CUES

By

Qingsu Cheng

Bachelor of Science
Nanjing University of Technology, 2006

Master of Science
Sichuan University, 2010

Submitted in Partial Fulfillment of the Requirements

For the Degree of Doctor of Philosophy in

Biomedical Engineering

College of Engineering and Computing

University of South Carolina

2013

Accepted by:

Ehsan Jabbarzadeh, Major Professor

James Blanchette, Committee Member

Esmaiel Jabbari, Committee Member

Tarek Shazly, Committee Member

Qian Wang, Committee Member

Lacy Ford, Vice Provost and Dean of Graduate Studies

DEDICATIONS

To

My wife, Yuan Ma

My parents, Rushen Cheng and Qiaomei Xu

My parents in law, Mingdong Ma and Yuejian Liu

ACKNOWLEDGEMENTS

I really enjoyed my time in University of South Carolina. I made new friends from the entire world. With the help from my colleagues, collaborators and friends, I was able to make this dissertation.

I would like to express my deepest appreciation to my advisor Ehsan Jabbarzadeh, who supervised me on my graduate study with his great talent and genius. His enthusiasm of pursuing new findings and novel innovations in science and engineering inspires me to explore the unknown territories of the research. Creative strategies to bypass the equipment shortages and practical solutions to unexpected experimental problems came out during our regular discussions.

Multiple collaborators helped a lot. Dr. Tarek Shazly's and his group member, Jahid Ferdous and Eva Juares-Perez, did me favors in mechanical test. Dr. Qian Wang and his group member, Dr. Xinjie Zan and Pongkwan Sitasuwan, help me work out the roughness test. Dr. Blanchette and his group member, Dr. Mathew Skiles and Dr. Suchit Sahai, always glad to provide convenience on microscope.

There is a lot of great experience with the group members in Jabbarzadeh group. I gained experience in building chemical facility and chemical synthesis with Konstantinos Zonaras who built the carbon nanotube facility. Dr. Marina Pryzhkova trained me on molecular cell biology. Greg Harris and I had valuable discussion on our project. Katy Rutledge helps me on improving English written skill. Many other group members:

Marc-Olivier Blais, James Raymond Cormany III, Jason Lauer, John snider, Richard Doe also and Maria Pioli are very helpful.

Many friends in Columbia SC have made me go through all the difficulties and taste all the sweetness in life. Particular thanks to: An Zou, Chen Zhang, Yuewen Xu, Ping Li, Dr. Fang Yang, Wei Zhao, Zhiyong Wang, Fan Wu, Jui-Heng Tseng, Dr. Will Reed, Kayla Pate, Sungtak Kim, Dr. Ozan Karaman, Daniel Bratti, *etc*.

Finally, there are always supports from family. I want to thank them from the deepest in my heart.

ABSTRACT

The unique properties of CNTs lead CNTs attractive in biological engineering applications. It is expected to use CNT based biomaterials for clinic use in the near future. CNTs can be used to tune cellular fate through bother extracellular pathway and intracellular pathway. CNT based biomaterials has been applied into bone, nerves, and cardiovascular system. There has also been progress in the use of CNTs in controlling cellular alignment, to enhance tissue regeneration, growth factor delivery and gene delivery.

Pluripotent stem cells (hPSCs) offer a promising tool in tissue engineering strategies, as their differentiated derivatives can be used to reconstruct most biological tissues. These approaches rely on controlling the extracellular and intracellular cues that tune the ultimate fate of hPSCs. In this context, significant effort has gone to parse out the role of conflicting matrix-elicited signals (*eg.* topography and elasticity) in regulation of macroscopic characteristics of cells (*eg.* shape and polarity). A critical hurdle lies in our inability to recapitulate the nanoscale spatiotemporal pattern of these signals. We used CNTs as a tool to tune nanoscaled architecture in cellular microenvironment in Chapter 2 and Chapter 3. After recapitulating the basic understanding of how CNT pattern controlling cellular polarization and human embryonic stem cell attachment in 2D substrate in Chapter 2, we took a step forward by developing a porous scaffold with appropriate mechanical strength and controllable surface roughness for bone repair in

chapter 3. We found that the incorporation of CNTs led to an enhanced surface roughness and mechanical strength of CNT-PLGA composites, which led significantly higher rate of osteogenic differentiation of osteoblasts on CNT/PLGA scaffolds compared to the control PLGA scaffold. All these basic understanding lead us to enhance the utility and efficacy of using CNTs for directing stem cell fate by both 2D and 3D substrate.

On the other hand, cancer has arisen to be of the most prominent health care issues across the world in recent years. Doctors have used physiological intervention as well as chemical and radioactive therapeutics to treat cancer thus far. As an alternative to current methods, gene delivery systems with high efficiency, specificity, and safety that can reduce side effects such as necrosis of tissue are under development. Although viral vectors are highly efficient, concerns have arisen from the fact that viral vectors are sourced from lethal diseases. With all this in mind, rod shaped nano-materials such as CNTs have become an attractive option for drug delivery due to the enhanced permeability and retention effect in tumors as well as the ability to penetrate the cell membrane. In Chapter 4, we successfully engineered PLGA functionalized CNTs to reduce toxicity concerns, provide attachment sites for a pro-apoptotic protein, caspase-3 (CP3), and tune the temporal release profile of CP3 within bone cancer cells. Our results showed that CP3 was able to attach to functionalized CNTs, forming CNT-PLGA-CP3 conjugates. We show this conjugate can efficiently transduce cells at dosages as low as 0.05 μg/ml and suppress cell proliferation up to a week with no further treatments.

Overall, our results showed CNTs were promising to tune cell fate both externally and internally.

TABLE OF CONTENTS

LIST OF TABLES

LIST OF FIGURES

LIST OF SYMBOLS

N_A	Avogadro's constant.
ρ	density.
MW	polymer molecular weight.
Θ	XRD Scanning angle.

LIST OF ABBREVIATIONS

2D.....Two Dimension

3D.....Three Dimension

ABS.....Absorption

ALP.....Alkaline Phosphatase

AFM.....Atomic Force Microscope

APAF1.....Apoptotic Protease Activating Factor 1

BAK.....BCL-2 antagonist or killer

BAX.....BCL-2-associated X protein

BCL-2.....B Cell Lymphoma 2

BH3.....B Cell Homology 3

BSA.....Bovine Serum Albumin

CNT.....Carbon Nanotube

CP3.....Caspase 3

DAPI.....4’-6-diamidino-2-phenylindole

DC.....Direct Current

DI.....Deionize

DMSO.....Dimethyl Sulfoxide

DOS.....Density of State

EDC.....N-(3-Dimethylaminopropyl)-N′-ethylcarbodiimide

FADD..... FAS-associated death domain protein

FDA.....The Food and Drug Administration

FTIR.....Fourier Transform Infrared

HA.....Hydroxyapatite

hESC .....Human Embryonic Stem Cell

HIV .....Human Immunodeficiency Virus

HUVEC.....Human Umbilical Vein Endothelial Cell

MAPK.....Mitogen Activated Protein Kinase

MCNT.....Multi Wall Carbon Nanotube

MES .....2-(*N*-morpholino)ethanesulfonic acid

MOMP ..... Membrane Permeabilization

MSC ..... Mesenchymal Stem Cell

MTT .....(3-(4,5-dimethylthiazol-2-yl)-2,5-diphenyltetrazolium bromide

NHS.....N-hydroxysuccinimide

PEG.....Polyethylene glycol

PGA.....Poly Glycolic Acid

PLA ..... Poly(lactic acid)

PLGA .....Poly(lactide-*co*-glycolide)

PMMA .....Poly(methyl methacrylate)

RAS..... Transforming Protein p21

PI3K .....Phosphatidylinositide 3 Kinase

PLK .....Polo-like Kinase 1

SCNT ..... Single Wall Carbon Nanotube

SEM ..... Scanning Electron Microscope

siRNA ..... Small Interference RNA

TEM .....Transmission Electron Microscope

UV..... Ultra Violet

CHAPTER 1

Introduction: Carbon Nanotubes in Biomedical Engineering Applications

1.1. Carbon nanotubes

Carbon nanotubes (CNTs) were first discovered by Iijima and Baughman [1, 2]. A single CNT is one or multiple layers of graphene sheets which roll up. Depending on the number of the graphene sheets, CNTs are mainly categorized into single wall carbon nanotubes (SCNTs) and multi wall carbon nanotubes (MCNTs) (Figure 1. 1) [3]. SCNTs (Figure 1. 1A) has a diameter close to 1 nm with a varied length from nanometer to centimeters. There are two models for MCNTs (Figure 1. 1B): one is Russian doll model, while the other is parchment model. For Russian doll model, graphene sheets are arranged in concentric cylinders. For the parchment model, a single sheet of graphene is rolled up with several walls of grapheme sheets, like a scroll of newspaper. The interlayer of distance for MCNTs is approximately 0.34 nm for those two models of CNTs [3]. The Russian doll model are more commonly seen. In particular, double wall CNTs count for a special subcategory in MCNTs. It has a similar property as SCNTs, but its chemical resistance is more close to MCNTs [3, 4]. Besides these two major categories, there are also new categories existed since 1990s: torus CNTs [5], nanobud CNTs [6], graphened CNTs , nitrogen doped CNTs, peapod CNTs [7], cup stacked CNTs, extreme CNTs, *etc*.

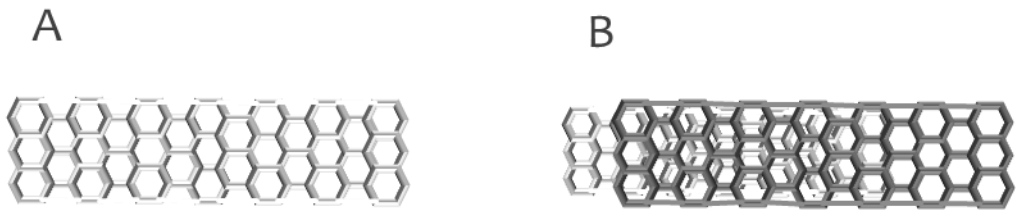

Figure 1. 1 Illustration of SCNT and MCNT. A. SCNT which has only a layer of graphene. B. Russian doll model MCNT, several layer of tubes were concentric arranged to form a MCNT.

Both CNT categories exhibit extraordinary chemical and physical properties. CNTs hold unique physical and chemical properties: such as high surface to volume ratio, high modulus, super electrical and thermal conductivity, super hydrophobic and inertia [8]. Owing to CNTs' extraordinary thermoconductivity, electroconductivity and mechanical property, CNTs find their applications as additives in structural materials such as golf stub, boat, aircraft, bicycles *etc*. Other than that, CNTs are extremely attractive in composite materials [9, 10], electrical device [11-14], hydrogen storage [15, 16], biomedical engineering [17-22], *etc*.. We are extremely interested in using CNTs in biomedical engineering applications.

1.1.1. Size

CNTs are nanosize materials. CNTs usually have a diameter smaller than 50 nm depends on the numbers of the graphene layers [23]. The length of CNTs are varied depending on the fabrication techniques and ranging from nanometers to even centimeters [24]. However, the diameters of CNTs are more stable at the range of several to several tens of nanometers, constructing as high aspect ratio as 132,000,000:1, Therefore, CNTs shape like a needle, facilitating the cellular penetration. Meanwhile, CNTs also maintain high ratio of surface area to volume, resulting a higher loading

capacity. Relying on those properties, CNTs could be very efficient in trafficking biological cargoes in biomedical engineering application.

1.1.2. Mechanical Strength

CNTs are one of the strongest and stiffest materials in the world in terms of tensile modulus and elastic modulus. Graphite, which has a similar structure as graphene, had an in-plane modulus of 1.06 TPa. Considering CNTs are layers of graphene, CNT should display a similar stiffness [25]. Therefore, a couple of groups focused on attenuating mechanical property of CNTs. Since 1990s, a number of groups have conducted tests to discover the mechanical strength of CNTs. They found that the modulus were ranging from tens to hundreds of GPa. With technique developed, it has been demonstrated the Yong's modulus of a single CNT was approximately 1 TPa [26-29], which was 5 times than stainless steel. Note that CNTs are extremely light that its density is approximately 1.4 $g \times cm^{-1}$, CNTs' specific strength can reach 4.8×10^4 $KN \times m \times Kg^{-1}$, which is 3000 times than high carbon steel. CNTs also had a high elastic modulus ~50GPa, with a ~15 % elongation at break. However, CNTs bundles were not as strong as individual CNTs. The weak shear interactions between CNTs and CNT layers led the mechanical strength at GPa level. CNTs' hollow structure and high aspect ratio also led CNTs to undergo buckling rather than elastic deformation. What's interesting was that CNT bundle would only withstand a pressure lower than 25 GPa [30]. All those data were usually obtained in axial direction of CNTs. The strength of CNTs in radial directions were believed to be softer than its axial direction, which was confirmed by AFM in the range of several GPa [31, 32]. Take a step forward, how do

CNTs maintain such a strong property? The answer is because their unique molecular structure. The carbon atoms which make CNTs up are bound by covalent sp^2 bond, which are stronger than sp^3 hybridization found in alkanes and diamonds.

Overall, CNTs can be used to strengthen the mechanical properties of composite materials as we mentioned above. However, particularly, CNTs were also used to enhance the mechanical property for bone tissue engineering by directly injection into and indirectly contact to bone tissue relying on CNTs' super mechanical performance [33, 34].

1.1.3. Electrical property

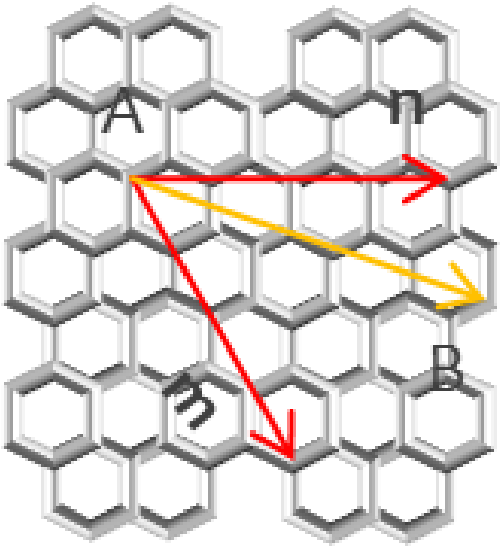

Figure 1. 2 m, n indices to describe the electrical nature of carbon nanotubes. Take the origin carbon as the number 1 carbon, draw vector a1 to atom 3 and draw vector a2 to atom 5. Coming from A to B, the number of atoms coming in a1 and a2 directions are m and n.

The electrical property of CNTs is based on how the graphene sheet is rolled up. The nature of the rolling up of CNTs is described using the indices (m, n) (Figure 1. 2).

In general, in a single phenol ring of CNTs, take the origin carbon as the number 1 carbon, draw a vector a1 to atom 3 and draw another vector a2 to atom 5. Coming from A to B, the number of atoms coming in a1 and a2 directions are m and n. For SCNTs, if m=n, the nanotube is described as armchair tube, which carbon patterns like an arm chair. If m or n equals zero, the CNTs form a zig-zag pattern. All the other cases of the indices refer as chiral tubes [35]. These indices can be used to predict the electrical properties of CNTs. Particularly, for the case of armchair pattern (m=n), CNTs exhibited metallic property with a band gap of zero eV. For the case of m-n≠3, CNTs were semi conductive with a band gap of approximately 0.5 eV. For the case of m-n=3, CNTs were semi metallic with a band gap of approximately 10 meV [35]. Based on these electrical properties, CNTs were able to be used as a chemical sensor, to monitor the environmental change, control chemical process, pre-screen diseases [36, 37]. For MCNTs, the electrical property was determined by each single layer of graphene sheets.

1.1.4. Optical properties

The optical properties of CNTs refer to absorption, photoluminescence and Raman spectrum. These optical properties allow us to characterize or detective CNTs quickly and nondestructively. These optical properties of CNTs derive from CNTs' electronic transition within one-dimensional density of states (DOS) [38]. Note that a single CNT can be considered as a one dimensional material. It should hold a typical feature of one-dimensional crystals. That is their DOS is not a continuous function of energy as a 3 dimensional material has, but it descends gradually and then increases in a

discontinuous spike. Those sharp peaks find in one-dimensional materials are called Van Hove singularities.

Due to Van Hove singularities, CNTs preserve 3 major remarkable optical properties: (A) Optical transitions occur between the cross over transitions v_1 - c_1 and v_2 - c_2. However, these crossover transitions were dipole-forbidden, thus were extremely weak and could only possibly be observed by using cross-polarized optical geometry [39]. Note these crossover transitions of semiconducting or metallic CNTs are traditionally labeled as S_{11}, S_{22}, M_{11}, *etc.*, or, if the conductivity of CNTs is unknown or unimportant, as E_{11}, E_{22}, *etc*.. (B) Considering that the energies between the Van Hove singularities depends on CNT structure. The optoelectronic properties of CNTs can be tuned and controlled by varying CNT structure, Such designing ability has been experimentally demonstrated by using UV illumination of polymer-dispersed CNTs [40]. (C) CNTs had rather sharp (~10 meV) and strong optical transitions. It is relatively easy to selectively excite CNTs having certain (n, m) indices, therefore giving us the chance to detect optical signals from that specific type of CNTs.

Optical absorption in CNTs originates from electronic transitions from crossover transitions. The transitions are relatively sharp and can be used to identify specific CNT types (m,n indices). However, it is not optimistic to distinguish different CNT types in a CNT mixture. This is because that the sharpness of the gap deteriorates with increasing energy. Many CNTs had very similar E_{22} or E_{11} energies, significant overlap of different types of CNTs occurred in absorption spectra [41-44]. Furthermore, CNTs were close to a black body (absorbance equals to 1) as well. For instance, vertically aligned SCNT

array could have absorbance of 0.98–0.99 from the far-ultraviolet (200 nm) to far-infrared (200 μm) wavelengths [45].

Raman spectroscopy requires very small amount of sample but still has good spatial resolution (~0.5 micrometers) and sensitivity for SCNT. The data obtained from Raman spectroscopy would also examine the purity as well. Consequently, Raman spectroscopy is becoming the most popular technique to characterize CNTs. Moreover, what put Raman scattering more attractive for SCNT is the resonant property would provide more applications in biomedical engineering [46, 47].

1.1.5. Thermal properties

All types of CNTs are good thermal conductor along tube direction as well. Measurement has shown that SCNT had a thermal conductivity of 3500 $W \times m^{-1} \times K^{-1}$ at room temperature. This was almost 10 times of the thermal conductivity of copper (385 $W \times m^{-1} \times K^{-1}$). What made SCNT's thermal properties more attractive was that the thermal conductivity along the radial direction was only 1.52 $W \times m^{-1} \times K^{-1}$, similar as soil. Considering CNT were very stable up to 2800 ^{o}C in vacuum and 750 ^{o}C in air, CNTs could be potentially used in one direction heat transfer [48, 49].

1.1.6. Hydrophobicity

CNTs are super hydrophobic materials as well [50]. Hydrophobicity is benefit in waterproof applications. However, hydrophobicity is usually the main cause of intrinsic toxicity of CNTs, leading cell to necrosis. Pristine CNTs would also tend to accumulated and agglomerated due the hydrophobic interaction in water phase [51]. Therefore, to

utilize CNTs in biomedical engineering applications, the functionalization of CNTs were usually required.

1.2. Functionalization of carbon nanotubes

As we mentioned above, the hydrophobicity of CNTs need to be changed to hydrophilic in order to reduce the intrinsic toxicity of CNTs. Another reason for to do so is that CNTs requires functionalization to be able to disperse in biological environment. In general, the functionalization of CNTs can be categorized into covalent and non-covalent [52]. Non-covalent binding relies on the interactions between CNTs and linkers. Covalent binding relies on chemical reactions to add reactive groups to CNTs which facilitate further modifications such as protein/polymer conjugation.

1.2.1. Non-covalent functionalization of carbon nanotubes

For non-covalent functionalization of CNTs, pristine CNTs remain intact and there is no atomic damage on either sidewall or terminal of CNTs. The dominant interaction between CNTs and their adducts is π-π stacking [53]. Aromatic molecules can be immobilized on the poly-aromatic graphitic surface of CNTs due to π-π stacking (Figure 1. 3 upper panel). For instance, Pyrene derivatives were used to stabilize CNTs from aggregation [54]. DNA and RNA were also able to immobilize CNTs due to the π-π stacking between nucleobase and CNTs [55, 56]. Moreover, proteins could be functionalized on CNTs by interaction between benzene groups and CNT sidewall. Besides π-π stacking, van der Waals forces and hydrophobic interaction are other key forces for CNTs and adducts. For example, amphiphiles were used to suspend CNTs in

water phase [57-59]. The hydrophobic methylene chain wrap over the CNTs Figure 1. 3 bottom panel) due to hydrophobic interaction. The hydrophobic backbone adhere to the body of CNTs and the hydrophilic water-soluble head enhance the ability of CNT conjugates to disperse in aqueous solution. Tween-20, Triton X-100 and pluronic triblock polymers, were used to reduce protein binding or to obtain a well suspended CNTs water solution. This non-covalent binding allows CNTs to be able to conjugate a variety of cargoes which have biological function. The newly formed biological conjugates can deliver these cargo into a living cell. There is another key advantage for non-covalent binding. That is the structure of CNTs are not broken down, which let non-covalent bounded CNTs preserve their unique physical and chemical properties. However, there are also critical concerns that A) non-covalent bounded molecules are more easily detached from CNTs; B) biological molecules are tending to be degraded; and C) amphiphilic surfactants are able to lyse cells and denature proteins.

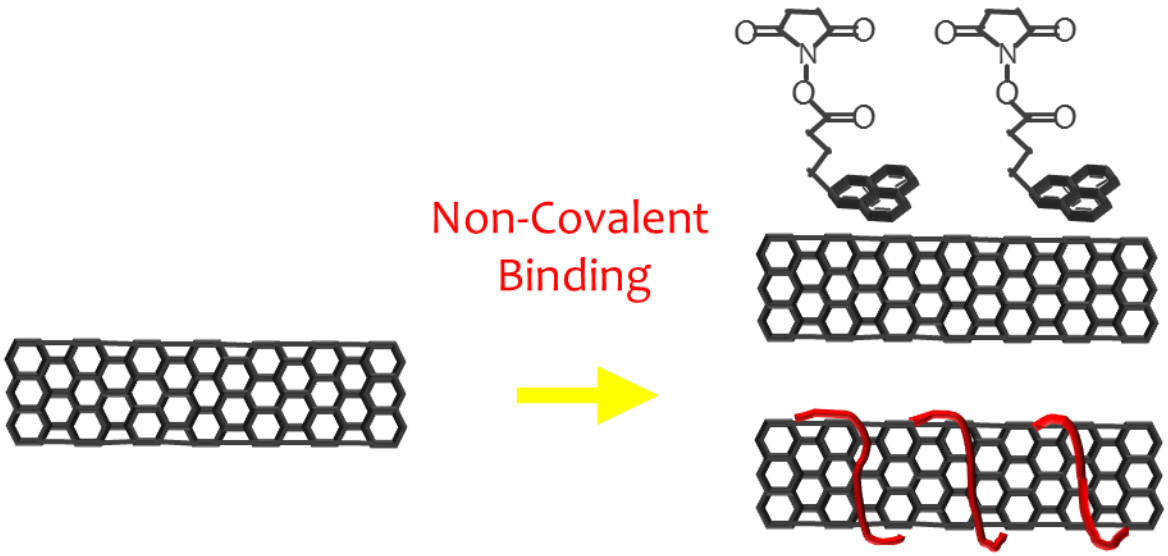

Figure 1. 3. Schematic of non-covalent binding of CNTs. Upper panel on the right showed aromatic rings of adduct molecules adhere to the main body of CNTs due to π-π stacking. Bottom panel on the right showed molecular chains adhere to main body of CNTs due to van der Waals interaction and hydrophobic interactions.

1.2.2. Covalent functionalization of carbon nanotubes

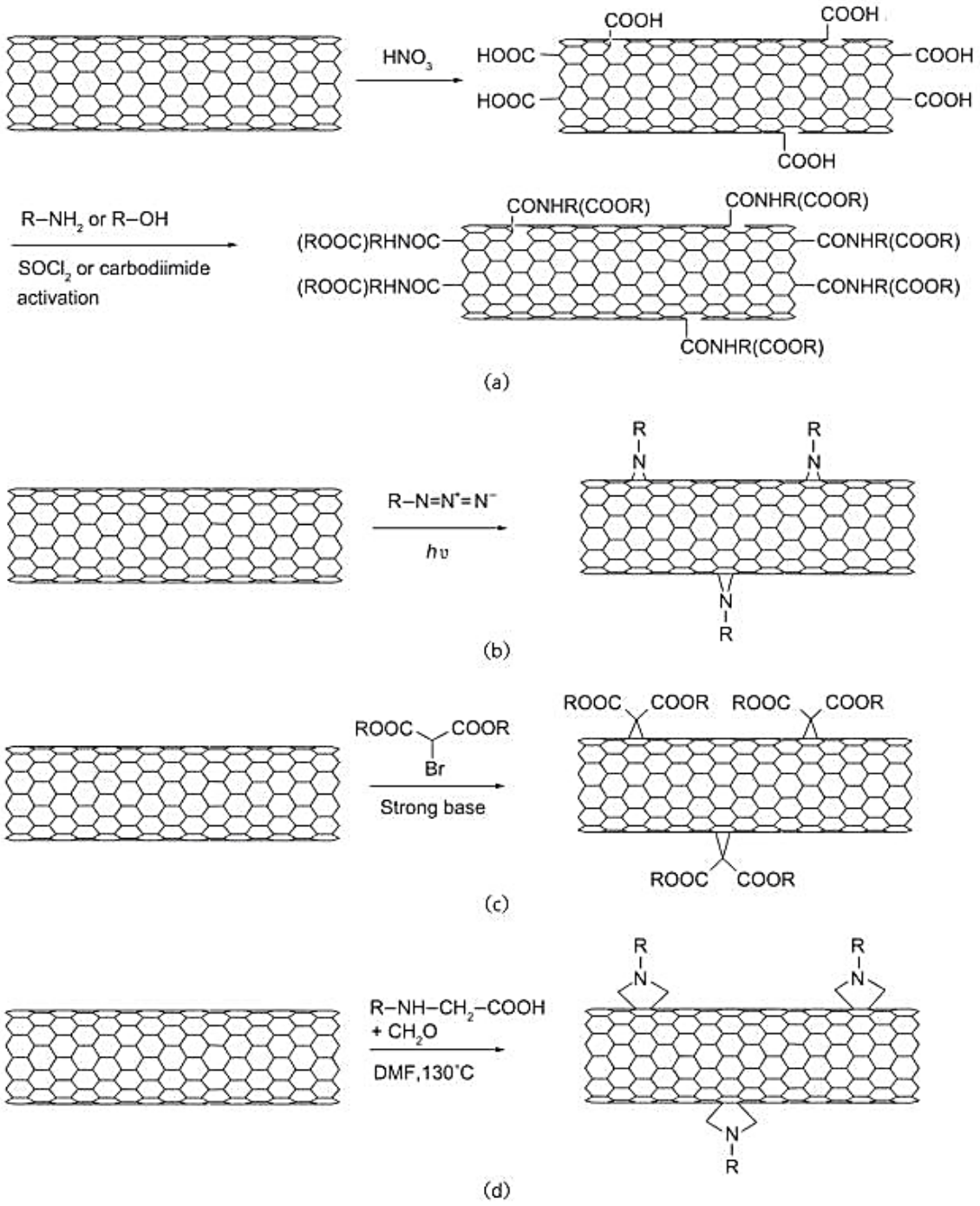

Figure 1. 4 Schematic of covalent binding of CNTs [52]. (a) CNTs are oxidized and then conjugated with hydrophilic polymers; (b) photoinduced addition of azide compounds with CNTs; (c) Bingel reaction on CNTs; (d) 1,3-dipolar cylcoaddition on CNTs. Further conjugation of bioactive molecules can be applied based on such functionalization.

For covalent binding (Figure 1. 4), the most commonly used functionalization method to function CNTs is oxidation [60]. In brief, oxidation reagent such as hydrogen peroxide and nitric acid is used to form carboxyl groups on the terminal or side wall of CNTs. These oxidized CNTs are further attached to hydrophilic polymers to prevent aggregation due to charge screening effects. In the community, a couple of different polymers such as PMMA [61], PEG [62], *etc*. were successfully attached to oxidized CNTs. This further conjugation of polymers allows attachment of biological functional molecules. In our group, we firstly fabricated CNT-PLGA conjugate for the use of gene delivery in biological system (Chapter 4).

Second route of covalent functionalization of CNTs is cycloaddition. This type of reactions happens on the sidewall of CNTs. One of the unsaturated bond in aromatic ring of CNTs is broken and a new cyclic adduct will be added on. There are three major cycloaddition reactions in functionalization of CNTs. Azides were introduced onto sidewall of CNTs by photochemistry [63]. Carbene compounds were generated on the sidewall of CNTs by Bingel reaction [64]. 1, 3-dipolar cycloaddition have also been used to generate functional groups to the sidewalls of CNTs [65].

These covalent reactions impair the atomic arrangement of carbon and reorganize electron cloud of CNTs. Therefore, the electron and thermal conductivity and optical properties are altered. Despite this disadvantage, covalent functionalization could have the biological cargoes linked to CNTs to be more stable in biological system. Functionalized CNTs were also be able to maintain temporal drug release profiles (as shown in Chapter 4).

1.3. Cell fate regulation

Tissue formation, function, regeneration after damage and pathology formation are the result of temporal and spatial organization of individual cell fates [66]. Individual cell fate is the consequence of the cross talk of cells to its microenvironment and neighboring cells. In brief, cells sense the physical cues and soluble chemical cues by the receptors on the cell membrane [67]. These signaling cues are read and translated into intracellular cues. Then, cells are able to differentiate to the desired lineage. Thus, we have two options to direct cellular behavior: (i) construct biomimic microenvironment which favors desired cellular differentiation; and (ii) deliver key intracellular cues into cell and control the cell fate.

1.3.1. Extracellular cues to regulate cellular behavior

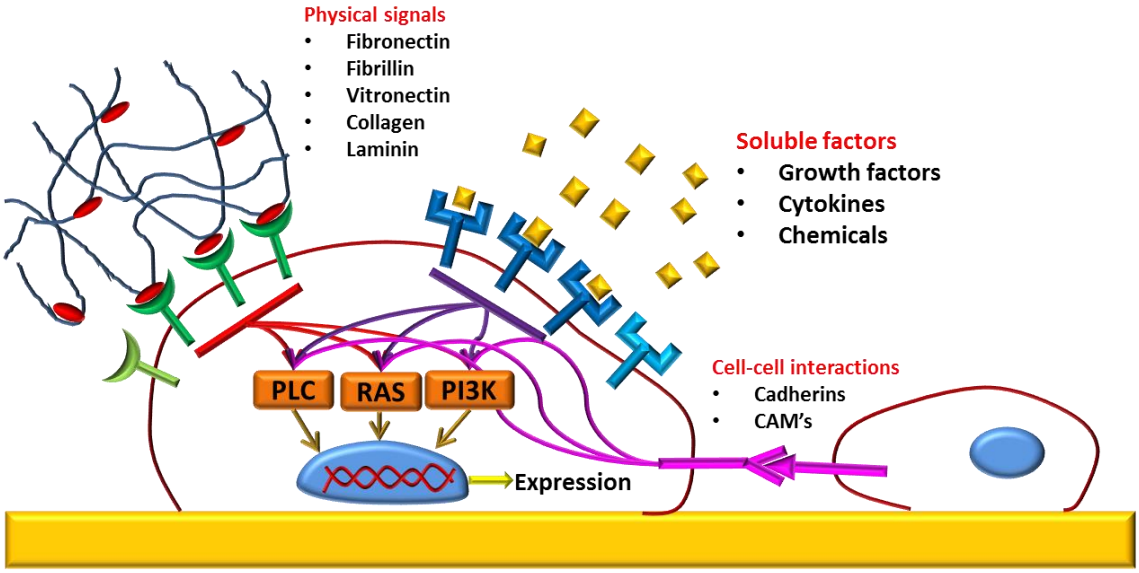

Figure 1. 5 Schematic of Extracellular matrix regulating cell fate. Cells will sense physical signals and soluble signals and express genes. The receptors translate signaling cues through PLC RAS and PI3K to gene expression. The extracellular cues includes physcial signals, soluble signals and cell-cell interactions. Physical signals includes fribronectin, fibrillin, vitronectin, collagen, laminin and other stromal properties. Soluble factors includes growth factors cytokins and outsourced chemical. Cell-cell interactions includes cadherins and CAM's.

Extracellular environment is the area full of surrounding cells and signaling molecules [66]. There are three major types of effectors: (1) insoluble signaling molecules, such as extracellular matrix proteins (ECM): collagen, fibronectin, vitronectin, elastin, *etc.*; (2) soluble signaling molecules such as growth factors and cytokines; and (3) cellular membrane proteins involved in cell-cell contact (Figure 1. 5).

In terms of engineering regenerative tissue by controlling extracellular matrix, scaffold architecture, fibrils organization, mechanical strength, in combination of surface topography are key effectors to modulate cell fate [66]. For instance, cellular behavior was found to be influenced by microenviromental stiffness [66]. Cells were less migrated due to reduced spreading and disassembling of actin while they are seeding on a weak gel, cells behaved the opposite on stronger scaffold in contrast [68]. Moreover, scaffold should be able to withstand cell contractile forces which generated by via cell and scaffold [69, 70]. On the other hand, cells preferred to proliferate, migrate and mature on substrate which has similar modulus as their donors. Bone exhibits strong mechanical properties since it provides structure stability for the body and it allows for millions of loading cycles throughout a person's lifetime [71]. However, both natural and synthetic polymers were low in strength which couldn't meet the requirement for bone tissue engineering that bone cement must meet approximate mechanical strength of where it is replacing, *eg*. human trebecullar bone's compressive modulus is 5 to 50 MPa. Either crosslinking or blending with high stiffness materials should be carried out to enhance the mechanical strength of polymer substrate for bone tissue engineering. As a result, high modulus materials are preferred for bone tissue engineering.

Surface roughness or surface topography is another important property that allows for osseointegration in scaffolds, as demonstrated by Goldberg group, Feighan group and D'Lima group [72-74]. Topography would affect cell spreading and cell activities [75], could significantly increase total surface area as well that cells would sense and migrate [76]. Additionally, Cells could sense surface grooves which would be either wide or narrow and in turn cytoskeleton would adjust to it [77]; cells also could respond to microscale changes of the surface by tuning cell orientation and motility [78]. These micro or nano scale differences could be achieved by fabrication process such as introducing nano materials into basal materials and using mirco/nano fabrication techniques. In Chapter 3, creating a scaffold with certain surface roughness is the first challenge. Then, cells would sense these factors by membrane receptors [67]. These factors would be transduced into intracellular signals, affecting gene expression through receptor mediated transduction pathways, such as integrin pathway, mitogen activated protein kinase pathway, mechano-transduction pathway, *etc*.. Therefore, to engineer microenvironment with proper property could lead cells to a desired fate.

1.3.2. Intracellular cues to regulate cellular behavior

Other than physical cues; genes, transcription factor, and signaling molecules can induce cell differentiation and control cell phenotype as well (Figure 1. 6). Subsequently, approved clinical gene therapy was started in 1990s [79]. More and more gene therapies either in experimental or clinical stages have been proved promising in curing human diseases. However, there is still a challenge that a safe, efficient and long-term delivery system is required [80].

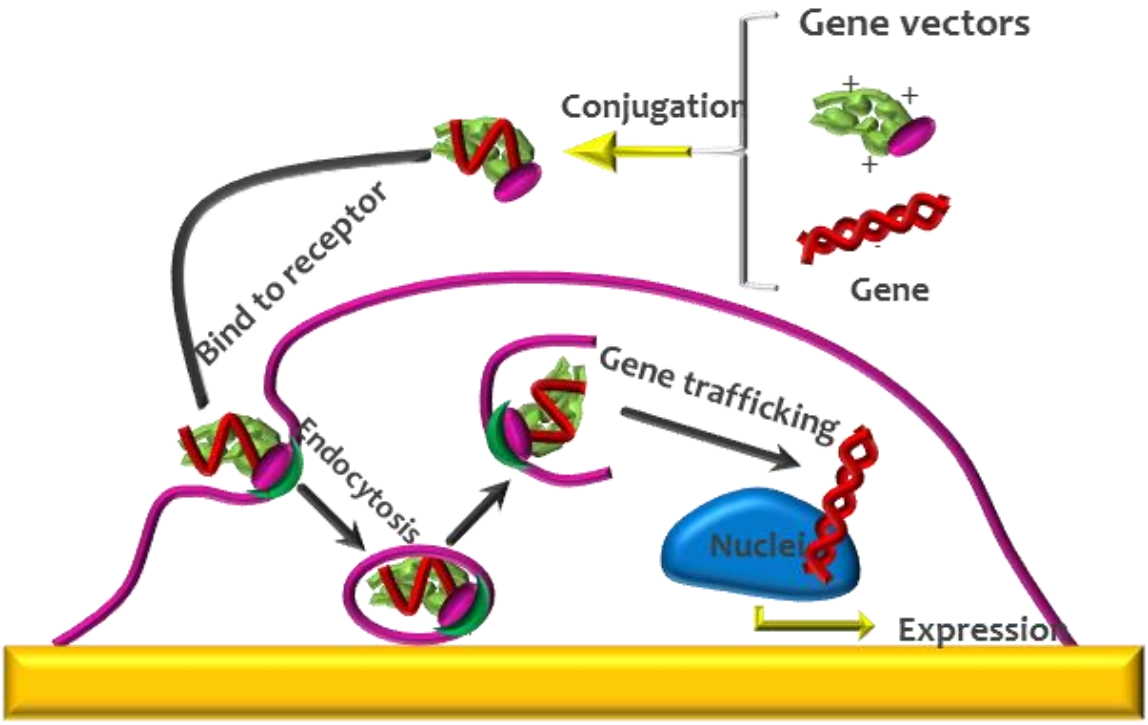

Figure 1. 6 Schematic of how intracellular cues to regulate cell fate. Genetic materials and transcriptional factors are delivered into cell and regulate gene expression. In brief, DNA or RNA conjugates to gene factors firstly, and then the whole conjugate will bind to membrane receptor. Through endocytosis the whole conjugate will be absorbed by cell. Thus, DNA or RNA will be released and finally affect gene expression.

Currently, retrovirus [81], adenovirus [82] and adeno-associate [83] viral vectors are major types gene vectors widely used due to their ability to infect cells and transfer target genes. The ideal gene vectors need to fit such requirements that (i) can transduce genes into specific target cells without infecting normal cells; (ii) can integrated into the target genome with high efficiency, and (iii) the transcriptional unit should be responded to the regulatory elements. Through viral vectors (Figure 1. 7) are beneficial in efficient delivery and transducing cells, there are still concerns which emphasized on that some of viruses are deadly diseases intriguer, such as human immunodeficiency virus (HIV) and human T-cell lymphotropic virus (HTLV) (Figure 1. 7). Additionally, some virus may still trigger immune response and result in lowing efficiency.

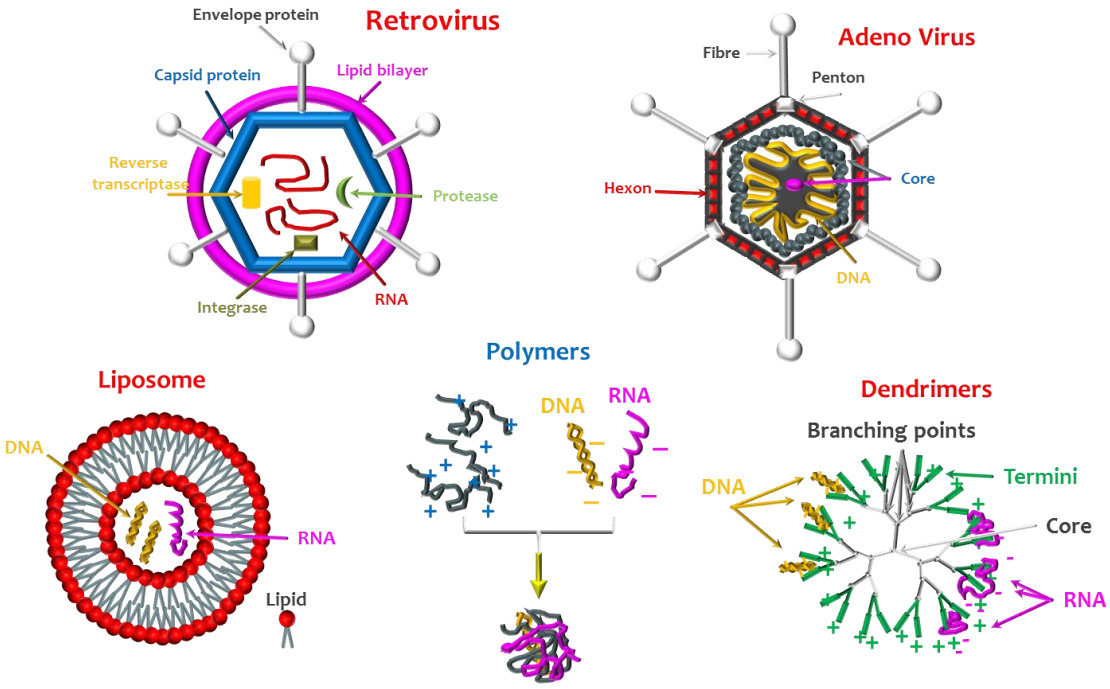

Figure 1. 7 Schematic of vectors used in gene therapy and drug delivery. There are two major categories: viral vectors and non-viral vectors. Commonly types of viral vectors are: adeno virus and retro virus, which differs from the genetic materials incorporated inside (RNA and DNA respectively). Commonly types of non-viral vectors are liposomes, polymers and dendrimers, which are usually positively charges in order to facilitate DNT/RNA conjugation.

Consequently, non-viral vectors (Figure 1. 7) are taken into considerations. Polymers and lipids are most commonly explored materials for drug delivery. Synthetic polymers such as PEG [84], PLA [85] and PLGA [86]; natural polymers such as chitosan [87], collagen [88] or gelatin [89] and lipids [90] were used to synthesize nanoparticles, liposomes and micells. These polymers and lipids can be either chemically modified or not modified to encapsulated drugs. Liposomes are spheres contain a separate liquid phase from the element which could protect the genes from degradation. Drugs are released in a controlled manner due to surface and bulk degradation or phase transition. However, concerns arise that immune response may

occur due to heterogeneity of ex-original materials and efficiency is low. Hence, there is a need to construct a high efficient non-viral vector.

1.4. Carbon nanotubes in biomedical engineering applications

The unique properties of CNTs lead CNTs more attractive in biological engineering applications. It is expected to use CNT based biomaterials for clinic use in the near future. CNTs can be used to design mechanical enhanced scaffold to stimulate cellular growth. CNT based biomaterials has also been applied into bone, nerves, and cardiovascular system. There has been progress in the use of CNTs in controlling cellular alignment, to enhance tissue regeneration, growth factor delivery and gene delivery.

1.4.1. Carbon nanotubes to controlling cell alignment

As we indicated above, area of cell expansion and topography play important role in cell survival, differentiation, vascularization and cancer development. A few studies have already demonstrated that mesenchymal stem cells (MSCs) can be differentiated into multiple cell line by simply controlling the disorder or the dimension of nanostructures [91]. The result showed the differentiation found not many differences in the case where soluble cues were used. Cell polarization induced by alignment could be an answer to the critical hurdle of tissue engineering: lack of enough vascularization in the scaffolding materials (200 μm deeper in the scaffolding materials). More interestingly, take tumorigenic fibroblast as an example, they lay down collagen in an

aligned fashion, facilitating cell migration and tumor generation. Normal fibroblast only lay down collagen in a random fashion, forming normal phenotype.

CNTs are nanosized rod-like materials. Despite their fascinating electrical and thermal conductivity, they can be used to engineering nano topography on 2D substrate in an aligned manner. Currently, there were several methods have been developed to align CNTs. Microfluidic flow [92], DC electricity [93], centrifugal forces [94], and micro patterning [95] were all used to align CNTs on 2D substrate. A variety of cell lines such as MSCs [96], Chinese hamster ovary cells [97], *etc*. was successfully aligned on this 2D substrate. The successful alignment of CNTs on 2D substrate would also increase the future application of electrical shock and growth factor conjugation for further induction of either differentiation of stem cells or the maturation of adult cells. We may also utilize this CNT to study cell polarization and tumor genesis. In our group, we were trying to develop a CNT based 2D substrate for cellular attachment and alignment for both adult cells and single human embryonic stem cells (hESCs) (Chapter 2). The further application would have been utilize this substrate for inducing hESC differentiation at single cell level.

1.4.2. Carbon nanotubes for bone tissue engineering

CNTs have been used to study neurogenesis [98], cancer treatment [99] and especially in osteogensis [100]. There have been several reports of the influence of CNTs on osteoblastic cells *in vitro*, most of these studies indicated that CNT promote the proliferation and cell growth of osteoblastic cells [34, 101, 102]. This is a valuable characteristic of CNTs for its application in bone tissue regeneration. Furthermore,

investigators have shown that CNTs possess compatibility with bone tissues that CNTs neither increased the inflammation of the bone tissue, nor blockd the bone tissue regeneration. In contrast, CNTs provided assistance in bone tissue regeneration and showed integration with the tissue [103]. More interestingly, they could integrate successfully into bone tissue [8].

Zanello et al. discovered that osteoblasts change morphology and express plate shape crystals in the presence of CNTs [34]. These osteoblasts which exposed to CNTs were more differentiated and osteocyte-like as compared to osteoblasts cultured on a glass surface which exhibit a flat morphology [104]. Plate shaped crystals aggregated in clusters outside the cells and were similar in shape to hylauic acid found in woven bone [105]. In another route, Yi et al. found gold nanoparticle coated surface promote osteogenic differentiation through mitogen-activated protein kinase p38 MAPK pathway. Osteoblasts sensed gold nanoparticles via integrin receptors and induced p38 kinase activation which upregulated osteogenic differentiation gene expressions [106]. Kim et al. also demonstrated Ti surface roughness enhances osteoblast differentiation via mediating MAPK pathway. Bone formation genes were expressed by activating protein kinase A (PKA) due to occupation of integrin receptors [107]. Moreover, studies have shown genes code BMP-2, osteonectin and osteopotin have been upregulated under exposure of CNTs [108-110].

As a result, more CNT composites are taken into account for bone tissue engineering. Abarretegi et al. developed a chitosan/CNT scaffold and evaluate its effect in tissue engineering. Scaffold performed a satisfactory result of cell adhesion, cell viability, and cell proliferation on the external surface [111]. Meanwhile, with the

addition of rhBMP-2, cells were differentiated towards osteogenic lineage. Furthermore, Mikos et al. fabricated an ultra-short single wall CNT nano composite and evaluated the effects of mechanical strength, porosity and material composition on bone marrow stem cells. Results showed CNT materials hold promising potential in bone tissue engineering with tunable porosity and mechanical strength [112]. Edward et al. developed a PLGA/CNT electronic spinning nanofibers, not only are cell growth supported, but also full range of electronic conductivity and mechanical property of CNT are fully utilized [113]. It has been suggested that CNT is a good type of material for bone regeneration. Thus, a promising chapter in the study of biological applications of s in bone tissue engineering has begun (Chapter 3).

1.4.3. Carbon nanotubes for neurogenesis

Another more sophisticated application for using CNTs in tissue engineering is Neurogenesis [114]. The great electrical conductivity would provide superb environment for neural progenitor cells to develop axons [115]. Quite a few studies have been developed to study neurogenesis on CNT based substrate using different cell lines. As early as in 2000, Mattson et al. provided the fundamental study of neuronal differentiation of rat embryonic stem cell on pristine CNTs [116]. A few years later, Hu et al. reported they successfully tested the signal transfer between the synapse of neuron cells cultured on CNTs based substrate [117, 118]. Other than the neuron cell maturation, CNTs could also induce differentiation of hESCs to neuron lineage on a 2D substrate composed of CNTs [119]. It has been demonstrated that CNTs were biocompatible to neuron cells. Now researchers are more focused on using CNTs to assemble aligned

networks for neuron network regeneration, which could be potentially a big leap in neuron regeneration. Overall, there is one extra credit of using CNTs than using micro patterning: CNTs will not only provide axon growth direction, but also facilitate electrical signal to transfer along CNTs alignment. These properties in turn help neuron regeneration.

1.4.4. Carbon nanotubes for drug delivery

CNTs are needle like and very easy to penetrate the cell membrane due to its high volume to radius ratio. However, CNTs are not suitable for directly transferring genes in biological system. Subsequently, scientists discovered that functionalized CNTs have decreased their intrinsic toxicity [120]. The major modifications of CNT are covalent and non-covalent functionalization [52] as we discussed above. For a quick reminder, oxidation and cylcoaddition reaction are common methods in covalent functionalization to add functional group to CNTs' sidewall or ends [121, 122]. For non-covalent functionalization, CNTs are coating with a layer of molecules by π-π stacking or the small interactions between the molecules.

On the other hand, as a matter of fact, drug carriers in nano sizes have advantages in drug delivery systems: (i) protection of delicate drugs, (ii) enhance absorption in selective tissues, (iii) control drug distribution profile and (iv) enhance intracellular penetration [123]. But the CNT cellular uptake mechanism may differ depending on the functionalization and size of the CNTs [124]. CNTs have been used to efficiently shuttle various biological cargoes, ranging from small drug molecules [125] to biomacromolecules, such as proteins [126, 127] and DNA [128, 129] and RNA [130],

into different types of cells via endocytosis [131]. Moreover, small amount of CNTs was found to be biocompatible to cells.

Carbon based biomaterials is leading a new trend in various medical areas especially in tissue engineering. Functionalized CNTs based biomaterials which enhanced its biocompatibility can continuous contact with biological systems and can be used as scaffold to support the cells and to deliver drugs. Liu Z. et al have successfully delivered siRNA by phospholipid PEG (PL-PEG) functionalized CNTs into tumor cells and tissue to inhibit cell proliferation and tumor ingrowth and enhance CXCR4 expressions ex and *in vivo* [132-134]. siRNA was released by cut off S-S bond attached to PL-PEG which would not last for a longer period. Therefore, CNT are found to be an effective gene deliver vesicle but a long term release profile using CNT is still needs to be investigated.

1.4.5. Carbon nanotubes for disease imaging and detection

Because CNTs hold intrinsic optical properties, CNTs are good candidate for optical imaging. SCNTs have small band gaps on the order of 1 eV, makes it auto fluoresce in the near infrared range. The excitation and emission bands of SCNTs are separated broadly. The background fluorescence can be reduced. Relying on this properties, a few groups have developed imaging SCNTs within the cell body. Pilot study using SCNTs for biomedical imaging *in vivo* was first conducted by Weisman group. They successfully imaged food bio-distribution in larvae. SCNTs were also promising in cancer imaging that tumor retains naosized materials by EPR effect. Researchers reported that functionalized SCNT signals was observed in living mice

model. The *in situ* and *in vivo* imaging utilizes the photoluminescence property of SCNT. SCNT has an auto fluorescence in the near IR range, allowing real time, *in vivo* and in situ imaging in a living organism. Despite that, CNTs could be also used for cancer imaging by adding receptor target adducts or CNTs itself would be retain in tumor tissue due to EPR effect [135-140].

1.5. Toxicity of carbon nanotubes in biomedical engineering application

The toxicity of CNTs has been drawing attention of researchers in biomedical nanotechnology. As of 2007, preliminary results highlighted the difficulties in evaluating the toxicity of this heterogeneous material. CNTs have so many parameters which have considerable impact on the toxicity of CNTs. These parameters includes: structure, size distribution surface area and chemistry, surface charge, agglomeration and purity. Interestingly, available data clearly showed that, CNTs could cross membrane barriers by its own property. Then here comes out a paradox. If raw materials reach the organs, they can induce harmful effects such as inflammatory and fibrotic reactions. Thus, functionalization of CNTs are preferred. Overall, CNTs are very promising in cancer therapy and controlling cell fate internally [141, 142].

More specifically, except the use of CNTs in cancer therapy, toxicity concerns are always there for either stem cell differentiation or adult cell maturation. In early years, a number of studies have demonstrated that CNTs could have potential toxicity in biomedical engineering applications. Others claimed there was no toxicity at all. These findings are complicated and paradox. Recently, many comprehensive studies revealed convincing data about CNT toxicity. CNTs retain intrinsic toxicity due to that their

inherent properties: super hydrophobicity and high surface area. For example, Ding et al. discovered that CNT increases apoptosis of human skin fibroblast [143]. In addition, the HEK 293 cell proliferation was found to be inhibited by co-culture with CNTs. Note, CNTs used in these studies were not functionalized. Liu et al. tested the cytotoxicity of oxidized CNTs; they found that differentiation and proliferation of MSCs were inhibited by oxides CNTs [144]. Not only MSCs, lymphocytes were also has been induced apoptosis after exposure of CNTs [145]. Since simple oxidization didn't show promising in cytotoxicity, researchers then moved to decrease the toxicity by decreasing the intrinsic hydrophobicity of CNTs. PEGylated CNTs showed minimum toxicity *in vitro* studies. Several other reports has demonstrated the polymer functionalized CNT are not toxic to a variety of cell lines at all.

CNTs are not going to be used only for *in vitro* studies. To address more clearly for the side effect of CNTs in human body, researchers use animal models as references. There were a few studies discovered pristine CNTs definitely do damages to pulmonary system, suggesting aerosol exposure of CNTs needs to be avoided. Some further study demonstrated that the toxicity of the CNTs could have been size dependent. The toxicity of CNTs with smaller size in nanometer scale was significantly different from the CNTs with larger size in micrometer scale [146]. Then, more research focused on functionalized CNTs were accumulated in spleen and liver. However, little toxicity has been observed by using functionalized CNTs. Because of the successful minimization of toxicity by functionalization, the bio-distribution of functionalized CNTs was studied. Interestingly, the functionalized CNTs were able to be cleared by urea within hours. No

uptake or accumulation was found in organs such as liver and spleen by radioactive labeling.

1.6. Summary

CNTs for biomedical engineering has been an emerging area due to the special and fascinating physical and chemical properties CNTs hold. Although a few conclusion drew from some groups may be paradox, CNTs are promising candidate in tissue engineering, biomedical imaging and gene delivery. However, more research attention should be focused on basic chemistry of CNTs functionalization and basic biology of degradation, distribution and clearance of CNTs in human body. In the following three chapters, we demonstrated the ability of CNTs as extracellular and intracellular regulators to control cellular behaviors.

As extracellular matrix, we developed an aligned CNT substrate to align HUVEC and culture hESCs at single cell level (Chapter2). It is well acknowledged that culturing single hESCs is extremely difficult. By either mechanical or enzymatic breakdown of hESC colony, it is able to culture single hESCs. However, these single cells still tend to migrate to crowd together. With our newly developed CNT substrate, we could culture hESCs at single cell level, and could control their migrating as well. This is the great novelty in the Chapter 2. By culturing single hESC, we could take a step forward to differentiate single hESCs to desired phenotype with limited heterogeneity.

We also developed a CNT containing PLGA scaffolds for bone regeneration in Chapter 3. Previous study has showed that CNT addition increased either stiffness or

surface roughness, which in turn increased osterogeneis. The great novelty in Chapter 3 lies in that by developing a 3D CNT content scaffolds, we were able to coupling the surface roughness and mechanical strength to osteogenesis. As we confirmed, the increase of nano roughness and mechanical strength together helped improve osteogensis.

As intracellular cue vesicles, a number of biological cargo has been already delivered intracellularly by a several types of linkers such as PEG or not. We developed a new CNT-PLGA conjugate to delivery biological cargoes into cells in Chapter 4. The innovative aspect of our DDS system based on CNT-PLGA is that we can tune temporal release profile by controlling the molecular weight and PGA to PLA ratio.

CHAPTER 2

Alignment of Carbon Nanotubes: An Approach to Modulate Cell Orientation and Asymmetry

2.1. Introduction

Stem cells are promising in tissue engineering, as their differentiated derivatives can be used to reconstruct most biological tissues. These approaches heavily rely on biophysical cues that tune the ultimate fate of stem cell and provide by cellular microenvironment [147]. Particularly, topography plays a crucial role in affecting cell behavior such as spreading, migration, and differentiation among other characteristics [148-150]. Focal adhesion is a key component by which cells are able to adhere to substrates. As cells bind to extracellular matrix (ECM) ligands, integrins are clustered and therefore form focal adhesion. Cells sense topographical structure through focal adhesion, therefore control cellular alignment and other cell behaviors [149]. Cellular alignment is crucial for the function of certain tissues in the human body. For instance, the mechanical strength of bone depends heavily on the cytoskeletal alignment of osteoblasts [151]. This allows us for engineering a unique topographical substrate, which enables integrin to attach in a controlled manner therefore affect the cell behavior and ultimately tissue function.

However, the mechanism for the change of cell behavior induced by cell alignment remains somewhat elusive. Mechanotransduction signaling pathways are generally hypothesized with tension forces being transmitted from focal adhesions

through the cytoskeleton and ultimately to the cell nucleus [152, 153]. These forces are mediated by trans-membrane adhesion proteins and can therefore affect the expression of signaling proteins [154-156]. For instance, collagen type I is a ligand for integrins that are bound to integrin linked kinase. Integrin linked kinase activation has been reported to increase cytoplasmic levels of β-catenin, which positively affects the Wnt-β catenin signaling pathway. This signaling cascade can potentially result in the neurogenic differentiation of embryonic stem cells [154-157]. Additionally, nuclear shape changes via connections between the cytoskeleton and the nuclear matrix [158].

Nano and micro engineered topographies are of current interest to develop cellular alignment [159]. Stem cells were differentiated into a neuronal lineage with significant neurite extensions confined in the nanogrooves [159] or along with direction of electronic spun fibers [160]. The differentiation of exoderm or endoderm can be determined via controlling the colony size of embryonic stem cells by micropatterning technology [161]. These studies mostly focus on a view of how cellullar alignment is affected by the microscale substrate. Few reports have focused on the alignment of cells induced by nanoparticles. Thus, we are interested in using CNTs to engineer nano topographies.

CNTs have become an attractive option to biological applications for their unique characteristics [162, 163]. CNTs have been used as a developing platform to enhance nano roughness [19] among other applications [164-166]. Specifically, it has been confirmed statistically that CNTs were able to increase the number of focal adhesions and expression of vinculins [167]. Rigid dash like and dot like focal adhesion structures have also been monitored on CNT substrates [168]. Our previous study also demonstrated

increased number of cell attachment by addition of CNTs [169]. Recently, Namgung et al. successfully aligned human mesenchymal stem cell on CNT coated surface using a spin coating procedure [96]. These findings inspire us to tune cellular alignment through focal adhesion sites by regulating CNT substrates.

With these in mind, our goal is to develop a platform coating aligned ligand functionalized CNTs to provide attachment sites, which cells can decipher and bind to. Our hypothesis underlies that cells will be able to recognize and adhere only to those CNT patterns, such that cytoskeleton will organize to adopt the aligned fashion through focal adhesions.

To achieve the goal, we functionalized carboxyl CNTs with the ligand proteins and aligned these CNT-ligand conjugates on an Au coated glass substrate by spin coating. We characterize the CNT-ligand and the surface properties of substrate by various techniques. In addition, we used human embryonic stem cells (hESC) and human umbilical vein endothelial cells (HUVEC) as model cells in order to demonstrate the spreading and cytoskeleton organization on the substrate. The uniqueness of this paper lies in the ability of these patterns to control cell attachment and shape through the tenability of density and dispersion of these CNT-ligand conjugates.

By developing this aligned CNT pattern, we were able to tune single hESC attachment and alignment of HUVEC. We have provided a new approach to tune hESC culture at single cell level. This would allow us for better understanding differentiation of hESC at single cell level. Most importantly, the differentiation of hESCs could be conducted at single cell level by using this CNT pattern. Potentially heterogeneity could avoid in hESC differentiation.

2.2. Materials and methods

2.2.1. Substrate preparation

Coverslips were rinsed in sterilized water for 5 min, dried with lab provide air blow for 5 min, and cleaned with an ozone cleaner (BioForce Nanoscience) for 3 min. Coverslips were then coated with a first layer of 5 nm Ti and second layer of 10 nm Au through sputter coating (Denton Desk II Turbo Sputter Coater and Denton Desk II Sputter Coater respectively). For Ti coating, a vacuum at 10 Torr has been applied to the chamber with Ar gas blowing into the chamber. 15 seconds of sputter coating time was applied. For Au coating, a vacuum at 100 Torr has been applied with Ar air blowing into the vacuum chamber. 30 seconds of sputter coating time was applied. All Au coated samples were stored in petri dish sealed with parafilm till use to prevent dust.

Total of 100 µg of carboxyl CNTs (Nano Lab, purity>95%) were dispersed in 0.5 ml of 0.2 mol/ml 2-(N-Morpholino)ethanesulfonic acid (pH 5.6) (MES, Acros) buffer under sonication for 1 hour at room temperature. 0.25 ml of 0.8 mol/ml 1-(3-Dimethylaminopropyl)-3-ethylcarbodiimide hydrochloride (EDC, Acros) and 0.25 ml of 0.4 mol/ml N-Hydroxysuccinimide (NHS) (Acros) in MES solution were added to activate carboxyl groups [170, 171]. The mixture was washed with PBS and centrifuged in a MW 100 KDa cutoff centrifugal filter (Millipore) (4 ml) to remove EDC and NHS at 5000 g three times for 30 minutes each. Refill 4ml of PBS in centrifugal filter tube each time. Then, 5 µg of a model protein was added at 4 ^{o}C and incubated overnight. Finally, the mixture was washed and centrifuged in a filter to remove un-conjugated protein at 5000 g six times for 30 minutes each [171]. Refill 4 ml of PBS and sonicated for 10 mins to resuspend mixture before each following centrifuge. The final CNT-protein in PBS

solution (resuspend in 1 ml PBS) was collected and stored at -20 ^{o}C until use. These studies used Matrigel (Invitrogen), bovine serum albumin (BSA) (Sigma) and fluorescent BSA (fBSA) (Sigma) as model proteins for characterization of adhesion to CNTs. Fibronectin (Sigma) and Matrigel were used to provide cell attachment for human umbilical vein endothelial cells (HUVECs) and human embryonic stem cells (hESCs), respectively. The prepared CNT-ligand conjugations were stored in -20 ^{o}C until use.

In order to obtain the aligned CNT pattern on the surface, substrates were rinsed in CNT-ligand solution for 12 hours. Then CNT-ligand conjugates were aligned on the Au coated substrate through spin coating (Chemat Technology). The solution was spun at 800 rpm for 10 seconds and 5000 rpm for 1 minute. After incubation in ambient conditions in a petri dish sealed with parafilm for 30 minutes, aligned CNT substrates were gently washed with PBS and ethanol twice to remove any unseated CNT-ligand and remaining particles. Poly(ethylene) glycol (PEG) thiol (Sigma) is placed in ethanol solution (1 µl/ml) and coated onto the CNT-ligand substrate for 10 minutes to passivize rest of Au coated area and prevent non-specific cell attachment.

2.2.2. Substrate characterization

For transmission electron microscope (TEM) characterization, several droplets of homogenized carboxyl CNTs and Geltrex conjugated CNTs solution were coated onto 200 mesh copper grids and dried at room temperature for 10 minutes. TEM images of carboxyl CNTs and Geltrex conjugated CNTs were visualized by a Hitachi H-8000 TEM system.

For scanning electron microscope (SEM) characterization, prepared substrates with carboxyl CNTs were imaged with a Zeiss Ultra Plus SEM system. We use carboxyl CNTs instead of CNT-ligand conjugates due to the consideration of conductivity.

Immunofluorescent images were captured with fBSA conjugated CNTs on substrates and imaged by a Nikon Eclipse 80i microscope.

UV-Vis Spectrum characterization was done with 5 μg/mL BSA solution and 5 μg/mL carboxyl CNT homogenized solution prepared by sonication (30 mins). 5 μg/mL BSA conjugated CNT solution was prepared with 1 hour incubation of 5 μg/mL BSA and 5 μg/mL carboxyl CNTs at 37^{o}C followed by 1 hour incubation at room temperature. The unconjugated BSA was then removed with a 100K molecular weight cutoff centrifugal filter (Millipore) at 5000 g for 30 min for 6 times. The UV-vis spectrum was recorded using a Beckman Coulter DU 730 UV-Vis spectrometer with a step of 1 nm.

2.2.3. Cell Culture

Human umbilical vein endothelial cells (HUVECs) (Lonza) at passages 8-12 were used for this study. Cells were seeded on CNT aligned substrates at a density of 5,000 cells/cm^2 in Ham's F12K medium (Invitrogen) supplemented with 2 mmol/L glutamine (Invitrogen), 1.5 g/L sodium bicarbonate (Sigma), 0.1 mg/mL heparin (Fisher), 0.03-0.05 mg/mL endothelial cell growth supplement (BD Biosciences), 10% FBS (Invitrogen) and 1% penicillin-streptomycin (Invitrogen). Medium were changed every 3 days, HUVECs were passaged every 7 days.

hESC line H9 was purchased from WiCell with cell lines grown on a mouse embryonic fibroblast (MEF) (CF-1, Millipore) feeder layer in DMEM/F12 (Invitrogen)

with 20% KnockOut Serum (Invitrogen), 0.1 mM MEM Non-Essential Amino Acids (Invitrogen), 3.5 mM L-Glutamine final concentration (Invitrogen), 100 µm 2-Mercaptoethanol (Sigma) and supplemented with 10 ng/ml human recombinant bFGF (PeproTech) as shown in WiCell protocols. Medium was changed daily and cells were passaged on every fifth day of culture with collagenase type IV (Invitrogen).

MEF were grown in DMEM (Invitrogen) with 10% FBS (Invitrogen) and 100U/100µg/ml of penicillin/streptomycin (Invitrogen). Medium were changed every 3 days. MEF cells were passaged every 7 days. The passages 6 of MEF were used as feeder layer.

hPSC monolayer culture with single cell passaging was established as described [172]. Briefly, hPSC were switched from feeder-dependent culture to feeder-free conditions with 20 gauge sterile steel tips. hPSCs were grown as colonies for 2-3 passages on growth factor reduced Geltrex (Invitrogen) coated 6-well plates (BD Biosciences) in MEF conditioned medium supplemented with 10 ng/ml bFGF. Cells were passaged mechanically on day five.

Conditioned medium was prepared as described, mitotically inactivated MEF through Mitomycin C (Sigma) treatment at 10 µg/ml for 2.5 hours were plated on gelatinized flasks (Sigma) at a density of 60,000cells/cm^2, the following day cells were washed with PBS (Sigma), medium was changed to hESC medium without bFGF addition at 0.5ml/cm^2 and collected every 24 hours for 7 days.

Before cell culture the conditioned medium was filtered and supplemented with 10 ng/ml bFGF. On the following passage, hPSC colonies were treated with TrypLE Select (Invitrogen) for 1 minute, gently dissociated to single cells and plated to new wells

at approximately 80-100,000 cells/cm^2. Cells were grown under the same culture conditions and single cell passaged upon reaching confluence. After stabilization of the cell culture cells were routinely passaged as single cells on each fourth day with a seeding density of 50,000 cells/cm^2.

2.2.4. Immunochemistry

HUVEC and hPSC single cells were allowed 2-4 hours for attachment to CNTs and fixed with formalin (Sigma) for 15 mins at room temperature, permeabilized in 0.1% Triton X-100 (Sigma) at 4 ^{o}C for 10 mins, and blocked in 4% goat serum solution at room temperature for 30 minutes. HUVECs were stained primarily for PECAM-1 at a 1:500 dilution ratio (Cell Signaling) for 60 mins. PSC single cells were stained primarily for Oct4 at a 1:500 dilution (Santa Cruz Technology) or vinculin at a 1:100 dilution (Sigma) for 60 mins. Secondary antibodies were purchased from Invitrogen and used at a 1:100 dilution for 60 mins. Rhodamine phalloidin at a 1:100 dilution (Invitrogen) was used to visualize cytoskeleton structure of HUVECs and hESCs (20 mins incubation). DAPI (Sigma) was used to visualize nuclei (1:40).

2.3. Results and Discussion

2.3.1. Preparation and Characterization of Aligned CNT Substrate

As shown in Figure 2. 1, Au coated coverslips were rinsed in a homogenized CNT-ligand solution. CNT-ligand conjugates would be able to stick to Au coating due to electrostatic interactions. Then, centrifugal force was applied by spin coating. The CNT-ligand conjugates would adopt the centrifugal force and would be organized into an

aligned fashion over the substrate. The concentration of conjugates, rinse time, and spin coating procedure were adjusted to achieve an ideal performance of CNT-ligand conjugates on the surface for cell attachment. To prevent non-specific binding of cells to the non CNT-ligand area, the area with no CNT-ligand conjugates was passivized in PEG-SH solution at determined concentration. At last, cells were able to attach to CNT-ligand particles only.

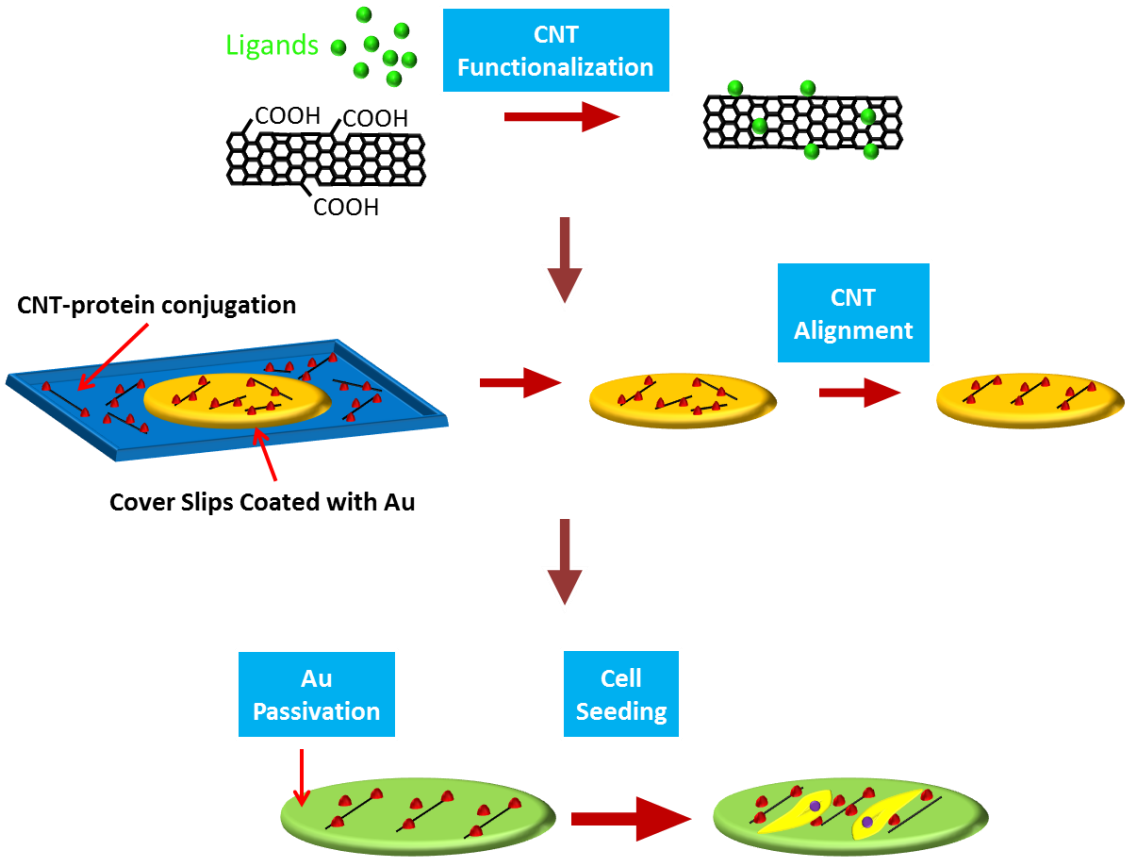

Figure 2. 1 Schematic diagram showing experimental procedure for CNT substrate. In brief, carboxyl CNTs were functionalized with protein ligand and CNT-ligand conjugates were aligned on Au surface by spin coating. Then Au surfaces without CNTs were rendered non-adhesive by thiolated polyethylene glycol (PEG-SH) and cells were cultured on the substrates.

Multiwall carboxyl CNTs were commercially purchased from Nanolab and characterized through TEM. As shown in Figure 2. 2A, the length of the carboxyl CNTs

used in this study is approximately 5 μm with the diameter shown in Figure 2. 2B of approximately 20 nm. These specifications were larger than the single wall CNTs, facilitating more ligand conjugate to each single MCNT. Consequently, the density of conjugated protein per CNT will be higher than SCNT. This was a desired property which facilitates cell adhesion and migration [173, 174]. As we mentioned above in Chapter 1, toxicity concerns of CNTs in biomedical engineering would need functionalization of CNTs. Although using CNT as extracellular cues *in vitro* would significantly reduce the toxicity concerns of CNTs, there is still critical hurdle that CNTs need appropriate functionalization to desired application: provide cell attachment sites. There are two major types of functionalization including covalent and non-covalent reactions [52]. To achieve covalent binding, reactive groups [175, 176] are formulated to allow for further attachment of polymer [177], protein [178], and DNA [179]. In contrast, non-covalent binding is based on π-π stacking between CNTs and aromatic groups from the linkers [180]. Both functionalization would provide certain degree of protein attachment. However, there were reports suggesting non-covalent bound biological stuff may not remain stable in serum containing situations [181]. Thus, based on our goal to provide cell attachment sites on CNTs, we functionalized CNTs through covalent reactions that directly link protein ligand to CNTs.

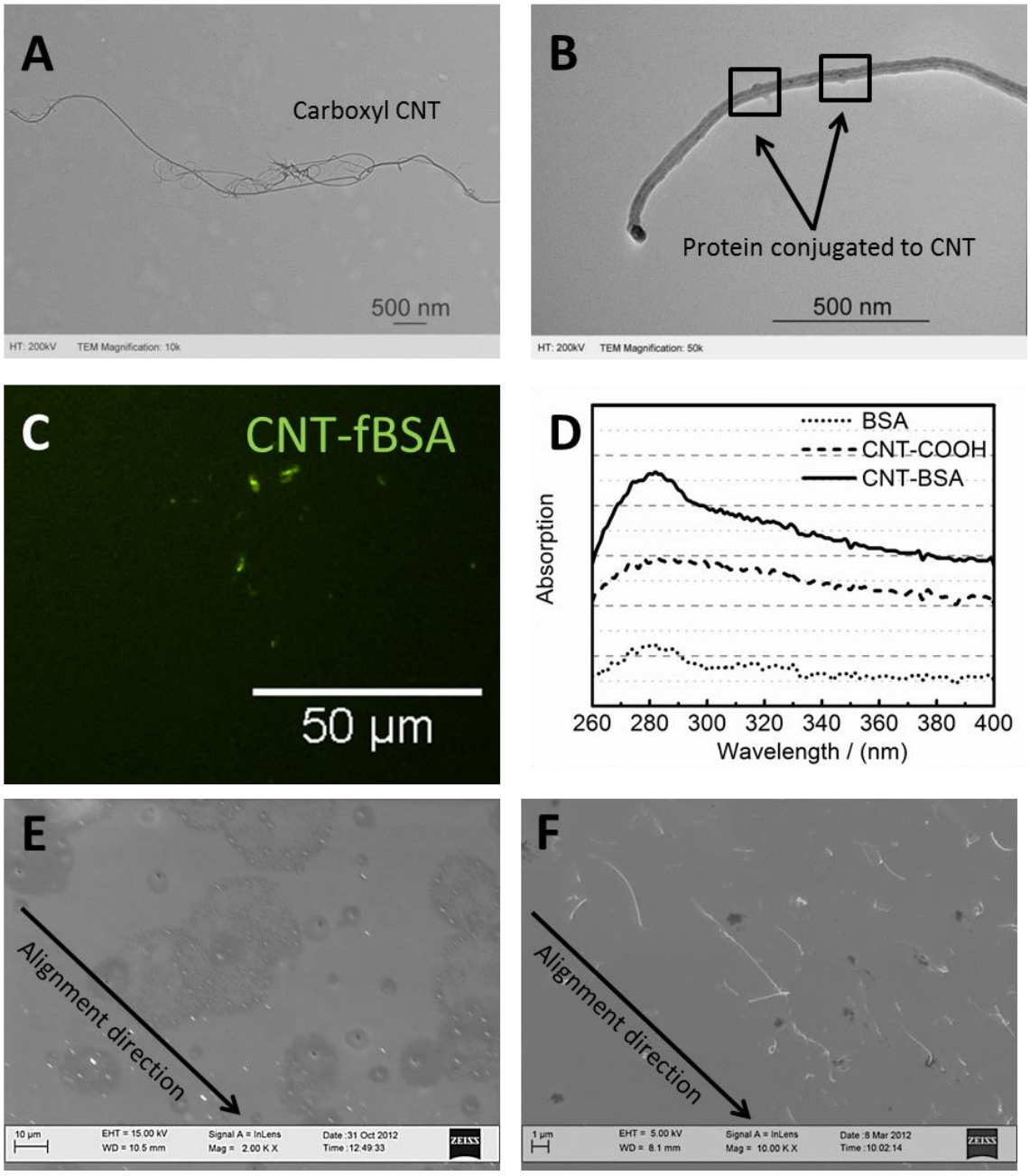

Figure 2. 2 Characterization of CNT-ligand conjugates and aligned CNT substrate. A. TEM of carboxyl CNTs. Carboxyl CNT is about 5 µm in length and 20 nm in diameter. B. TEM image of Geltrex conjugated CNTs. There were several protein particles attached to the CNTs' sidewall as squared. C. Fluorescent image of CNT-fBSA conjugation on Au substrate. Green shows the positive signal of CNT-fBSA on substrate. D. UV-vis spectrum of CNT, BSA and CNT-BSA conjugates. CNT-protein conjugates and its dispersion confirmed on Au surfaces which allow cell attachment for HUVEC and hESCs. E. Low-magnification SEM image of aligned CNT substrate. F. High-magnification SEM image of aligned CNT substrate. Cleary we've seen CNTs were in an aligned fashion.

We were able to show highly specific protein conjugation to CNTs for cell attachment as shown in Figure 2. 2B. This high magnification TEM image showed Geltrex protein conjugated to CNTs with protrusions from the sidewall of these CNTs to the space. The sizes of these protrusions were found to be approximately 2 nm, which correlated with the calculated size of the proteins comprised in Geltrex according to the equation $r = (\frac{3MW}{4\pi\rho N_A})^{\frac{1}{3}}$ [182]. Where MW is the molecular weight of the protein, N_A is Avogadro constant. ρ is the density of the solution. Note, the molecular weight for common extracellular matrix is under 10-100 KDa range, resulted the diameter around 2 nm. fBSA was used as another sample protein for demonstration as shown in Figure 2. 2C through microscopy. CNT-fBSA were shown positively signals on the 2D substrate. We saw green fluorescence emitted from rod like CNTs, which is generated from fBSA excited by 488 nm laser. This confirms protein conjugation to CNTs on substrate, demonstrating the ability of CNT-ligand to provide cell attachment site on substrate. UV-Vis absorption was also used to test the conjugation spectrometrically. As shown in Figure 2. 2D, CNT-BSA conjugates exhibited an enhanced absorption at 280 nm, which was the typical absorption of a protein. This type of UV absorption was similar to other studies of analyzing proteins [183]. With all these in mind, we confirmed the ability of a fibronectin or Geltrex protein could be conjugated to CNTs covalently. Therefore, the CNT-ligand conjugates would provide enough attachment sites for cell adhesion.

Recent studies have also shown that aligned topographies were highly effective in directing cell differentiation and adopting specific cell behavior [154, 184-189]. Besides dip pen nanolithography [190], UV lithography [191] and electro-spin nanofibers [191, 192], we were able to align CNT-ligand conjugates on Au coated coverslip. As observed

in low-magnification SEM images (Figure 2. 2E), the rod shaped tubes representing carboxyl CNTs were well aligned in the direction of centrifugal force. In the high magnification SEM image of Figure 2. 2F, carboxyl CNTs with different lengths were clearly shown in an aligned fashion throughout the substrate. Our results correlated well with previously report, which aligned single wall CNTs on a poly-*l*-lysine substrate by spin coating [193, 194]. Through the parameters listed in this paper, we have successfully developed a highly aligned multiwall carboxyl CNT substrate for its utility in cell culture systems.

2.3.2. Adhesion of HUVEC and hESC single cell on Aligned CNT Substrate

Cellular adhesion to the matrix is a key contributor to many cell functions including proliferation and apoptosis. Significant interest has been directed into how factors such as the topographical and mechanical cues presented in cell adhesion affect cellular behavior. These microenvironments have been shown to control cell spreading, migration, and differentiation among other characteristics. A combination of matrix factors such as topography, mechanics, and ligand density have all been implicated in the direction of cell behavior and fate [155, 174, 195]. However, these factors and interplay between factors remain poorly understood and have been identified as a crucial portion to cellular function.

These microenvironment also play a crucial role in cell shape, which in turn also can affect cell behavior [148-150]. Stem cells are particularly interesting to observe cell shape because of the capability of differentiating into the many cell types in the body and contain significant potential for use in regenerative medicine and tissue engineering [159,

196, 197]. It is understood that mechanical and topographical cues from the hESC's immediate environment can affect its cell shape and therefore differentiation lineage in addition to the more studied soluble factors [66, 147, 196]. Nano-engineered topographies are of current interest because they are able to avoid the use of biochemical factors, which are both expensive and difficult to control in terms of concentration [159]. Cellular alignment is crucial for the function of certain tissues in the human body, for instance, the mechanical strength of bone structures depends heavily on the cytoskeletal alignment of osteoblasts and their surrounding collagen matrix [151]. hESC differentiation can be induced by physically aligning the cells in a uniaxial manner. hESCs have also been shown capable of differentiation along osteogenic and neurogenic lineages when cultured on nanoengineered substrates [159, 197].

Cellular alignment is highly important in bodily tissues, especially endothelial cells. The effects of shear stress and nanotopography on human umbilical vein endothelial cell (HUVEC) alignment have been studied extensively. HUVECs exposed to 1.5 Pa shear stress demonstrated actin filament alignment after 16 hours of exposure28. Combined effects of micropatterned surfaces and fluid shear stress on the alignment of human endothelial cells were studied by Vartanian et al [198]. Nano-fibrous structures have also been considered as an alignment tool. Human corneal endothelial cells are another cell type that is able to align along the length of Type-I collagen fibrils mediated by integrins $\alpha 2$ and $\beta 1$ [199]. CNTs are another highly sought after option for alignment of cells such as aligning cells for growth and differentiation [200].

Focal adhesions formation is a key component to which cells are able to adhere to flat substrates. As cells bind to ECM ligands integrins are clustered and focal adhesions

are able to form while the cell undergoes spreading. Ryoo et al. has statistically confirmed that CNTs were able to increase the number of focal adhesions per cell of NIH3T3 cells as well as the expression of vinculin [167]. Zhang et al. also observed dash like and dot like focal adhesion structures on CNT substrates [168]. Cells sense micro-environmental signals through focal adhesion, controlling cell shape and function by integrating physical cues [149]. These findings inspire us to tune focal adhesion sites by regulating CNTs patterns. With these principles and properties of CNTs in mind, this work establishes a platform which contains aligned CNTs to provide attachment sites to which cells can decipher and bind. Cells will then be able to adhere migrate in an aligned fashion on these CNT patterns. The uniqueness of this paper lies in the ability of these patterns to be used in a wide variety of cellular, particularly hESC, applications to promote attachment, migration, and differentiation of cells through the tunability of these CNTs.

Endothelial cells are highly sensitive to shear stress with the ability to be easily oriented [201] as well as the ability to control orientation and migration of endothelial cells by distinct fluid flows [202, 203]. Independent to fluid flow, reports show the use of localized α4 integrin phosphorylation to align endothelial cells [204], while others have discovered laminin gradients affect endothelial alignment to a high degree as well [205]. Collagen based nanofibers [206] and topographic cues [207] have also induced migration and orientation of endothelial cells without the use of fluid flow which have lead us to use aligned CNTs to orient endothelial cells for a variety of applications. With the CNT fabricated substrates shown here, our results coincide with previous studies in showing

alignment and migration and to this end, we believe this CNT based substrate can be used to tune cell growth and migration in a controlled manner.

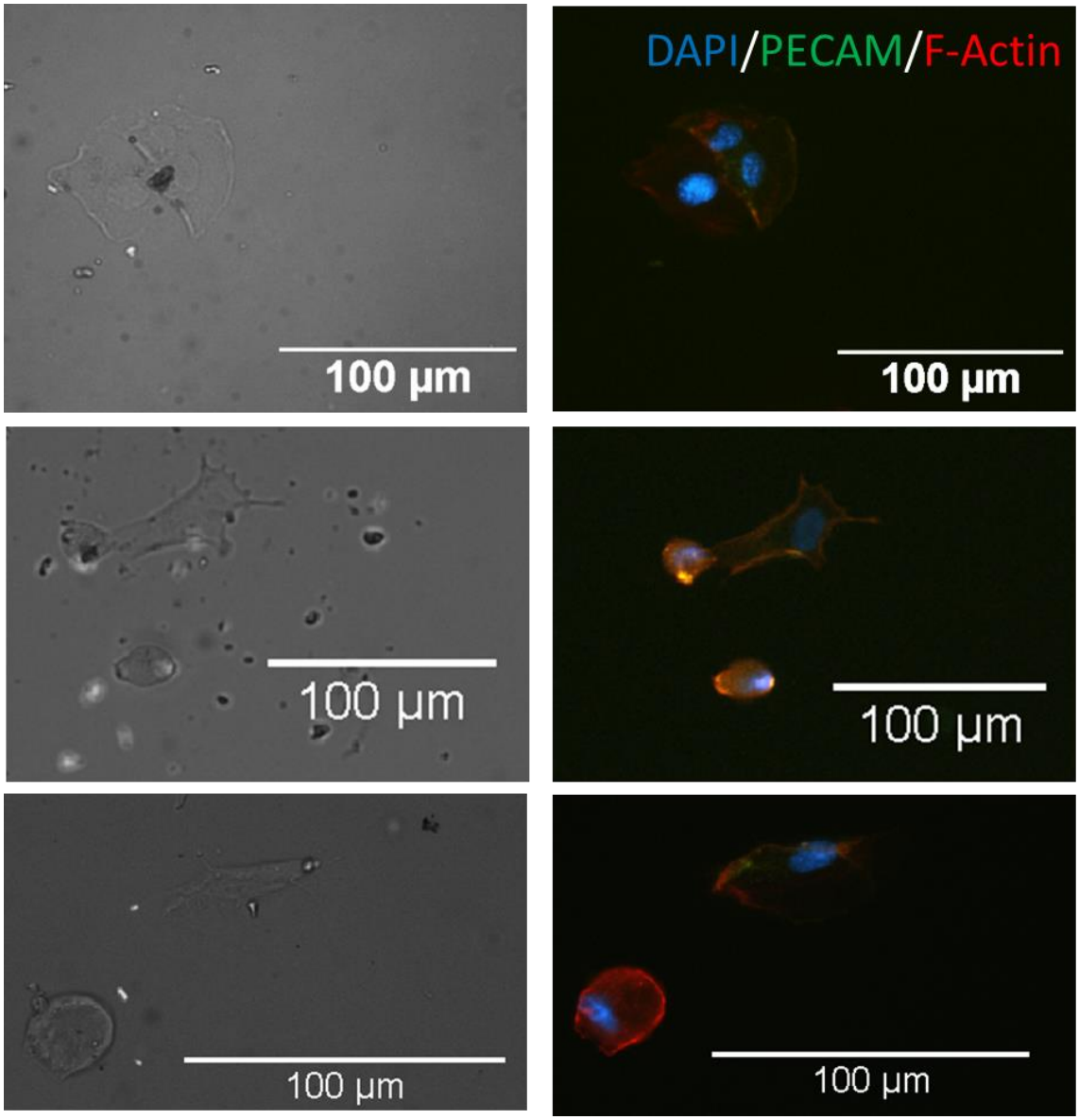

Figure 2. 3 Immunofluorescent images of HUVECs on CNT substrates. DAPI (blue), PECAM (green), F-actin (red) are shown. HUVECs are randomly distributed on CNT randomly assembled substrate, either confined by CNTs or spread over CNTs.

Cell adhesion of HUVEC was performed on both randomly assembled CNT substrate (Figure 2. 3) and aligned CNT substrate (Figure 2. 4). HUVEC were not in an aligned fashion on randomly assembled CNT substrate. HUVEC organized cytoskeleton in random orientations and was confined in a small adhesive area. PECAM-1 staining

showed a significant lack of cell-cell contact junction indicating cells have limited mobility on randomly assembly CNT substrate [208]. Consequently, HUVEC cells were able to sense and recognize CNT-ligand conjugates on substrates ash showed in Figure 2. 3.

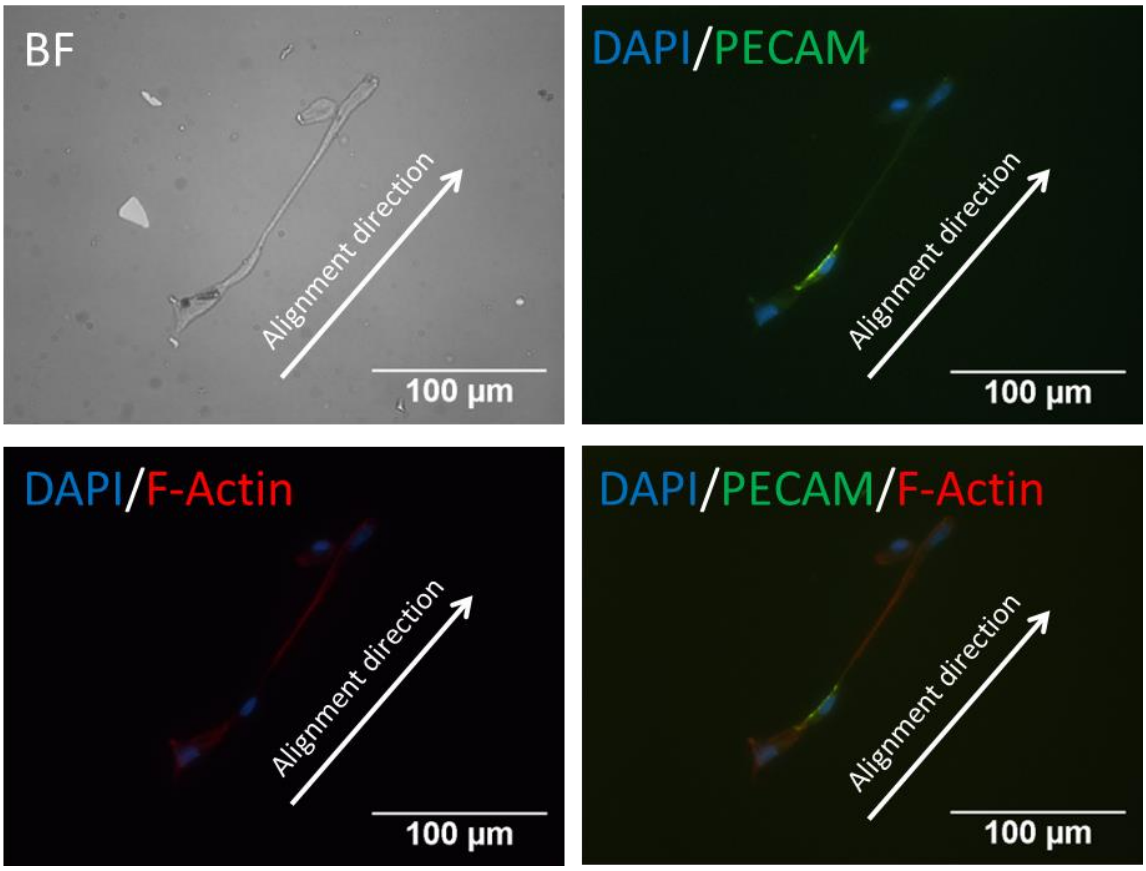

Figure 2. 4 Immunofluorescent images of HUVECs on substrates. DAPI (blue), PECAM (green), F-actin (red) are stained. HUVECs are able to bind to aligned CNT-ligand conjugates and show a spread, aligned phenotype along CNTs aligning direction.

In contrast, HUVEC behaves an aligned fashion on aligned CNT substrate. As shown in Figure 2. 4, immunofluorescent images of HUVECs on aligned CNT substrate showed that HUVEC cells adapt to the CNT alignment. PECAM-1 staining showed HUVEC cells had distinct cell-cell contact junctions along with aligned CNT direction. Cytoskeletal organization was highly stressed towards aligned CNT direction as well.

Note that HUVEC cells were able to migrate and orientated on collagen based nanofibres [206] and aligned topography [207], our aligned CNT substrate could provide potential capability of controlling vascularization and directing stem cell differentiation to those cells which have specific alignment characteristics, e.g. cardiomyocytes and neurons.

Traditionally maintaining hESC cultures *in vitro* requires MEF feeder layers and manual passaging of individual colonies. This method does not lend themselves to large scale production of pluripotent cells for high throughput experiments. Enzymatic dissociation of pluripotent stem cells has recently been reported as a method to higher scale passaging of pluripotent cells for future clinical possibilities [209-211]. However, problems occurred with enzymatic passaging of hESCs. It is hard to maintain hESCs within certain size [210, 212, 213]. There is also the possibility of genetic and epigenetic changes in hESCs [214-216]. Overcoming these obstacles is harnessing hESC research to decipher single cell level interactions. With a homogenous population of hESC single cells, it will be feasible to study cell-substrate interactions in greater depth than previously. Thus, we are trying to use CNT substrate to bring us closer to decipher hESC-substrate interactions within highly tunable CNT substrate.

Fluorescent images of single hESC were showed in Figure 2. 5. hESC adhesion experiments were also demonstrated the utility of aligned CNT substrate to be related to stem cells research. We studied cell adhesion of H9 cell at single cell culture level to demonstrate the ability to selectively bind to a CNT-ligand conjugates and retain initial pluripotency. This was preferential over colonies due to the ability to expand hESCs as a homogeneous population in contrast to cells grown in colonies [217, 218].

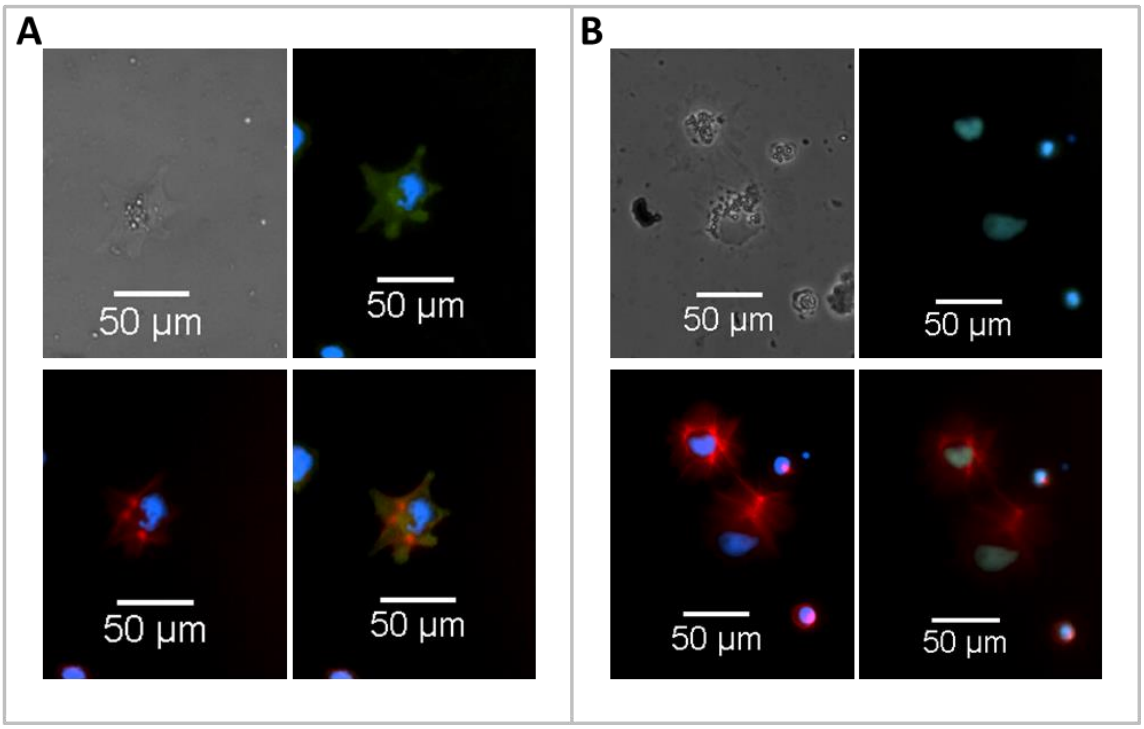

Figure 2. 5 Fluorescent images of single hESC on CNT substrate. A. Top left showing bright field image of single H9 cell line, top right showing vinculin in green and DAPI in blue, bottom left showing actin in red and DAPI in blue, bottom right showing merged image. This demonstrates H9 cells are able to bind to CNT substrate with normal focal adhesion structure and spreading tendencies. B. Top left showing bright field image of single H9 cell line, top right showing Oct4 in green and DAPI in blue, bottom left showing actin in red and DAPI in blue, bottom right showing merged image. H9 cells are able to attach and spread on CNT substrate while retaining initial pluripotency.

Single cells were able to bind to CNT substrate with a small percentage of cells being able to fully spread. To test whether CNT substrate affect initial hESC properties such as pluripotency, cytoskeletal formation, or spreading tendencies of single ESCs, markers for Oct4 and F-actin were labeled with antibodies. As shown in Figure 2. 5, cells retained pluripotency by expressing markers of Oct4 and flattened cell morphology. As shown with phase contrast in Figure 2. 5, these cells exhibited a more irregular outline showing more prominent filapodia extensions to surrounding CNT-ligand conjugates. Focal adhesions were shown to be normal and intact indicating a normal cell phenotype

on the CNTs as shown in Figure 2. 5A. This shows the function of the CNT substrate and the ability to parse the substrate-hESC interaction in future studies.

2.4. Conclusion

In summary, we have fabricated a substrate patterned with aligned CNT-ligand conjugates to be used in a variety of potential applications. We test the utility of HUVEC cells and hESC single cells to recognize, attach and bind to CNT-ligand conjugates with normal phenotype and function. We found that (A) CNT substrate was able to provide focal adhesion binding sites for cell adhesion. (B) Through aligning CNT-ligand conjugates, we are able to align cells in unique direction. (C) This study provides foundation in specific lineage directing of hESC single cells.

We have provided a new approach to tune hESC culture at single cell level. This would allow us to culture and induce cell differentiation of single hESCs for a better understanding differentiation of hESC at single cell level.

CHAPTER 3

Carbon Nanotube-Poly(lactide-co-glycolide) Composite Scaffolds for Bone Tissue Engineering Applications

3.1. Introduction

Bone has the inherent ability to repair small fractures; however, larger bone defects resulting from trauma, tumor resection or muscuoloskeletal diseases heal over a long period of time. Orthopaedic surgeons currently employ two approaches to treat bone defects: (i) autografts, in which the patient's own healthy bone tissue is used, and (ii) allogenic grafts, in which bone tissue is obtained from another donor. Autografts are presently considered to be the best treatment option for their osteoconductivity, osteinductivity and osteogenecity [219, 220]. However, the use of autografts is restricted by the shortage of supply and need for a secondary surgery. The use of allografts also faces major hurdles including the risk of immune response and disease transmission.[221-224] In addition, long-term storage of allografts renders the bone structurally weak and destroys most of the osteoprogenitor cells. In recent years, tissue engineering (Figure 3. 1) has been evolving as an alternative strategy to develop bone grafts. This approach relies on the use of combinations of specific cell types, growth factors and three dimensional (3D) porous scaffolds [225-227].

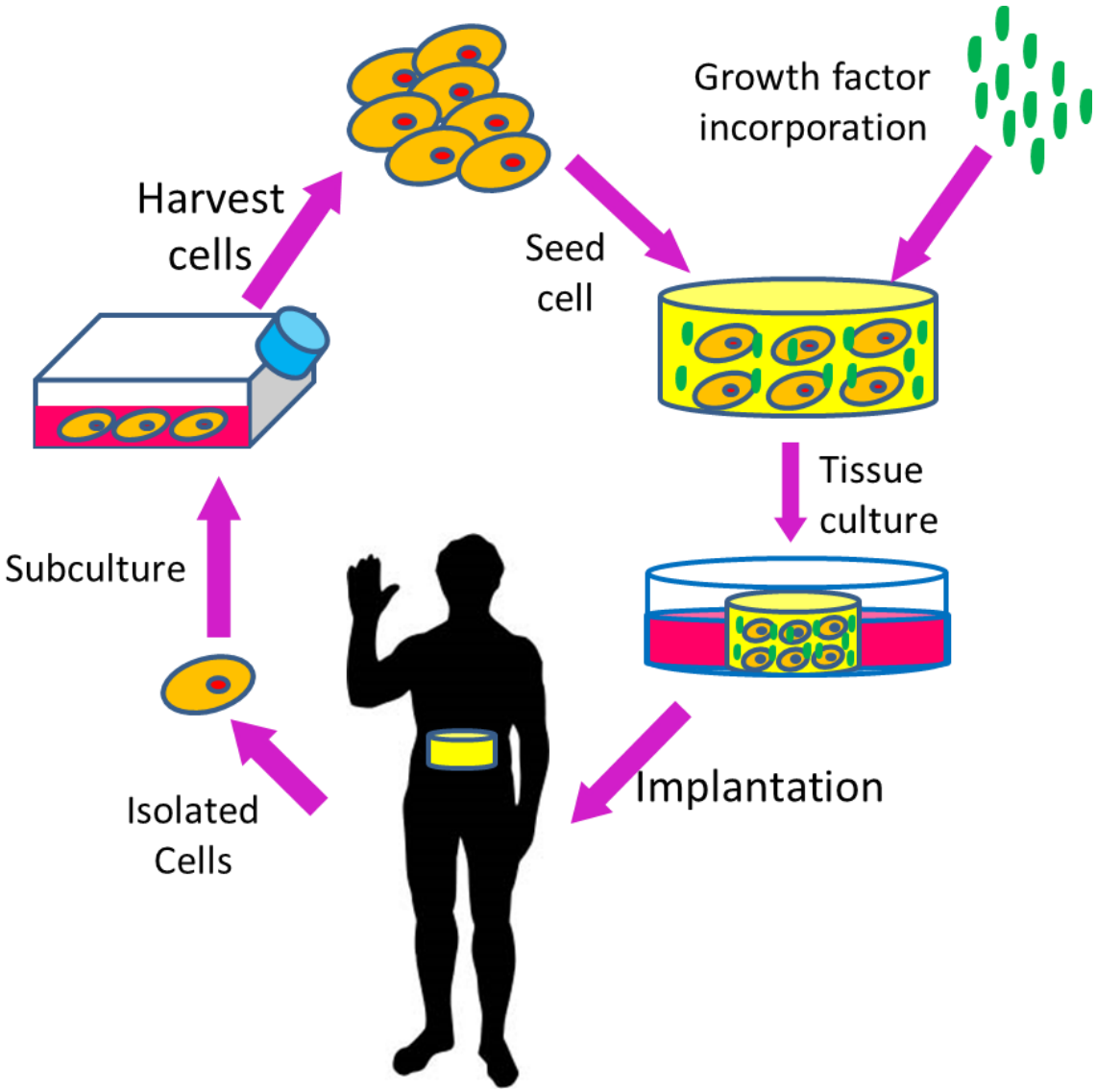

Figure 3. 1 Schematic of tissue engineering. In brief, cells are isolated to expand in *in vitro* culture. Next, scaffold with growth factor are recruited to regenerated tissue *in vitro*. Then, the regenerated tissue is transplanted into human body to replace the failure tissue. Finally with the successful implantation of regenerative tissue, the tissue failure could be cured.

A main focus in musculoskeletal tissue engineering is the design of 3D scaffolds, which guide the intricate dynamic cell signaling processes that governing the migration of host cells, differentiation of transplanted cells and formation of bone extracellular matrix (ECM) [228]. In this context, significant effort has gone to fine tune the nano-

scale structure and chemistry as well as the mechanical properties of scaffolds in order to recapitulate the *in vivo* natural bone development.

One important obstacle in construction of engineered tissues is the proper perfusion of nutrients and oxygen through scaffolds. To overcome this limitation, highly porous scaffolds, through which nutrients can diffuse, are often preferred. However, higher porosity may compromise the mechanical properties of scaffolds. Towards optimizing scaffold properties, there is a need to establish the correlation between structural parameters (*eg*. pore size and porosity) and mechanical parameters (*eg*. compressive modulus and strength). Bone exhibits strong mechanical properties as it provides structure stability for the body and it allows for millions of loading cycles throughout a person's lifetime. The compressive modulus of an adult trabecular bone is over 150 MPa; thus, high modulus materials are suitable for bone tissue engineering applications. Polymers such as poly(lactic acid) (PLA), poly(glycolic acid) (PGA), their copolymers poly(lactic acid-glycolic acid) (PLGA) as well as ceramics such as HA have been used to develop 3D scaffolds using various fabrication methods [229-238]. Because of their biocompatibility, osteoconductivity, and appropriate range of mechanical properties, these materials have received substantial attention for skeletal repair and regeneration.

Surface roughness is another important property that allows for osseointegration of scaffolds [72-74]. In general, cells can sense surface topography and adjust their shape and cytoskeletal organization accordingly [77, 78]. In the context of bone tissue engineering, reports have demonstrated osteoblasts to preferentially adhere to substrates with nano-grooves, as compared to substrates with a smooth surface [239, 240]. As an

example, Khang et al. showed that the nano and submicron structured Ti surface upregulates the expression of osteogenic differentiation markers. Interestingly, peaks of 2-4 nm in height induced reorganization of cell cytoskeleton, increased cell spreading and subsequently enhanced osteogenic differentiation [241]. These studies, all together, demonstrate the importance of tuning scaffold surface roughness for desired tissue engineering applications.

We developed an approach to incorporate CNTs into a PLGA scaffold. We hypothesized that CNTs will increase the mechanical strength of scaffolds and allow for tuning the surface roughness, which in turn increases the osteogenic differentiation and bone mineralization. This hypothesis is based on previously published reports demonstrating the potential of CNTs to (i) reinforce mechanical strength of composites[8], (ii) accelerate the proliferation of cells, and (iii) create nano-scale rough substrates leading to improved cell function [34, 101, 242]. To this end, we examined the effects of homogenously dispersed CNT density on the structural and mechanical properties of composite CNT/PLGA scaffolds. This was followed by an *in vitro* evaluation of MC3T3-E1 osteoblast-like cell proliferation, cytoskeletal organization and bone mineral deposition on composite CNT/PLGA scaffolds. The innovative aspects of this project include: (i) the development of a scalable method based on the use of CNTs to fine tune the nano-roughness of 3D scaffolds, (ii) the establishment of a fundamental relationship between the CNTs concentration, homogenous/heterogeneous dispersion, degree of aggregation, and mechanical strength in a PLGA polymeric composite system, and (iii) introduction of CNT/PLGA composite scaffolds as an osteogenic matrix for bone repair.

We have demonstrated the ability of CNT containing PLGA scaffolds for bone regeneration in this chapter. To the best of our knowledge, previous study has showed that for CNT addition increases either stiffness or surface roughness, which in turn increases osterogeneis. The great innovative aspect in Chapter 3 lies in that by developing a 3D CNT content scaffolds, we were able to coupling the surface roughness and mechanical strength together to enhanced osteogenesis. As we confirmed, the increase of nano roughness and mechanical strength together help improve osteogensis.

3.2. Materials and methods

3.2.1. Synthesis of carbon nanotubes embedded PLGA scaffolds

The fabrication process was showed Figure 3. 2. CNTs were obtained from Nanolab which were 1-5 μm in length and 20 nm in diameter with a purity larger than 95%. CNT/PLGA scaffolds were fabricated using a solvent casting/particulate leaching method. Briefly, 30 mg of PLGA (Lectone, 85:15) was dissolved in 300 μl of CNT/dichloromethane solution. A sonication process was used to uniformly disperse CNTs in dichloromethane in three concentrations of 1 mg/ml, 3 mg/ml and 5 mg/ml before adding PLGA. The mixture of PLGA in CNT/dichloromethane was gently vortexed for 60 mins and sonicated for 30 mins, allowing for the PLGA to fully dissolve homogenized. Next, the mixture was added into a Teflon mold wells (5.5 mm in diameter and 2 mm in depth) with 60 mg of NaCl (Sigma) in diameters ranging from 104 to 214 μm. Following the evaporation of dichloromethane for 12 hours, the CNT/PLGA scaffolds were extracted from the wells of the model, stirred in DI water for 2 days and

dried at 37 ^{0}C in a vacuum oven. The scaffolds were stored in sterile tubes sealed with parafilm until cellular analysis.

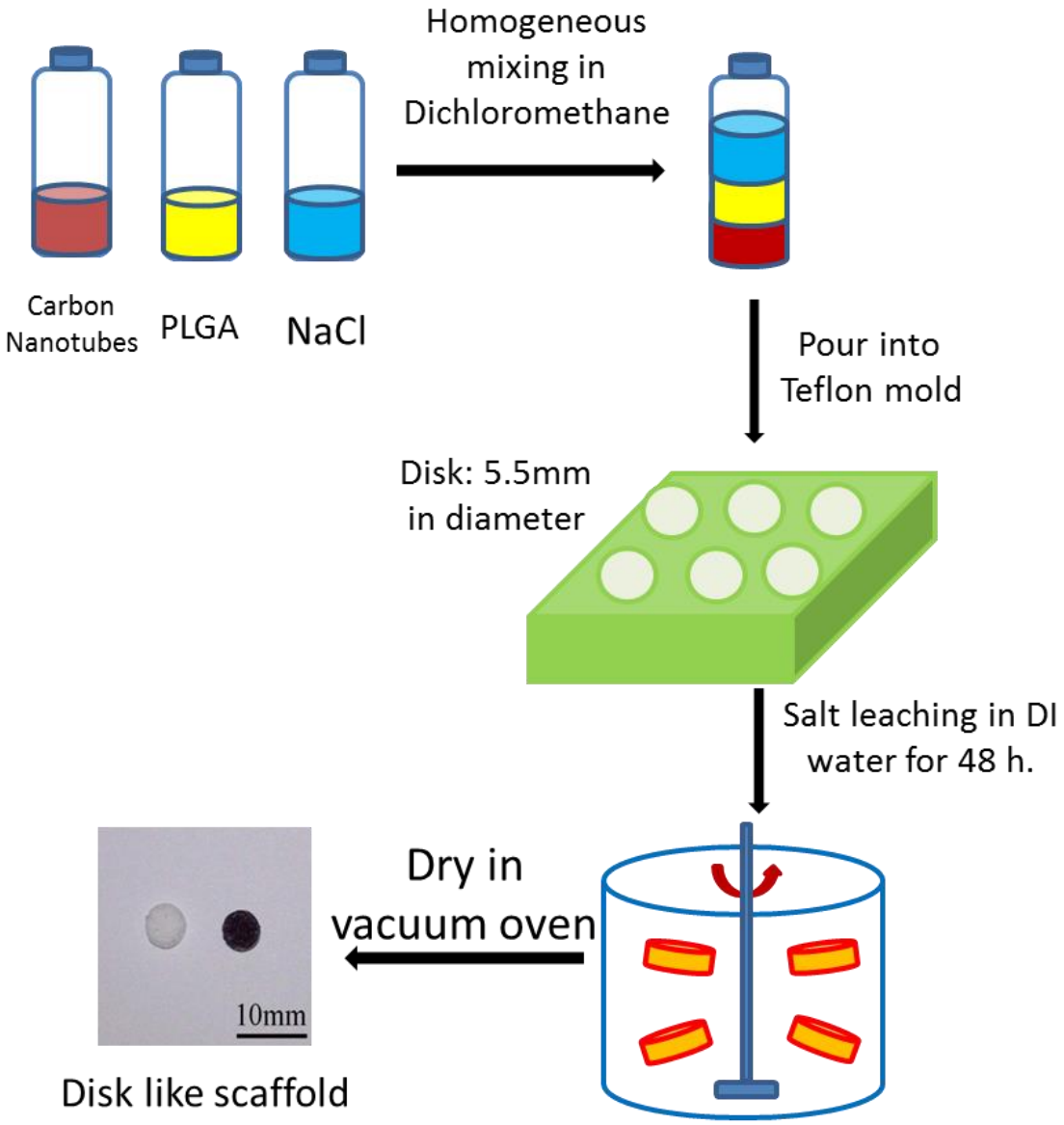

Figure 3. 2 Schematic of salt leaching method. In general, a mixture of porogen and scaffolding materials in certain solvent was homogenized dispersed and place in a model. Next, a scaffold without pores were formed in a desired shape by evaporation of that certain solvent. Lastly, porogen was extract by another solvent which will not dissolve scaffolding materials and left the space for the interconnected porous structure.

3.2.2. Structural, surface roughness and mechanical characterizations of scaffold

The morphology and pore structure of CNT/PLGA scaffolds were evaluated using scanning electron microscopy (SEM). In brief, scaffolds were attached to sample stubs and sputter coated with gold. In general, vacuum at 100 Torr has been applied with Ar air blowing into the vacuum chamber. Au was coated for 30 seconds for the purpose of conductive. The samples were viewed under SEM at an accelerating voltage of 10kV.

Atomic force microscopy (AFM) in combination with light microscopy was used to measure the surface roughness of and the degree of CNT aggregation in PLGA films containing CNTs at various concentrations. Briefly, PLGA was dissolved in a CNT/dichloromethane solution to give the total CNT concentrations of 1%, 3% and 5%. CNT/PLGA solution (100 μl) was dipped onto a 1 cm × 1 cm cover slip drop wisely. This was followed by a 24 h drying at room temperature in a sealed desiccator. AFM measurements on multiple locations of CNT/PLGA films were obtained using a NanoScope IIIA MultiMode AFM (Veeco) with contact mode. A scan field of 10 μm × 10 μm with a scanning rate of 1 Hz was used for these measurements. The data was analyzed using NanoScope imaging software.

The mechanical strength of three groups of CNT/PLGA scaffolds (5 mm in diameter and 2 mm in height) with various CNT densities (1%, 3%, 5%) were compared and controls were carried out using PLGA scaffolds. Compressive modulus testing was conducted using a mechanical testing machine (ElectroForce 3200) at room temperature in unconfined compression at 0.05 mm/sec between parallel nonporous plates while compressive force and displacement were recorded. Based on the monitored strain (σ) and stress (ε), the compressive modulus (E) was determined using the equation: $E=\sigma/\varepsilon$.

3.2.3. Cell seeding

In order to sterilize, scaffolds were immersed in 70% ethanol for 10 min, rinsed three times with sterile phosphate-buffered saline (PBS) and exposed to UV light for half an hour on each side. Next, scaffolds were transferred into 24-well culture plates and seeded with 20,000 MC3T3-E1 (ATCC) osteoblast-like cells per scaffold. Cells were cultured in α-MEM (Gibco) supplemented with 3 mmol/l glycerophosphate disodium (Sigma), 10 μg/l ascorbic acid (Sigma), 1% penicillin-streptomycin (Invitrogen) and 10% fetal bovine serum (FBS) (Invitrogen). Samples were maintained in a humidified incubator at 37°C with 5% CO_2.

3.2.4. Cell attachment, growth, and morphology

At predetermined time points, cell morphology was evaluated using SEM. Cells on scaffolds containing various CNT densities were fixed in 1% and 3% glutaraldehyde (Fisher) for 1 h and 24 h, respectively. The scaffolds were dehydrated sequentially by a series of ethanol concentrations (10%, 30%, 50%, 70%, 90%, 95%, and 100%) for 15 mins each. Scaffolds were then allowed to dry overnight, coated with gold/palladium, and observed under SEM. For Au coating, For a 30 seconds of Au coating, a vacuum at 100 Torr has been applied with Ar air blowing into the vacuum chamber.

Cell proliferation on scaffolds was assessed using 3-(4,5-Dimethylthiazol-2-yl)-2,5-diphenyltetrazolium bromide (MTT) (Alpha Aesar) calorimetric assay. In brief, scaffolds were washed with PBS, transferred into a new 24 well plate containing 1.5 ml of fresh culture medium and 300 μl MTT/PBS solutions and incubated at 37°C for 5 h. This was followed by the removal of medium/MTT solution and addition of 1.5 ml

dimethyl sulfoxide (DMSO) (Fisher) into each well. The resulting solution was diluted in a 2:1 ratio using DMSO and the absorbance was read at 550 nm using a Tecan SpectroFluo Plus reader. The cell number per scaffold was normalized through a calibration curve.

We used F-actin staining to confirm the cytoskeletal formation of cells on CNT/PLGA scaffolds. Briefly, cells on scaffolds were fixed at room temperature in 10% formalin for 30 min. After a 3X wash, cells were permeabilized using a 0.1% Triton X solution for 5 min. Cells were washed 3X with PBS and blocked using a 1% bovine serum albumin (Sigma) (BSA) solution for 1 h. TRITC-conjugated phalloidin (1:40) (Invitrogen) was used to stain the cytoskeletal protein actin for 1 h followed by nuclei staining with 4'-6-diamidino-2-phenylindole (1:30) (DAPI, Invitrogen). Stained cells were visualized using a Nikon Eclipse 80i microscope.

3.2.5. Assessment of osteogenic differentiation

Osteogenic differentiation was assessed by monitoring the expression of alkaline phosphatase (ALP) and deposition of calcium by cells cultured on scaffolds. This was evaluated for CNT/PLGA scaffolds with CNT densities of 1%, 3% and 5% while PLGA scaffolds were considered as a control.

ALP activity of the cells was measured quantitatively using an alkaline phosphatase substrate kit (BioRad). The basic of this method is to convert *p*-nitrophenyl phosphate into *p*-nitrophenyl in the presence of ALP where the rate of *p*-nitrophenyl is proportional to ALP activity. Cells were lysed with 1% Triton X-100 in autoclaved water for 5 min and then the cell lysates were collected and stored at -80^{0}C. Upon thawing, 100

µl of the cell lysate was added to 400 µl of *p*-nitrophenyl phosphate substrate and buffer solution mixture and incubated at 37 ^{0}C for 30 min. This was followed by addition of 500 µl of 0.4 mol/l sodium hydroxide to stop reaction. The production of *p*-nitrophenyl was determined by monitoring the absorbance at 405 nm using a Beckman Coulter DU 730 UV/Vis spectrometer. The ALP activity was normalized by the number of cells on each scaffold.

ALP activity staining of cells on scaffolds was also accomplished using an alkaline phosphatase kit #85 (Sigma). Briefly, samples were fixed in 10% formalin solution for 30 min and washed 3X with PBS. The staining solution was prepared by mixing the content of Fast Blue capsule in napthanol for 30 min. This was followed by 3X wash in PBS and incubation in the Mayer's Hematoxylin solution for 10 min. Stained cells were then photographed using a Nikon Eclipse 80i microscope.

The calcium deposition by cells was quantified using O cresolphthalein complexone (Sigma) method. In brief, at predetermined time points, the media was removed. Following a 3X wash with DI water quickly, samples were homogenized with 0.6 mol/l hydrogen chloride. This was followed by 4 h of shaking at 4 ^{o}C to extract calcium. Next, 37.8 ml of 2-amino, 2-methyl, 1-propanol (AMP) was dissolved in 150 ml DI water and adjusted to pH 10.4 by 6 mol/l HCl in the final volume of 250ml. AMP buffer were stored in dark at room temperature until use. Color reagent was prepared as describe: HCI (36.5%) (15 ml) was added to a 250 ml flask containing about 25ml of DI water. 25 mg 0-cresolphthalein complexone (Sigma) powder was added into the above prepared HCl solution. 250 mg of 8 hydroxy-quinoline (Sigma) was added as well. The color reagent was make up to 250 ml with DI water and stored in dark at room

temperature until use. A series of calcium in different concentration in DI water was prepared (1 mg/ml, 3 mg/ml, 5 mg/ml, 7 mg/ml and 10 mg/ml) as control.

Then, Tested samples and prepared calcium solution of different concentration, 100 µl each, were placed in 6 well plate with 2 ml AMP buffer and 2 ml color reagent. Incubated the 6 well plate at room temperature for 15 mins. And the absorbance was read using a spectrophotometer at 570 nm. A calibration curve was plotted by prepared calcium solution of different concentration. Calcium content of all tested samples were calculated accordingly.

Extracellular matrix mineralization was assessed using Alizarin Red S staining too. In brief, samples were fixed in 10% formalin for 30 min followed by a 3X wash in DI water. Next, samples were incubated for 5 min in 0.02 mg/ml Alizarin Red S (Sigma) staining solution (pH: 4.2-4.5). Samples were washed in ethanol and photographed under a Nikon microscope.

3.2.6. Statistical analysis

Five samples were analyzed per condition. Data in graphs represents mean ± standard deviation (SD). Comparison between the two means was determined using the Tukey test and statistical significance was defined as $p \leq 0.05$.

3.3. Results and discussion

3.3.1. Characterization of scaffolds

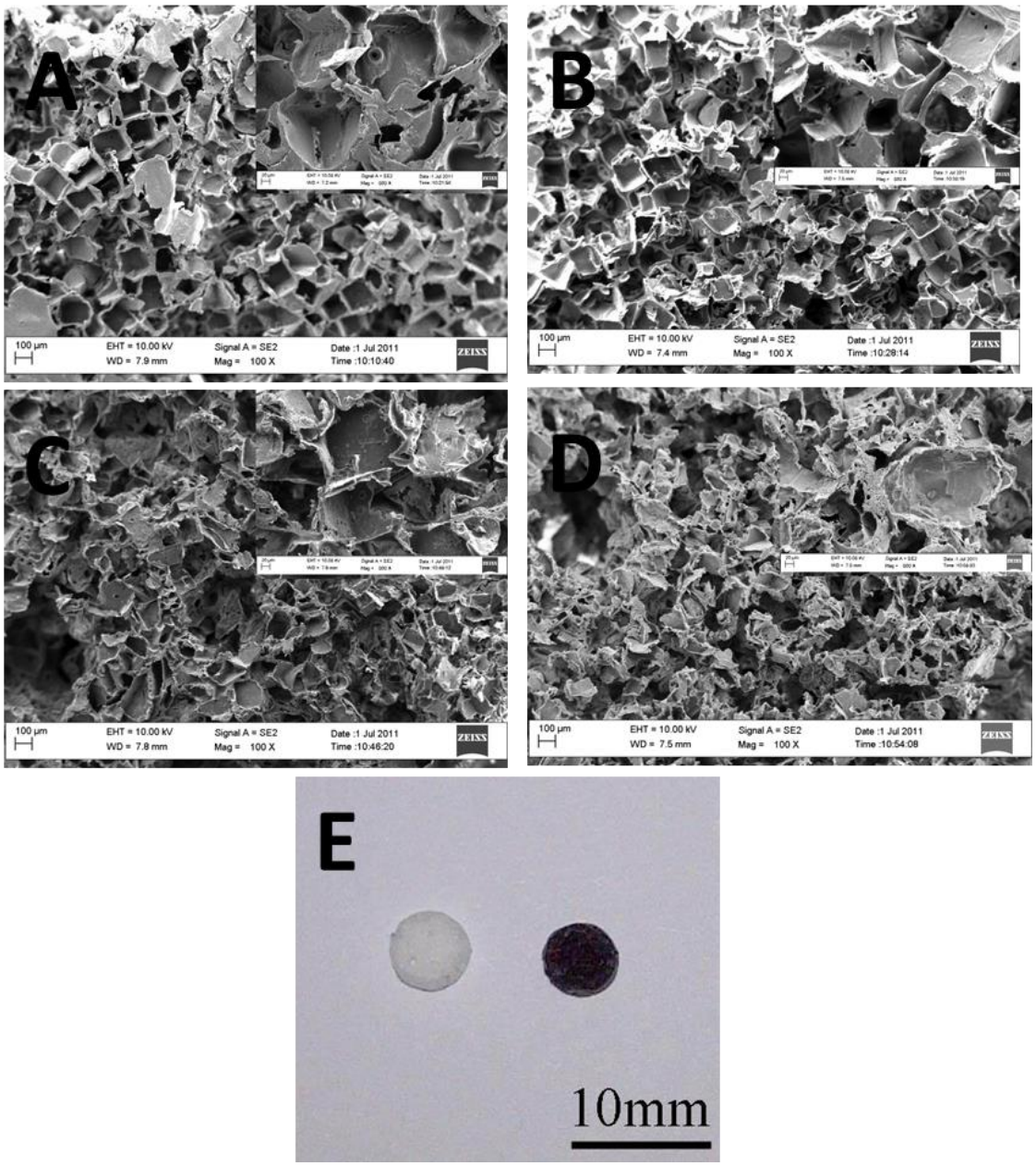

Figure 3. 3 SEM and digital camera images of CNT/PLGA composite scaffolds. (A) Control PLGA scaffold; (B) 1% CNT incorporated PLGA scaffold; (C) 3% CNT incorporated PLGA scaffold; (D) 5% CNT incorporated PLGA scaffold; (E) Photograph of PLGA and CNT/PLGA scaffolds made by salt leaching/particulate leaching method. White scaffold on the left is a PLGA scaffold and black scaffold on the right is a 1% CNT incorporated PLGA scaffold. All scaffolds were 5.5 mm in diameter and 2 mm in height.

Figure 3. 3 shows SEM images of PLGA (Figure 3. 3A), and 1% CNTs (Figure 3. 3B), 3% CNTs (Figure 3. 3C) and 5% CNTs (Figure 3. 3D) incorporated PLGA scaffolds, respectively. All scaffolds were highly porous with an interconnected pore structure. The diameters of cubic pores ranged between 100 μm to 200 μm, as determined by the NaCl particle size used in scaffold synthesis. Figure 3.3E showed a photograph of PLGA and 1% CNTs incorporated PLGA scaffold. Scaffolds made from pure PLGA appeared to be a white disk with a diameter of 5.5 mm and height of 2 mm while the incorporation of 1% CNTs changed the color of scaffold to black.

Bone tissue engineering strategies rely on the ability to develop 3D porous scaffolds with mechanical, structural and ECM compositional characteristics of natural bone. Bone tissue is organized into 5 different tissue type categories: (i) the macrostructure which is composed of cortical and cancellous bone, (ii) the microstructure which is made up of osteons, haversian systems, and trabeculae, (iii) the sub-microstructure made up of lamellae, (iv) the nanostructure composed mainly of collagen fibers and (v) the sub-nanostructure which has components such as mineral, collagen, and other organic proteins [243]. Recreation of the complexity of native bone is major challenge in scaffold based bone tissue engineering approaches. Further studies are warranted to elucidate the individual role of scaffold design parameters on the rate of *in vitro* osteogenesis and *in vivo* osteointegration.

Table 3. 1 Surface roughness of PLGA and CNT incorporated PLGA films as measured by AFM. The addition of CNTs resulted in an increase in the roughness of films.

Substrate	RMS (nm)
PLGA film	7.17±1.62
1% CNT incorporated PLGA film	43.95±10.74 *
3% CNT incorporated PLGA film	103.05±9.93 *
5% CNT incorporated PLGA film	169.17±12.72 *

* represents significant difference in surface roughness of CNT/PLGA films compared to PLGA films at significance levels of $p<0.05$.

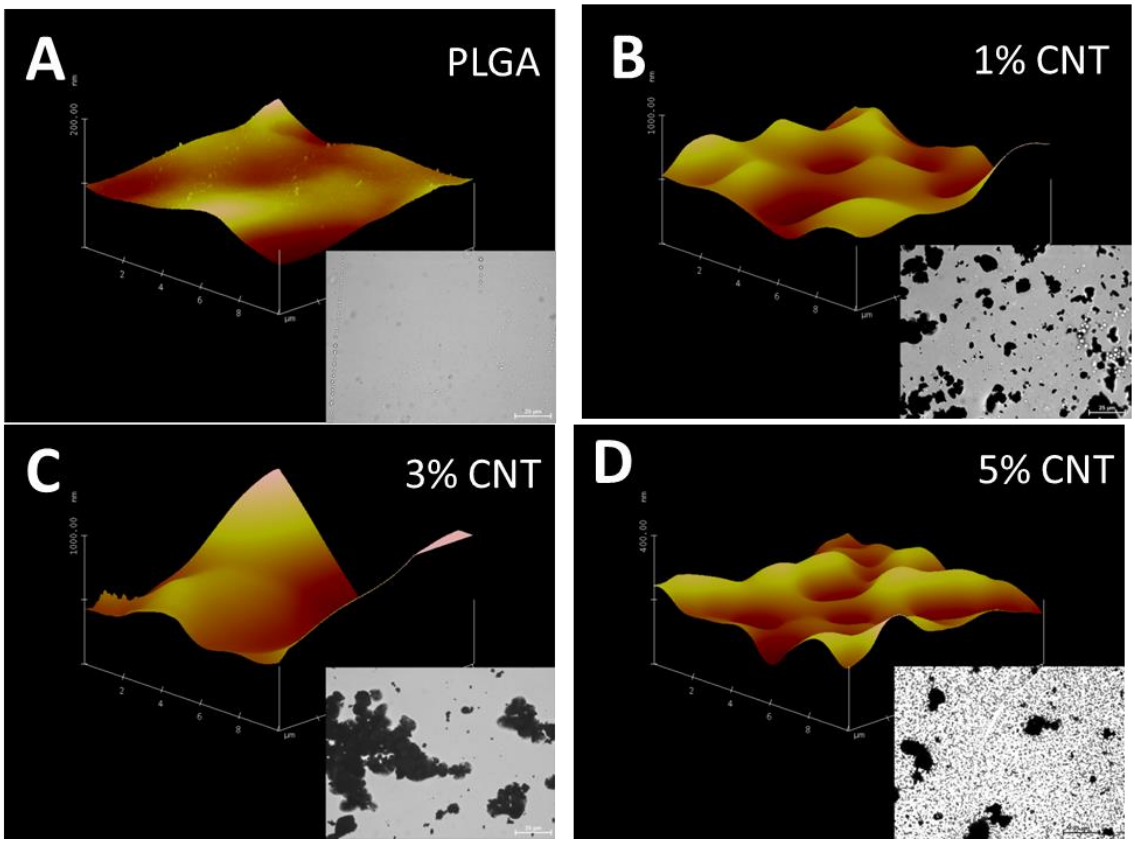

Figure 3. 4 AFM images of PLGA and CNT incorporated PLGA films. (A) Control PLGA film; (B) 1% CNT incorporated PLGA film; (C) 3% CNT incorporated PLGA film; (D) 5% CNT incorporated PLGA film. The addition of CNTs led to an increase in surface roughness and aggregation of nanotubes.

The research work described in this manuscript focuses on the design and development of CNT/PLGA scaffolds for bone tissue engineering applications. It was hypothesized that the addition of CNTs to PLGA would combine the enhanced

mechanical competence of porous scaffolds with the benefits of the increased nano-scale surface roughness. A rationale for this work was based on recently published reports demonstrating the extraordinary ability of CNTs to reinforce polymeric composites. This unique capability stems from high surface to volume ratio and modulus of CNTs [1, 2].

Figure 3. 4 demonstrated the representative AFM images of PLGA and CNT/PLGA films. Our results demonstrated a direct correlation between the CNT concentration and surface roughness. The addition of CNTs would significantly increase the surface roughness of CNT/PLGA composites. Table 3.1 summarized the average calculated roughness for PLGA and PLGA/CNT films. We observed that the roughness increases from 7.17±1.62 nm to 43.95±10.74 nm with the addition of 1% CNTs. We hypothesized that the degree of aggregation and homogeneity in dispersion of CNTs define the roughness. To confirm this hypothesis, we performed light microscopy of PLGA films containing CNTs at various ratios. Our results, shown in Figure 3. 4, demonstrated a homogenous dispersion of single CNTs at 1% ratio and bundling of CNTs at 3% and 5% ratios to a degree that individual nanotubes become undetectable.

Another major motivation for this study stems from the previous reports demonstrating the osteogenic properties of CNTs in 2D and 3D systems. In this context, several groups have attributed the enhanced osteoblast proliferation and unregulated rate of differentiation to the increased surface roughness resulting from the addition of CNTs [108-110]. In particular, Zanello et al. recently demonstrated that osteoblasts change morphology and express plate-shaped crystals in the presence of CNTs [34]. In another study, osteoblasts exhibit an osteocyte-like morphology as compared to cells cultured on a glass surface and expressed a higher level of osteogenic differentiation and maturation

[104]. The osteogenic effects of nano-roughness has been shown in other systems in which nanoparticle coated surfaces promoted differentiation through the activation of mitogen-activated protein kinase (MAPK) pathway [106]. In line with these findings, Kim et al. demonstrated MAPK to be the dominating pathway in regulating the osteogenic response of cells to surface roughness on Ti substrates. This effect has also been demonstrated in 3D scaffolds, where Edward et al. demonstrated a higher degree of osteogenic differentiation on eletrospun PLGA fibers containing CNTs [112].

We used AFM to confirm that CNT incorporation affects the surface roughness of scaffolds. We accomplished this analysis in films since the AFM measurements in 2D yields a more consistent information than 3D scaffolds. Films of PLGA containing CNTs at concentrations of 1%, 3% and 5% were chosen for this study and the results were measured in terms of average roughness in nanometers. As depicted in Figure 3. 4 and Table 3. 1, we observed an increase in roughness of the PLGA films with the addition of CNTs. This trend was consistent with a previously published report by Tseng et al. in which they demonstrated the surface roughness of CNT/Polyimide films to increase with the concentration of CNTs [244]. To illustrate the mechanism behind the impact of CNT concentration on roughness, we used light microscopy to visualize nanotubes within the films. At 1% CNT/PLGA ratio, we observed individual nanotubes to create wrinkles within the PLGA film in all directions leading to an enhanced roughness. With the increase of concentration to 3% and 5%, CNTs started to aggregate at a higher rate. We postulate that this phenomenon is responsible for the increased surface roughness of the films as well as the decreased mechanical strength of scaffolds.

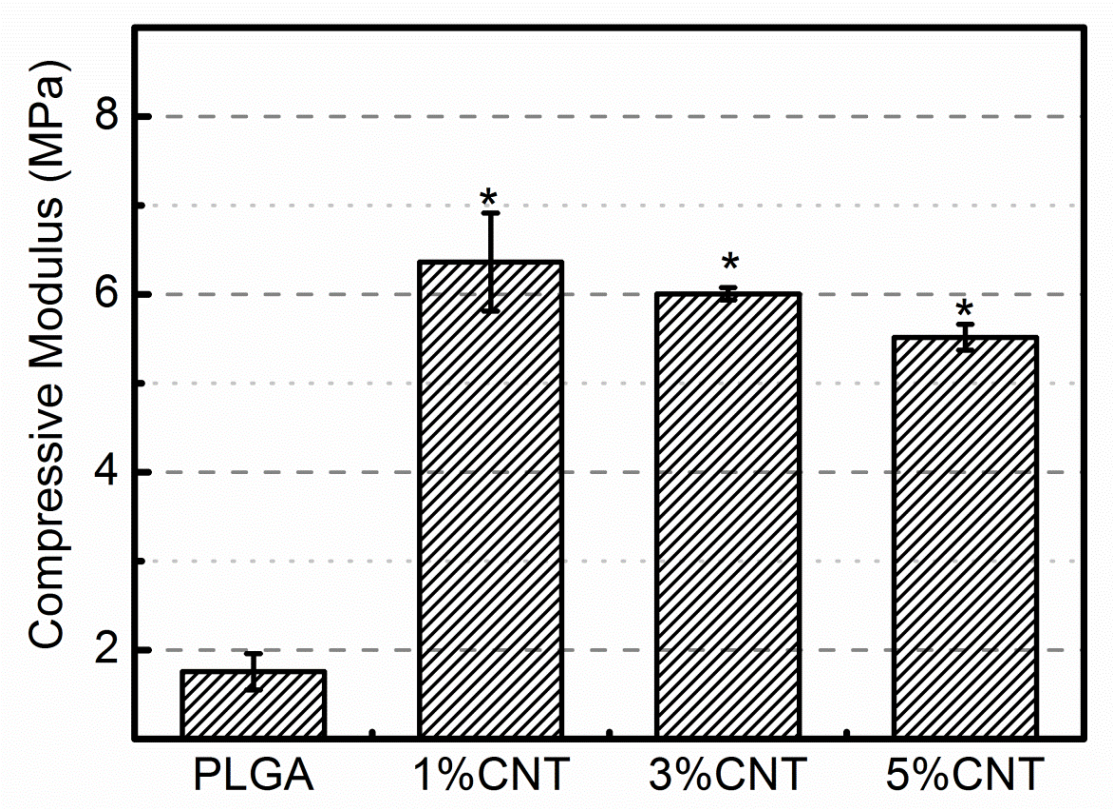

Figure 3. 5 Compressive modulus of PLGA and CNT incorporated PLGA scaffolds. * denotes significant difference when CNT/PLGA scaffolds, as compared to PLGA scaffold ($p<0.05$) the mechanical strength has been increased by addition of CNTs. However, CNT content more than 1% leads a slight decrease in Young's modulus compared to 1%.

The mechanical properties of scaffolds were assessed by compressive modulus testing. Interestingly, as shown in Figure 3. 5, CNT/PLGA scaffolds demonstrated a significantly higher compressive modulus than control PLGA scaffolds. The average compressive modulus of PLGA, 1% CNT/PLGA, 3% CNT/PLGA and 5% CNT/PLGA scaffolds were 1.75±0.20 MPa, 6.36±0.55 MPa, 6.0±0.06 MPa and 5.51±0.14 MPa, respectively. The addition of 1% CNTs into the PLGA scaffolds resulted in 3.6 fold increase in compressive modulus demonstrating the potential of CNTs as to fabricate composite scaffolds with desired mechanical strength.

In this study, we used solvent casting/particulate leaching to develop scaffolds. A major advantage of this fabrication method is that it allows for control over the porosity

and pore size through the use of NaCl particles with selective size ranges [245]. In line with our hypothesis, the results demonstrated a 3.4 fold increase in compressive modulus with the addition of 1% CNTs to PLGA scaffolds. Interestingly, the higher CNT ratios led to a decrease in mechanical strength. We attribute the reduction in mechanical strength of scaffolds to the aggregation and heterogeneous distribution of CNTs within the scaffolds. The tendency of CNTs to aggregate stems from their nano-structure, van der Waals interaction and limited dispersibility [246] It is important to note that this phenomenon has been also observed in other studies on mechanical properties of composites. For instance, Narimissa et al. showed a gradual decrease in Young's modulus of graphite/PLA nanocomposite due to aggregation of graphite [247]. In another study, Saotome et al. demonstrated a reduction in modulus with as larger fullerene nano-particple aggregates formed within the polycarbonate nanocmposites [248]. Take a step forward, we used percolation theory to explain the mechanical behavior of our scaffolds. This theory allows for calculating the threshold that describes the critical volume fraction separating the two phases in the mixture. Interestingly, the percolation threshold for CNT/polymer system is dependent on size and distribution of CNTs [249, 250]. Specifically, the percolation threshold for a rod-like filler for mechanical enhancement could be calculated according to this equation: $V_{fc}=0.7/(L/d)$. Where L and d represents length and diameter of a filler [251, 252]. Since our CNTs are 1-5 um in length and 20-40 nm in diameter, the calculated threshold is about 1.2%. Consequently, a drop of Young's modulus has been observed when more CNTs than 1% was added into scaffolds.

3.3.2. *In vitro* evaluation of CNT/PLGA scaffolds

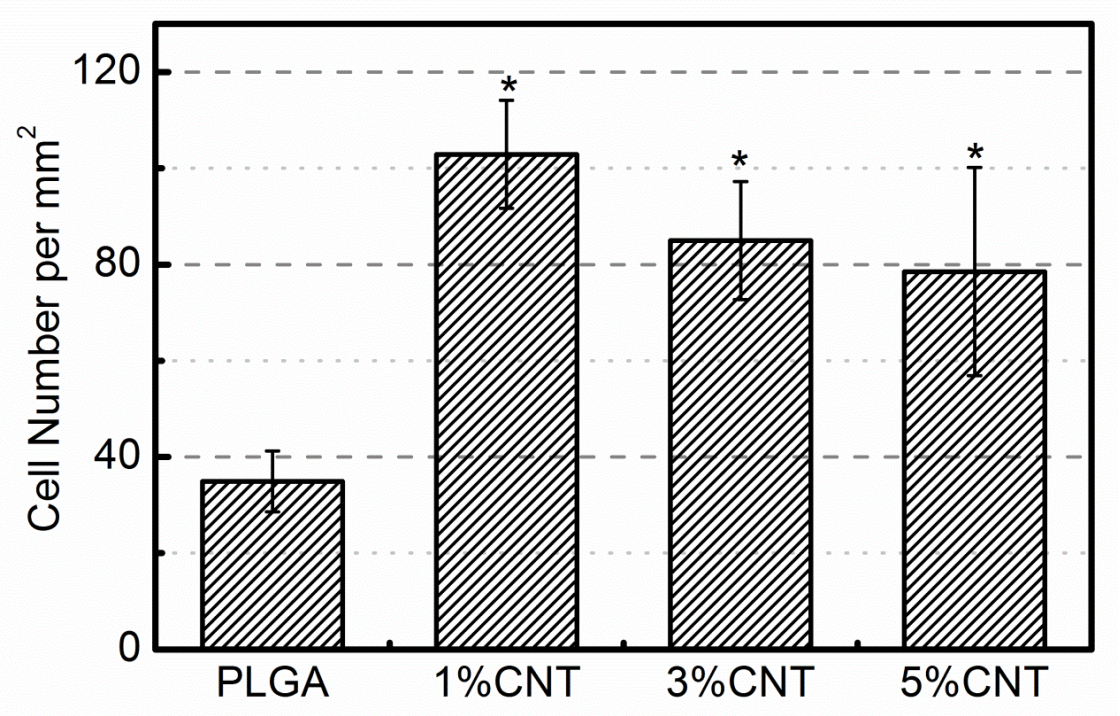

Figure 3. 6 Cell attachment on PLGA and CNT/ PLGA films after 1 day of cell seeding. * denotes significant difference in cell number on CNT incorporated PLGA scaffolds compared to PLGA scaffolds ($p<0.05$) the cell number adhere to film has been increased by addition of CNTs. However, CNT content more than 1% leads a slight decrease in the number of cell attachment compared to 1%.

To assess the effect of CNTs on initial cell attachment, we measured cell number on PLGA, 1% CNT/PLGA, 3% CNT/PLGA and 5% CNT incorporated PLGA films after 4 hours of cell culture (Figure 3. 6). Average cell number attached on films showed an increase with the addition of CNTs to PLGA. Cell number appeared to be highest on 1% CNT/PLGA films demonstrating a 2.9 fold increase per mm^2 compared to PLGA.

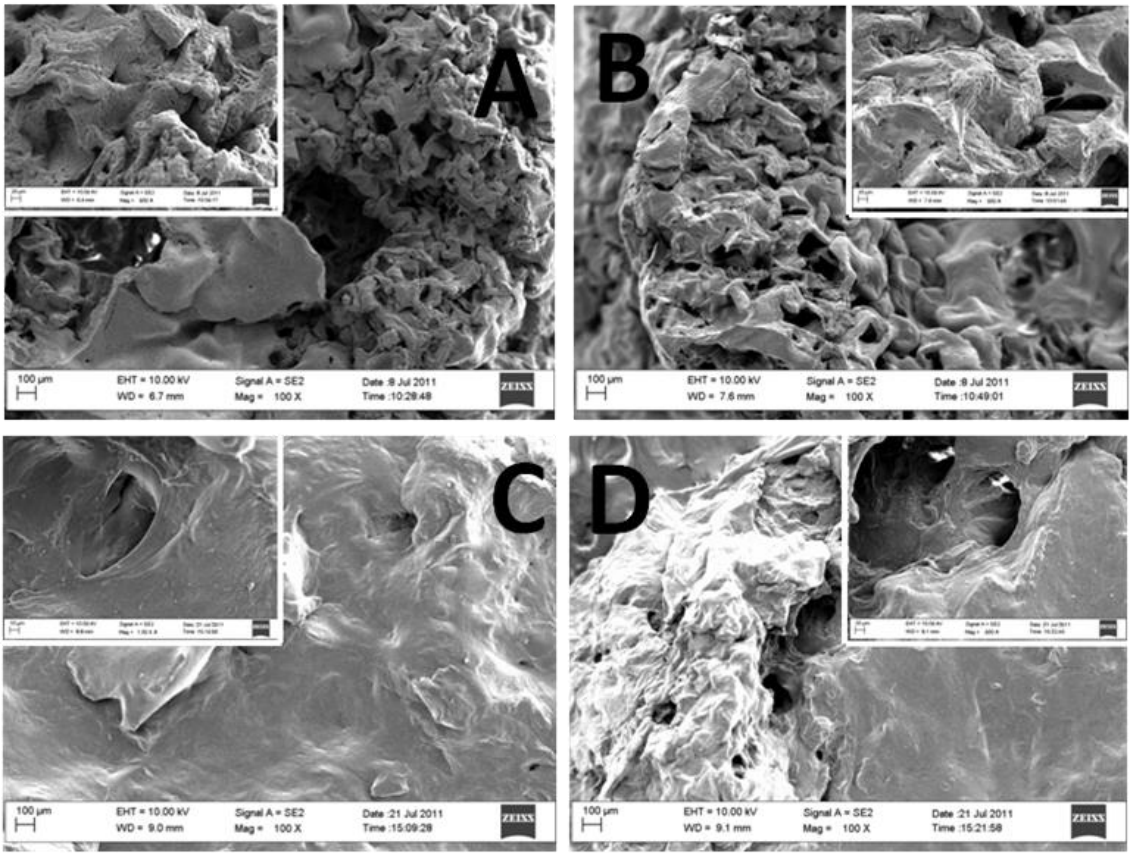

Figure 3. 7 SEM images of MC3T3-E1 osteoblast morphology and growth on PLGA (A and C) and 1% CNT/PLGA scaffolds (B, D) at days 7 and 21 respectively. No significant difference in cell morphology was noticed between the two groups.

Cell morphology and growth on scaffolds were visualized using SEM (Figure 3. 7). Cells first attached to the wall of pores and formed cell bridges between cell walls. All of the scaffolds were fully confluent after 7 days meanwhile pores could still be seen. At day 21, we observed a layer of cells covering the surface of scaffolds and filling the pore spaces.

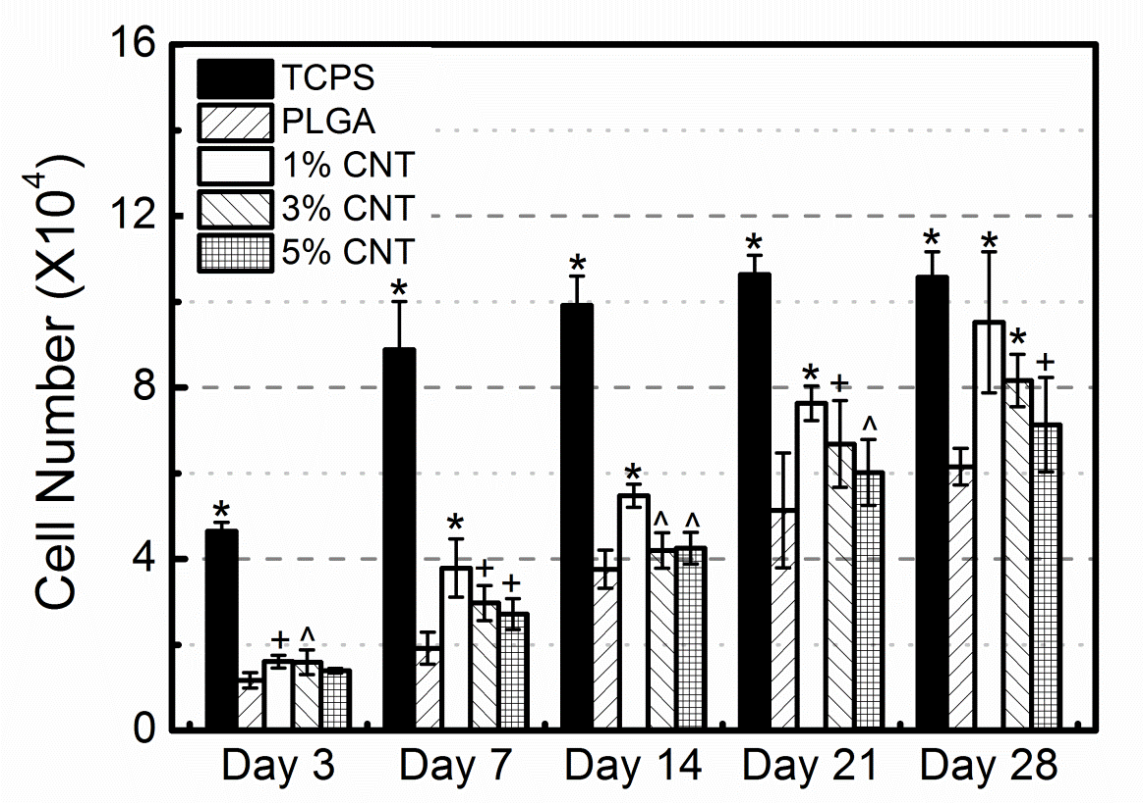

Figure 3. 8 MC3T3-E1 osteoblast proliferation on TCPS, PLGA and CNT incorporated scaffolds. *, + and ^ represents significant difference in cell proliferation on CNT/PLGA scaffolds compared to PLGA scaffold at the same time point at significance levels of $p<0.05$, $p<0.1$ and $p<0.5$, respectively.

Cell proliferation on 3D scaffolds was assessed quantitatively using MTT assay, as presented in Figure 3. 8. Four groups of PLGA, 1% CNT/PLGA, 3% CNT/PLGA and 5% CNT/PLGA scaffolds were considered for this study. Tissue culture polystyrene (TCPS) control group was included to confirm the status of cell culture conditions. The data presented growth in cell number as a function of time for all the groups. Strikingly, the incorporation of CNTs into the scaffolds resulted in a significant increase in cell proliferation for all time points and reached a plateau at day 28. Consistently in all time points, the maximum increase in cell proliferation as compared to PLGA scaffolds was observed in scaffolds containing 1% CNTs.

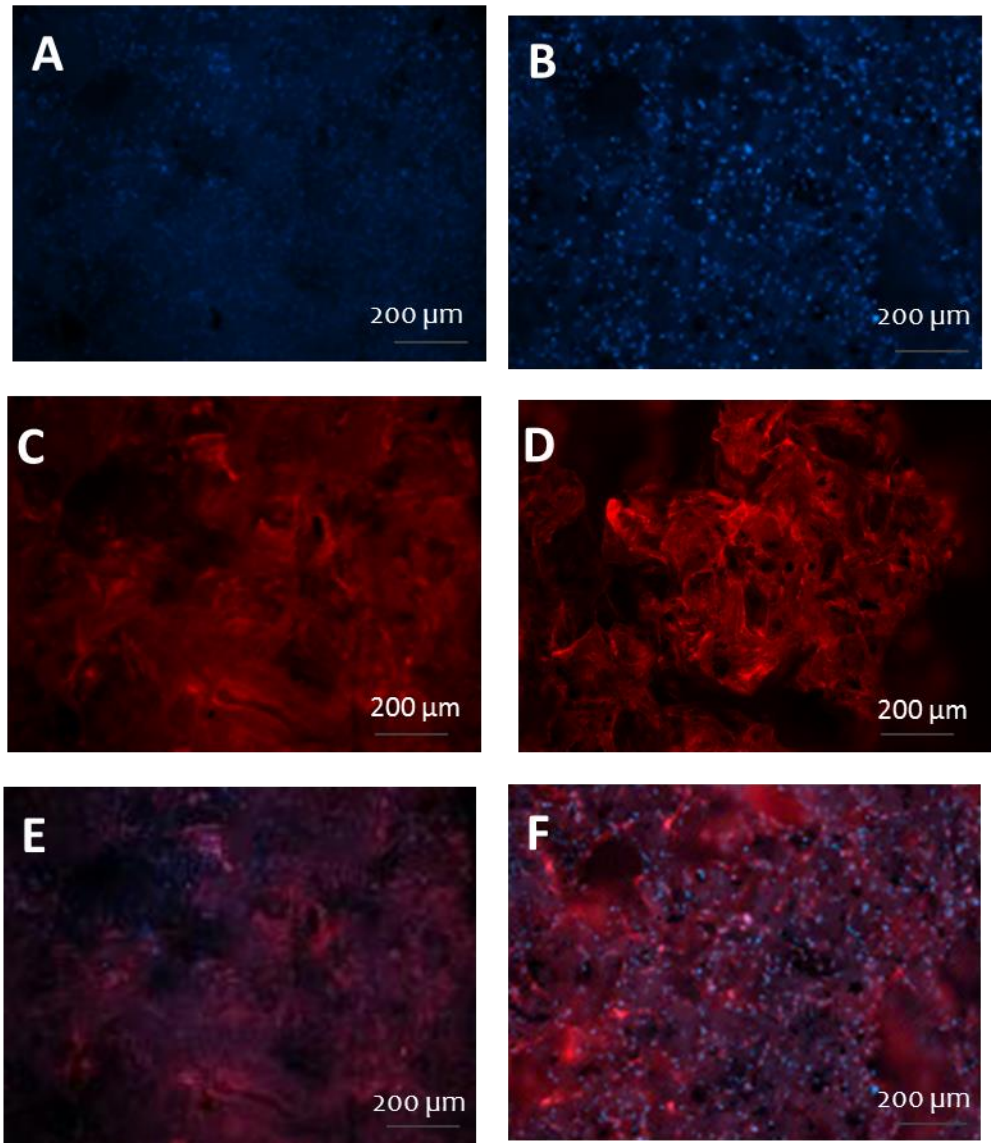

Figure 3. 9 Immunofluorescent staining of (A-B) nuclei, (C-D) cytoskeletal protein actin, and (E-F) actin-nuclei double staining of MC3T3-E1 osteoblasts cultured on PLGA (left column) and 1% CNT/PLGA (right column) scaffolds for 21 days. No significant difference in cell morphology was noticed between the two groups.

Cell cytoskeletal organization and morphology within the scaffolds were visualized via immunofluorescent staining with nuclei DAPI and cytoskeleton protein actin. Figure 3. 9 illustrates cell nuclei and actin double staining of cells cultured on PLGA and composite CNT/PLGA scaffolds. We observed that cells proliferated on the

surface and within the pores of scaffolds. There was not a noticeable difference in cytoskeletal organization between the control and CNT incorporated scaffolds.

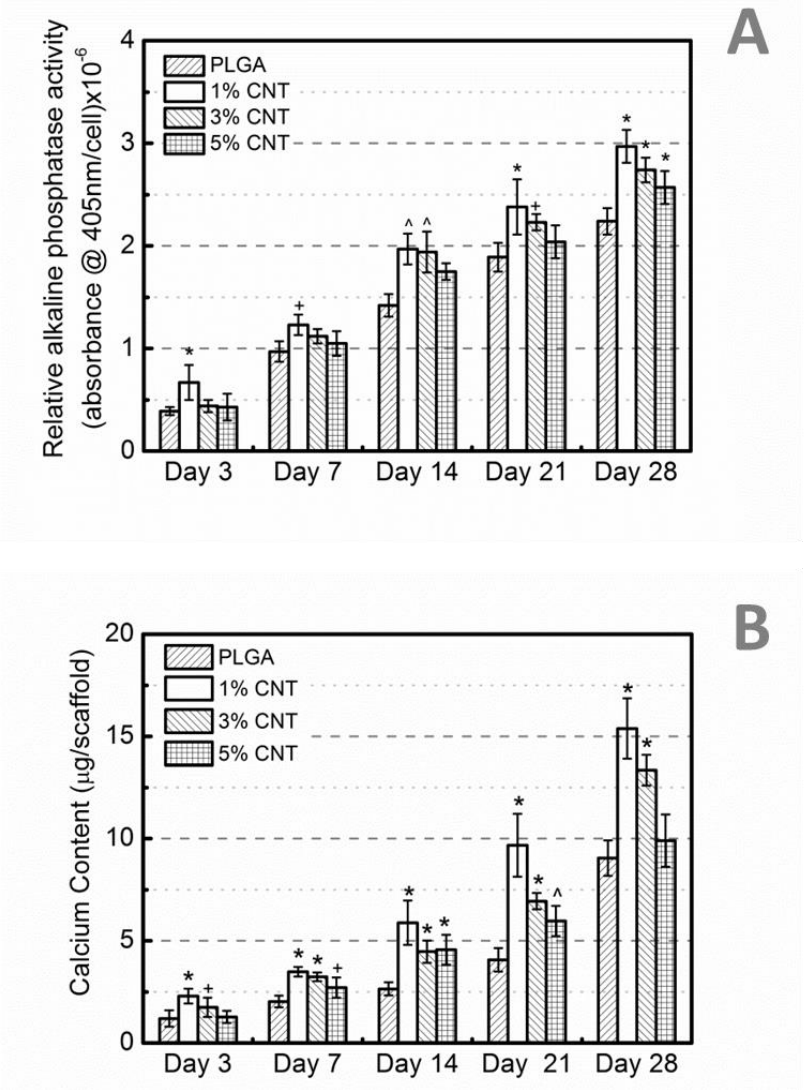

Figure 3. 10 Alkaline phosphatase activity and calcium expression of MC3T3-E1 osteoblasts on PLGA and CNT/PLGA scaffold. *, + and ^ represents significant difference in ALP activity and calcium expression by cells on CNT/PLGA scaffolds compared to cells on PLGA scaffolds at the same time point at significance levels of $p<0.05$, 0.1 and 0.5, respectively. A slight increase of calcium content was observed in first two weeks and a sharp leap of calcium content in after that. A moderate increase of ALP activity was observed through 4 weeks.

Osteogenic differentiation of cells was assessed by quantifying ALP activity and calcium content combined with qualitative Alizarin red mineral and ALP staining. Figure 3. 10A showed ALP expression level by cells grown on control PLGA scaffolds as well as scaffolds containing 1%, 3%, and 5% CNTs.

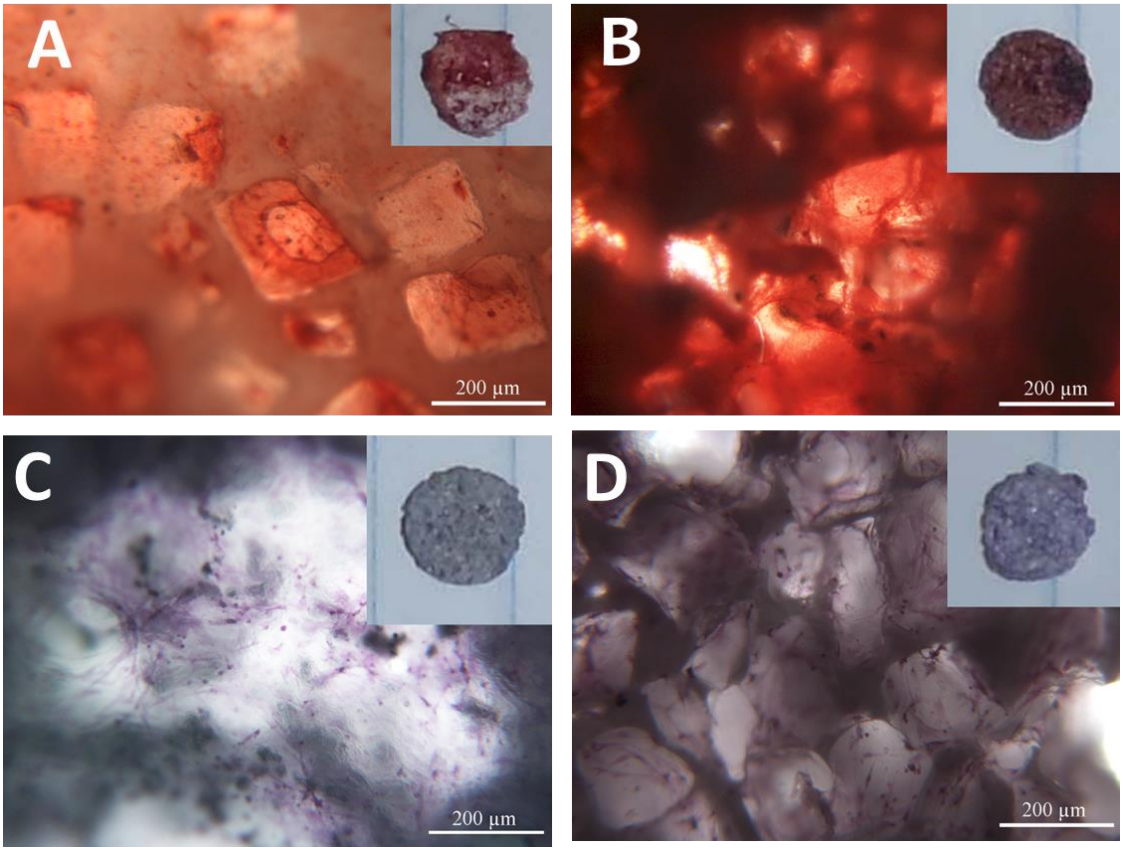

Figure 3. 11 (A-B) Alizarin red S staining and (C-D) alkaline phosphatase staining of MC3T3-E1 ostoblasts on PLGA (left) and 1% CNT/PLGA scaffold (right) at day 21. Calcium and ALP staining were showed positively, respectivly.

For all groups, ALP expression increased as a function of time. While the addition of CNTs resulted in enhanced osteogenic differentiation, the group containing 1% CNTs demonstrated the highest level of ALP expression. These results were consistent with the results of calcium content quantification (Figure 3. 10B). The data demonstrated an increase in calcium content on control PLGA scaffolds as well as PLGA scaffolds containing CNTs as a function of time. Strikingly, 1% CNT/PLGA scaffolds

demonstrated the highest amount of calcium with 1.5 fold higher level than control PLGA scaffolds after 28 days of culture.

We confirmed the mineral deposition and ALP expression by cells cultured on PLGA and 1% CNT/PLGA scaffolds, as demonstrated in Figure 3. 11. It was observed that cells express ALP enzyme and deposit mineral on the surface and within the pore spaces of scaffolds. Interestingly, the addition of CNTs to the scaffolds resulted in a faster rate of mineralization and higher rate of ALP expression by cells. These results all together demonstrate that CNTs enhance early stage osteogenic differentiation and late stage mineralization of osteoblastic cells on 3D PLGA scaffolds.

In line with other published reports, our *in vitro* results demonstrated a higher degree of MC3T3-E1 osteoblast-like cell adhesion and proliferation rate on PLGA scaffolds containing CNTs. The decrease of number of cell attachment accompany with more addition of CNT was due to that agglomeration of CNTs. More dispersed CNTs are preferred for cell attachment. Moreover, large agglomeration will also decrease the available surface area for cell attachment as well. Progressive osteoblast proliferation was observed throughout the scaffold 3D structure and resulted in the formation of cellular extensions covering the entire scaffolds and filling the pore spaces. Cell growth quantification results were consistent with the immunofluorescent images of actin cytoskeleton in showing osteoblasts preserved cellular structure integrity throughout the scaffolds. When exposed to the differentiation media, cells underwent osteogenic differentiation in 28 days on both control PLGA and CNT/PLGA scaffolds. Our scaffolds shows a good biocompatibility to MC3T3-E1 osteoblast-like cells.

The extent of differentiation was assessed through quantification of ALP activity and calcium content combined with qualitative Alizarin red mineral and ALP staining. ALP activity is an early marker of osteogenesis, which usually dominates in the first two weeks. Calcium content is the late marker for osteogenesis, which usually dominates after two weeks. We did observed a slow increase of calcium content on Day 7 and Day 14 and a sharp leap of calcium content in after that on Day 21 and Day 28. However, we didn't observe any ALP activity drop on Day 21 and Day 28. This was because the cells were mature outside from inside at a different rate. Cells in the middle of scaffold were migrated slowly into and need more time mature due to oxygen and nutrition limitation.

Moreover, our results collectively showed that the presence of CNTs led to a significant elevation in expression of osteogenic markers. This was manifested in quantified ALP and calcium content measurements as early as day 7. Interestingly, scaffolds containing 1% CNT stimulated the growth and differentiation of osteoblastic cells at the highest rate. The mechanism of the stimulatory effects of CNTs and inhibitory effects of high CNT loading is yet to be determined. However, this can be attributed to the higher surface roughness and stiffness as well as the excess bonding of growth factors to CNTs. Further studies are warranted to elucidate the mechanisms by which CNTs modulate protein adsorption and the consequent stem cell response to exogenous adsorbed growth factors.

The enthusiasm for the biomedical applications of CNTs has been dampened for toxicity concerns. In general, the toxicity of CNTs has been reported to be function of high surface area and intrinsic surface properties [253]. A recent report by Donaldson et al. demonstrated that CNTs are harmful to lung and illicit immunological responses [254].

Further studies by this group showed that long term inhalation of CNTs will cause pulmonary tumors. In another report, the fullerene distributed in tissues accumulated rapidly in liver and spleen [255]. However, recent work by Mikael et al. suggested that CNTs in low concentration and high purity evoke minimum cytotoxicity [256]. Tremendous effort has gone to characterize the nature of CNTs toxicity and modify the surface properties of CNTs to diminish their adverse effects. An approach to accomplish this goal is the functional modification of CNTs to enhance dispersion in physiological solutions as well as excretion of CNTs from human body. Singh et al. recently demonstrated that CNTs functionalized with carboxylate and hydroxyl groups had varying affinities for liver, kidney, spleen and bone, and can be cleared through renal excretion route [257]. Our observations in this study provide the proof of principle for the use of CNTs combined with osteoblasts in treatment of bone disorders. A future extension of this study will include the modification of CNTs to diminish toxicity side effects.

Another future direction of this research involves studies on how to control the orientation of CNTs within 3D scaffolds. Alignment allows for control over the extent of cell spreading and regulation of phenotype. This has been demonstrated in 2D environments where the orientation of CNTs distributed on a surface impacted the directional migratory behavior as well as osteogenic differentiation of MSCs. The incorporation of CNTs also provides an opportunity to regulate phenotypic expression and lineage specification of stem cells by electrical cues. Earlier attempts to accomplish this goal led to the fabrication of CNT-based nanodices for neural as well as cardiac electrical stimulation [258, 259].

3.4. Conclusion

In this study, mechanically competent CNT/PLGA scaffolds were fabricated through a uniform dispersion of CNT in PLGA/dichloromethane solution followed by a solvent casting and particulate leaching step. The incorporation of CNTs allowed for tuning the mechanical strength without compromising the porous architecture of scaffolds. The *in vitro* potential of CNT/PLGA composite scaffolds for bone tissue engineering was evaluated by monitoring the behavior of MC3T3-E1 osteoblasts. Our results demonstrated that the addition of CNT to PLGA scaffolds leads to a significant increase in adhesion, growth and osteogenic differentiation of cells. We were able to confirm the coupling of matrix stiffness and mechanical strength to enhanced osteogenesis in 3D environment. Interestingly, scaffolds containing 1% CNT demonstrated the highest level of *in vitro* bone mineralization due to a more uniform distribution of CNTs throughout the PLGA scaffolds. These findings all together demonstrate CNTs to be a powerful tool in scaffolds design in stem cell based tissue engineering. A more detailed study is warranted to delineate the signaling mechanisms by which CNTs regulate osteogenesis.

CHAPTER 4

PLGA-Carbon Nanotube Conjugates for Intercellular Delivery of Caspase-3 into Osteosarcoma Cells

4.1. Introduction

Cancer is a principal concern in today's health care treatment with more than 10 million cases each year [260]. Oncologists generally utilize physiological intervention as well as chemical and radioactive therapeutics to treat different forms of cancer. The drawbacks to the current therapeutics are the removal or necrosis of healthy tissue in addition to the tumor tissue. These side effects are one of the major concerns for traditional cancer treatments. To this end, targeted drug delivery has paved another avenue in potential cancer therapy in recent years. The Food and Drug Administration (FDA) approved clinical gene therapy in the 1990s [79] and in experimental and clinical stages has since demonstrated the promise of drug delivery in curing human diseases. Retrovirus [81], adenovirus [82] and adeno-associate [83] viral vectors are the major types of gene vectors used in research today. Although viral vectors are efficient in both delivery and transduction of cells, there are concerns that these viruses are sourced from lethal diseases such as human immunodeficiency virus (HIV) and human T-cell lymphotropic virus (HTLV). A safe, inexpensive, and effective vector has yet to be

fabricated for use in gene therapy. Therefore, developing these safe and efficient delivery systems in a controlled manner is a major focus and challenge in research [80].

The enhanced permeability and retention (EPR) effect, which is inherent to tumor biology, can allow nano-sized drug carriers to accumulate, retain, and release drugs due to the fact that tumors have leaky blood vessels and poor lymphatic drainage [261]. In further researching nano-sized drug carriers, scientists have been able to begin to widen the window into the dark room of cancer therapy. The use of nano-sized drug carriers has a few key advantages including the protection of delicate drugs, enhanced absorption in selective tissues, controlled drug distribution profile, and enhanced intracellular penetration [123]. Thus, researchers have taken initiative and developed several methods to fabricate nano-sized drug delivery carriers.

Polymers and lipids have garnered the most attention thus far as materials for drug delivery. Synthetic polymers such as poly (ethylene glycol) (PEG) [84], poly (lactic acid) (PLA) [85] and PLGA [86] as well as natural polymers such as chitosan [87], collagen [88], gelatin [89] or lipids [262] can be fabricated as nanoparticles, liposomes, and micelles to deliver molecules by either chemical modification or physical absorption. Drugs are able to be released in a controlled manner due to either surface and bulk degradation or phase transition principles. However, there are concerns with these due to immune responses dealing with the heterogeneity of the materials used as well as the low transfection efficiency and specificity. In noting this, we sought to develop a highly efficient non-viral vector drug delivery system utilizing CNTs.

CNTs [2], silicon nanowires [263], gallium nanotubes [264], boron nitride nanotubes [265], titanium oxide nanotubes [266] and zinc oxide nano-rods [267] have

received an overwhelming amount of support and enthusiasm in biomedical research. CNTs are made of a layer of grapheme [268] and have been used to shuttle several different biological molecules, ranging from small drug molecules [125] to biomacromolecules such as proteins [127], DNA [128, 269] and RNA [130] into different types of cells via endocytosis efficiently[131]. Ricin A was also delivered into various cell line with conjugation of CNTs and induce cell death. Other than cell proliferation inhibition and induction of cell death, DNA plasmids were also delivered into cells and enhance certain gene expression. CNTs are able to easily penetrate the cells and give the opportunity to transport this biological cargo across the cell membrane due to an extremely high aspect ratio. However, health concerns have hampered the practical application of using inorganic CNTs in biological applications thus far. Toxicity issues still raise doubts about the practical applications of CNTs due to the intrinsic toxicity caused by a high surface area and hydrophobicity [253]. However, toxicity concerns may not be a critical issue in cancer therapy due to that (a) EPR effect will accumulate nanoparticles in tumor tissue only; (b) The potential toxicity of CNTs would be acceptable due to cancer therapy target on killing cancer cells; and (c) CNTs at small amounts or functionalized with other molecules have shown to evoke minimum toxicity to normal cell line [256, 257]. Therefore, functionalization of CNTs can prove to be a successful path to protein and gene therapy. For instance, Liu et al. have been able to successfully deliver siRNA with phospholipid PEG (PL-PEG) functionalized CNTs into tumor cells and tissue to inhibit tumor cell proliferation, tissue ingrowth, and CXCR4 expressions both *ex vivo* and *in vivo* [132-134]. siRNA was released by breaking the S-S bond, which attached the siRNA to PL-PEG. Other pristine CNT based delivery vectors

are able to rely on diffusion to unload biological cargoes [127, 128, 130, 269]. Although the cellular uptake mechanism may differ depending on the functionalization and size of CNTs [124], thus far the researchers have been unable to control the release profile in a specified manner.

In this study we hypothesized a method to engineer a novel CNT based delivery vector functionalized with a degradable PLGA coating. Through degradation of PLGA, transcription factors are able to be released in a controlled manner and tune cell behavior. Significant advantages to our proposed system include the ability to transfect cells efficiently with the unique needle-like shape of CNTs, reduce cytotoxicity of pristine CNTs through a biocompatible PLGA coating, and program protein release times by controlling the degradation profiles of the PLGA.

4.2. Materials and methods

4.2.1. Carbon nanotube carboxylation

CNTs (0.2g) were purchased from Nanolab Inc. with an average length of 1-5 μm, diameter of 15±5 nm, and purity higher than 95% was added into a single neck glass flask with 200 ml 70% nitric acid (Fisher). For carboxylation of CNTs, CNTs were homogenously dispersed in nitric acid by sonication for 60 minutes at ambient conditions. A condenser reflux apparatus was followed to equip on top of single neck glass falsk to prevent CNTs in nitric acid from drying out. A silicon oil bath was set up to heat up the oxidation experiment. The reaction temperature was set at 120 ^{o}C for 12 hours. The reaction was quenched by addition of 200 ml deionized (DI) water. The mixture was filtered by 0.45 μm cellulose filter paper (Fisher), washed with DI water to

neutral pH, and dried at 80 ^{o}C overnight [175]. The black leftover on filter paper was stored in a glass vial sealed with parafilm in a desiccator until use.

4.2.2. PLGA functionalization

Carboxyl CNTs (50 mg), as prepared in 4.2.1., were homogeneously dispersed in 50 ml dimethylformamide (DMF) (Fisher) by sonication for 2 hours at ambient conditions. A total of 2 ml oxalyl chloride (Acros) was added drop wisely under N_2 and stirred in ice water for 2 hours with a magnetic stirrer. This mixture was stirred for another 2 hours at room temperature. A CNT-acyl chloride has been formed. Then, the mixture was transferred into a silicon oil bath at 70 ^{o}C and stirred overnight to remove the excess of oxalyl chloride. PLGA (0.5 g) (75:25) (Lactel) was then added and stirred at 100 ^{o}C for 5 days. CNT-PLGA was then formed by that chloride of CNT-acyl chloride was replaced by PLGA through a nucleophilic reaction. Finally, the CNT-PLGA containing solution was cooled down, filtered by 0.45 µm cellulose filter paper (Fisher), and washed with DMF, ethanol (Decon Labs), and DI water. The PLGA linked CNTs (CNT-PLGA) were the black leftover on the filter paper and were dried at 80 ^{o}C overnight, collected and stored in a glass vial sealed with parafilm in a desiccator [177].

4.2.3. Protein attachment

CNT-PLGA (100 µg) was dispersed in 0.5 ml of 2-(N-Morpholino)ethanosulfonic acid (pH 5.6) (MES) (Acros) buffer under sonication for 1 hour at ambient conditions. 0.25 ml of 1-(3-Dimethylaminopropyl)-3-ethylcarbodiimide hydrochloride (0.2 mol/L) (EDC) (Acros) and 0.25 ml of *N*-Hydroxysuccinimide (0.1 mol/L) (NHS) (Acros) in

MES solution were added to the activated carboxylate groups [170, 171]. EDC reacts with a carboxyl group on CNT-PLGA, forming an amine-reactive *O*-acylisourea intermediate. This intermediate may react with an amine on proteins, yielding CNT-PLGA-protein conjugates. However, the intermediate is also susceptible to hydrolysis, making it unstable and short-lived in aqueous solution. The addition of NHS stabilizes the amine-reactive intermediate by converting it to an amine-reactive NHS ester, thus increasing the efficiency of EDC-mediated coupling reactions. Finally, the amine-reactive NHS ester intermediate has sufficient stability to form CNT-PLGA-protein conjugation in aqueous solution.

The mixture was washed with PBS and centrifuged in a 100 KDa molecular weight cutoff centrifugal filter (Millipore) to remove EDC and NHS at 5000 g three times for 30 mins. Then, 5 μg of protein, either bovine serum albumin (BSA) (Sigma), fluorescent BSA (fBSA) (Sigma), or caspase-3 (CP3) (BD) was added into the CNT-PLGA/PBS solution at 4 ^{o}C overnight. The mixture was finally washed and centrifuged in a cutoff filter to remove un-conjugated protein six times at 5000 g for 30 minutes [171]. The protein conjugated CNT-PLGA (CNT-PLGA-CP3/BSA/fBSA) solution was collected and stored at -20 ^{o}C.

Pro-Ject protein transfection kit (BD) was used as a reference. Liposomes nanoparticles were fabricated through the commercial manual. Note that the actual protein amount dosages were calculated equally to the amount CNT-PLGA-CP3 groups. In general, certain amount of caspase-3 was dissolved PBS. Dry Pro-Ject film was hydrated and dispersed well by caspase-3 containing PBS solution. The mixed solution was incubated at room temperature for 5 mins and ready to be used. According the BD

protocol provided. An incubation time of 3-4 hours in serum free medium was required for protein transfection. 96 well plate was used for Pro-Ject transfection control. 20, 000 cell/cm^2 cell seeding density was used.

4.2.4. Cell culture

Osteosarcoma cells MG-63 (ATCC) were cultured in 90% α-MEM (Lonza) and 10% FBS (Gibco) supplemented with 2 mmol/ml *l*-glutamine (Sigma). A serum free medium mentioned above was prepared without serum using the same recipe. Cells were placed in well plate with a seeding density of 20,000/cm^2. Testing conjugates were introduced after 4 hours. This time point was set as 0 and cells were then maintained in a humidified incubator at 37°C with 5% CO_2.

4.2.5. MTT assay

Cell viability was assessed using 3-(4,5-Dimethylthiazol-2-yl)-2,5-diphenyltetrazolium bromide (MTT) (Alpha Aesear) calorimetric assay at predetermined time points of 1, 3, 5 and 7 days. In brief, MTT/PBS solution was added into each well (1:5) and incubated at 37 °C for 5 h. This was followed by the removal of medium/MTT solution and addition of 1 ml dimethyl sulfoxide (DMSO) (Fisher). The resulting solution was diluted by DMSO in a ratio of 4:1 and the absorbance was read at 550 nm using Tecan SpectroFluo Plus reader. Cell viability was determined as the equation:

$$\text{Cell Viability} = \frac{\text{Abs}_{550\text{nm}} \text{ of Treated Sample}}{\text{Abs}_{550\text{nm}} \text{ of Control}} \times 100\%$$

4.2.6. Spectra measurement

XRD patterns were carried out on a Rigaku MiniFlex II with a scanning speed of 0.2 degree/minute. UV was measured on a Jasco UV 60 UV-Vis spectrometer from 250 to 500 nm. Fourier Transform Infra-Red (FTIR) spectrum was measured on a Nicolet 6700 FT-IR spectrometer from 3600 to 400 cm^{-1}.

4.2.7. Immunofluorescent images

To remain sterile, cover slips were rinsed in 70% ethanol for 10 minutes and washed with PBS. Cells were seeded onto cover slips and allowed 12 hours to expand on glass slides. The addition of 0.05, 0.1, 0.5, 1 and 3 µg/ml CNT-PLGA-fBSA conjugate was added and incubated for 4 hours. Then samples were washed with PBS, fixed with formalin (Sigma), and dried. Fluorescent images were taken with a Nikon Eclipse 60i microscope system and all images were analyzed with Nikon Elements NX4 software.

4.2.8. TEM

Cells were seeded onto 40 mesh carbon grids for 12 hours with a density of 20,000 cells/cm^2 followed by an addition of 3 µg/ml CNT-PLGA-BSA conjugate solution and incubated for 4 hours. Samples were then washed with PBS, fixed with formalin, and dehydrated by a series of ethanol treatments [164]. TEM images of the cell penetration of the CNT-PLGA-BSA conjugate were taken with a Hitachi H8000 TEM.

4.2.9. Temporal release profile of BSA from CNT-PLGA-BSA *in vitro*

CNT-PLGA (100 µg) was dispersed in 0.5 ml of 2-(N-Morpholino)ethanosulfonic acid (pH 5.6) (MES) (Acros) buffer under sonication for 1 hour at room temperature. 0.25 ml of 1-(3-Dimethylaminopropyl)-3-ethylcarbodiimide hydrochloride (0.2 mol/l) (EDC) (Acros) and 0.25 ml N-Hydroxysuccinimide (0.1 mol/l) (NHS) (Acros) in MES solution were added to the activated carboxylate groups [170, 171]. The mixture was washed with PBS and centrifuged in a 100 kDa molecular weight cutoff centrifugal filter (Millipore) to remove EDC and NHS at 5,000 g three times for 30 minutes. Then, 200 µg of BSA was added to the CNT-PLGA/PBS solution at 4 oC overnight. Lastly, the mixture was washed and centrifuged in a cutoff filter to remove un-conjugated BSA six times at 5,000 g for 30 minutes [171]. The removed filtered solution was collected each run to determine amount of loaded BSA.

The CNT-PLGA-BSA conjugates were then dispersed in 1 mL PBS by sonication (5 min) and incubated in a water bath (37 ^{o}C). The entire conjugate solution was centrifuged in a 100 kDa molecular weight cutoff centrifugal filter (Millipore) to remove the released BSA solution at each predetermined time point. The concentration of the released BSA was determined with a Jasco UV 60 UV-Vis spectrometer at 280 nm with a pre-made calibration curve.

4.2.10. Release of resveratrol from nanoparticles made of different PLGA *in vitro*

In general, 100 mg of PLGA (Lactel) in differing ratios of PLA to PGA and molecular weight (5,000-16,000/50:50, 16,000-29,000/50:50 and 75,000-100,000/75:25) along with 10 mg of resveratrol (Sigma) were dissolved in 5 mL acetone (Sigma). The

mixture was then slowly injected into 100 mL 0.25 mol/ml MES solution (pH 5.0) containing 2.5% PVA (Sigma) at a rate of 1 mL/min [170, 171]. After 24 hours of moderate stirring to remove traces of acetone, the nanoparticle solution was centrifuged 6 times to remove the non-incorporated resveratrol. The supernatants were collected to determine the loaded resveratrol. The collected nanoparticles were lyophilized and stored in a desiccator.

The nanoparticles (1mg) were dispersed in 1 mL PBS by sonication (5min) in an EP tube and incubated in a water bath (37 ^{o}C). The nanoparticle suspension was centrifuged to collect the supernatant at each predetermined time point. The concentration of released resveratrol was determined with a Jasco UV 60 UV-Vis spectrometer at 327 nm with a pre-made calibration curve (Supplementary Figure 3).

4.2.11. Statistical analysis

Five samples were analyzed at each condition. Data in graphs represents the mean ± standard deviation (SD). Comparison between the two means was determined using the Tukey test and statistical significance was defined as $p \leq 0.05$.

4.3. Result and discussion

4.3.1. PLGA functionalization

CNTs have been used previously to deliver biological materials across the cell membrane including proteins, DNA, and RNA. Developing the proper surface functionalization for CNTs is the most critical step for a desired application. The two major types of functionalization for CNTs are non-covalent and covalent bonds [52].

Non-covalent binding is based on π-π stacking between the CNTs and aromatic groups from the linkers [180]. Liu et al. showed previously that DNA could be immobilized on pyrene derivatives of functionalized CNTs [270]. Other than these pyrene derivatives, single stranded DNA can also be used to immobilize CNTs [271], however DNA can be cleaved by serum, suggesting non-covalent reactions may not be stable in some cases [181]. For covalent binding, reactive groups are usually formed by various oxidation methods [175, 176] which allow for further modifications to enhance polymer [177], protein [178] and DNA [132] attachment. Functionalized CNTs can also be easily dispersed in water, which allows for forming supermolecular bioconjugates such as PLGA and PEG. PLGA is a FDA approved polymer for clinic use with the unique ability to control degradation rate, which allows us to tune the drug release profile. PEG is another commercially manufactured clinic material which has been used to conjugate with CNTs to deliver siRNA by the instant cleavage of S-S bond. PEG has only one type of functional group and smaller average molecular weight compared to PLGA. Further modifications are required to attach active biological cargoes to PEG and control its release profile. To this end, a novel CNT-PLGA based drug delivery system has several advantages including a high transfection rate, reduced toxicity, and a highly controlled drug release profile.

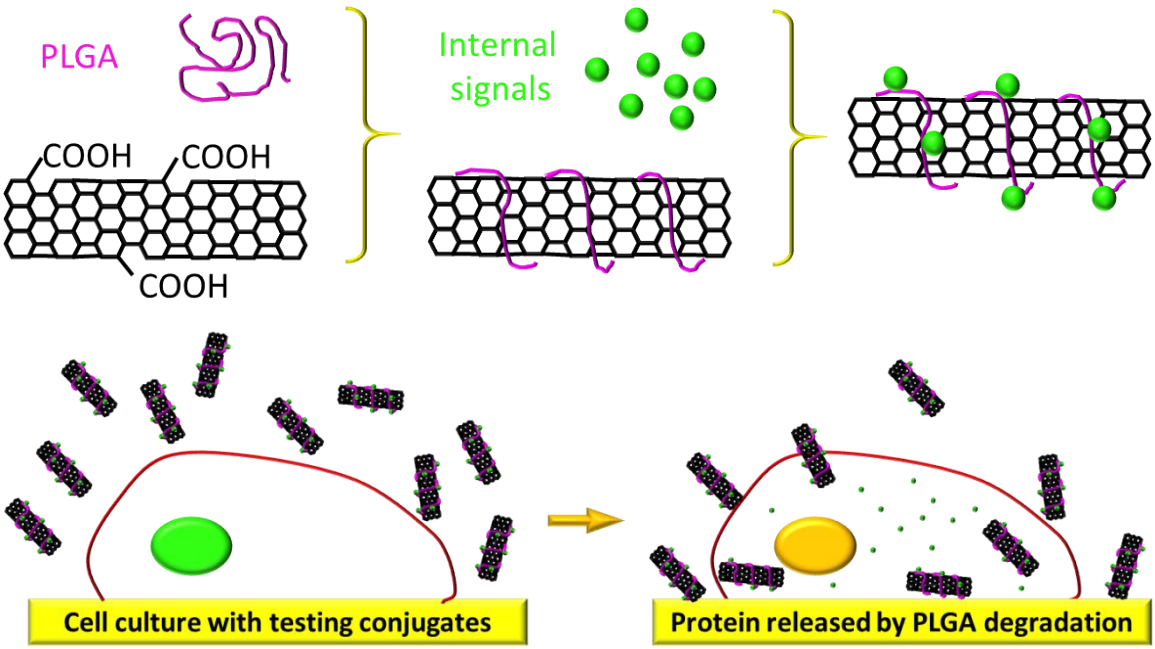

Figure 4. 1 Schematic of drug delivery into cells, carbon nanotubes is oxidized to form new carboxyl groups, linked with PLGA and functionalized by caspase-3. The conjugates penetrated into MG-63 cells and release caspase-3 by degradation of PLGA.

In this study, a novel CNT based drug delivery system as depicted in Figure 4. 1 was developed. In general, pristine CNTs as shown in Figure 4. 2 were oxidized in nitric acid to form carboxyl groups. Carboxyl groups of CNTs were then activated by oxalyl chloride forming CNT-acyl chloride and attached to the PLGA [177]. PLGA is able to provide attachment for the desired transcription factor CP3 by replacing chloride. The CNT-PLGA-CP3 conjugate can be easily dispersed in PBS without aggregation, which otherwise would hinder penetration of the cell membrane. Due to the enzymatic degradation of PLGA, CP3 would is able to be released gradually and induce cell apoptosis. The CNT-PLGA-CP3 conjugations are stable for weeks at -20 ^{o}C and the delivery profile can be tuned simply by changing the concentrations of PLGA.

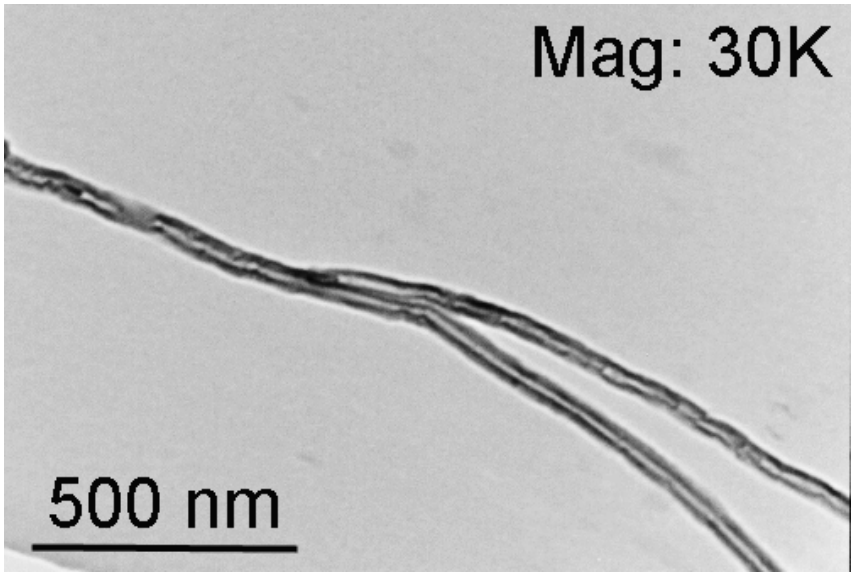

Figure 4. 2 TEM image of carbon nanotubes. The result showed that pristine carbon nanotubes has no outside coating. Our CNTs are about 5 μm in length with a diameter about 20 μm.

XRD, UV, IR and TEM were used to investigate the CNT-PLGA complex. In Figure 4. 3A, all XRD patterns were roughly the same in the region larger than 35 degrees which represents the crystal structure of the C-H bond, sp^2 hybrid C-C bond, and C-O bond [3]. However, PLGA patterns showed a peak, which denoted the amorphous region of PLGA polymers from 10-25 degree as shown in Figure 4. 3B. This peak can be determined as a characteristic of PLGA, which CNTs alone do not possess. A small peak at 22.7 degree for amorphous PLGA and a peak at 24.1 degree for CNTs were observed, indicating PLGA attachment to CNTs. However, this peak was not as pronounced as observed in pattern A. We believe only small amounts of PLGA were able to bind to CNTs resulting in a decreased signal.

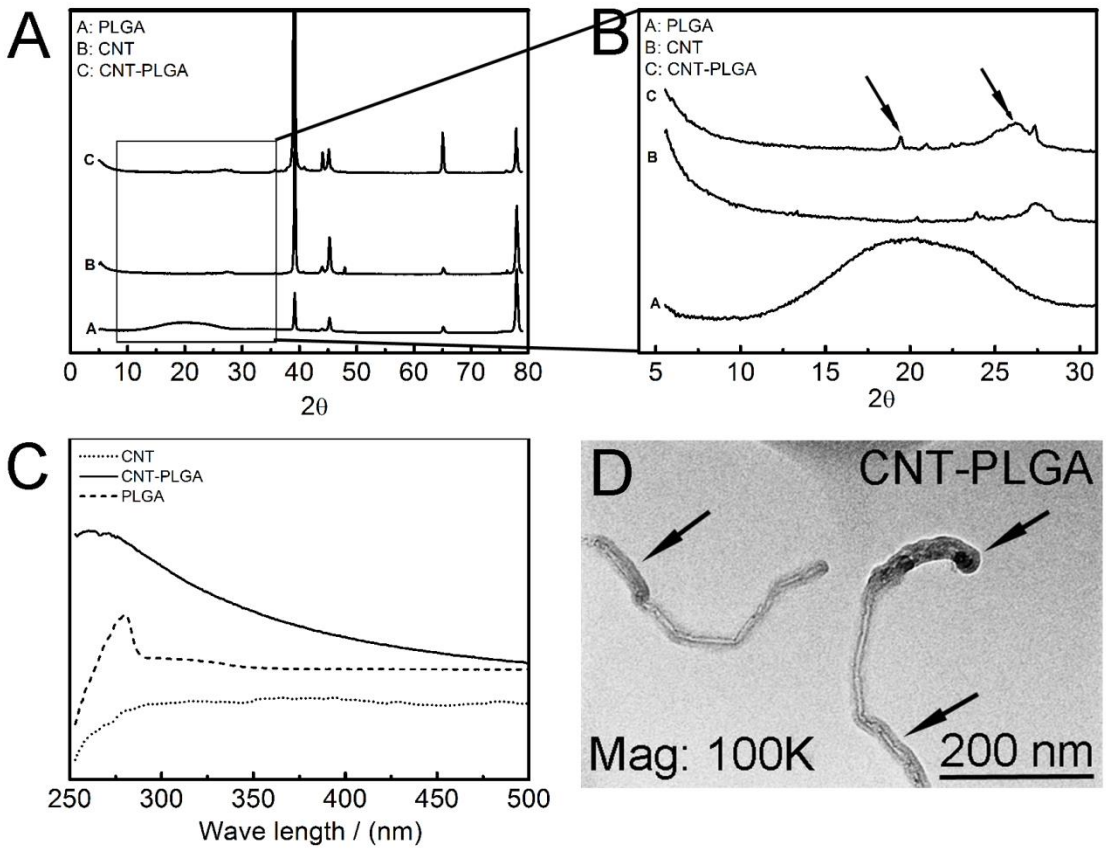

Figure 4. 3 Characterization of CNT-PLGA complex. A is XRD pattern, B is XRD pattern as well. C is UV-Vis spectrum, D is TEM image. Results showed that PLGA is successfully attached to carbon nanotubes. A small peak at 22.7 degree for amorphous PLGA and a peak at 24.1 degree for CNTs found in XRD pattern were indicating PLGA attachment to CNTs. UV absorption at 260 nm of CNT-PLGA indicated PLGA and CNTs were present. Dark PLGA layer clearly shown coated over the CNTs with a depth of several nanometers by TEM.

CNTs have a simple flat UV absorption and start to decrease from 280 nm as shown in Figure 4. 3C. PLGA didn't show a similar trend instead showing a strong absorption at 260 nm similar to Cheng's finding [272]. CNT-PLGA showed absorption at 260 nm indicating PLGA and a flat decreasing trend thereafter, indicating CNTs were present. This finding showed a similar trend to CNT-Paclitaxel [133]. Through FTIR spectra CNTs showed a typical sp^2 hybrid C-C stretching at 1200 cm^{-1}, while no O-H stretching was observed at 3400 cm^{-1} as shown in A. On the contrary, O-H stretching and

C=O stretching at 1650 cm^{-1} were observed in CNT-PLGA. This denoted a successful attachment of PLGA to the CNTs. In addition to FTIR, TEM was used to observe the PLGA linkage to CNTs. Pristine multi-wall CNTs in Figure 4. 2 with no PLGA functionalization was compared to the dark PLGA layer clearly shown coated over the CNTs with a depth of several nanometers in Figure 4. 3D.

4.3.2. Protein attachment

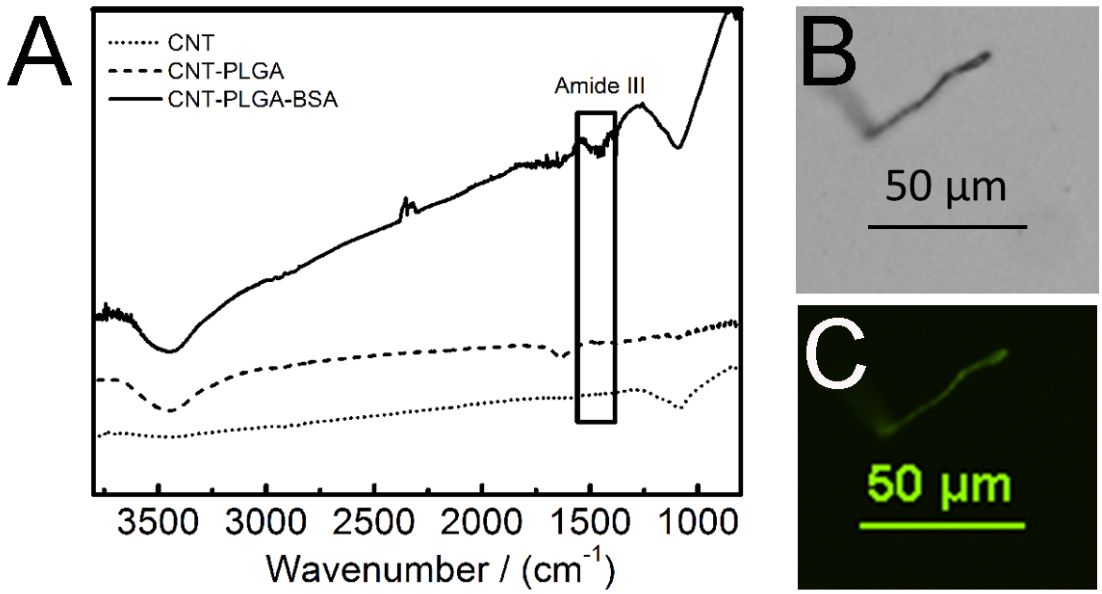

Figure 4. 4 Characterization of protein conjugation. A is Infra-red spectrum, B is light microscopy of CNT-PLGA-BSA, C is fluorescent images of CNT-PLGA-fBSA. Results showed that proteins has been successfully attached to CNT-PLGA complex, forming CNT-PLGA-BSA conjugates. CNT-PLGA-BSA showed a peak around 1400 cm^{-1} indicating amide III belt in IR, which is the typical peak of BSA. A single CNT-PLGA attached to fBSA was observed through immunofluorescence indicating successful conjugation.

DNA and RNA are the genetic material generally transported by functionalized CNTs. In 2004, Pantarotto discovered CNTs as a tool to transport DNA plasmids [128]. Further research found DNA was protected by CNTs during cellular uptake [273]. In

addition, Zhang et al. successfully transported telomerase inhibited small interference RNA into tumor cells and suppressed their growth [274]. However, researchers generally used protein fictionalization for stabilizing [275], labeling [276] and separating [277] CNTs rather than transporting functional protein to tune cellular behavior. Here, we were able to conjugate protein to CNT-PLGA complex.

Protein typically has a UV absorption at 280 nm due to sp^2 hybrid C-C in Phe, Tyr, and Trp which is a similar structure to CNTs. Protein also has a similar amorphous region in XRD pattern as most polymers. Therefore, XRD and UV are not appropriate methods to confirm protein attachment so we used FTIR and fluorescently tagged BSA to confirm the attachment of protein. As shown in Figure 4. 4A, CNT-PLGA-BSA showed a peak around 1400 cm^{-1} indicating amide III belt, which is the typical peak of BSA. fBSA was then used to attach to CNT-PLGA and in Figure 4. 4B and Figure 4. 4C, a single CNT-PLGA attached to fBSA was observed through immunofluorescence indicating successful conjugation. CNTs are generally auto fluorescent over 800 nm [278] but no fluorescent signal was observed at those wavelengths confirming the protein attachment.

4.3.3. Cellular transfection by CNT-PLGA-fBSA conjugates

The ideal vector to deliver biological material should have two basic characteristics being high efficiency and safety. In terms of efficiency, we investigated the cellular uptake ability of CNT-PLGA-fBSA and CNTs were found to have the ability to penetrate cells due to their nano-sized diameter and small radius to volume ratio [279]. In demonstrating the high efficiency to penetrate cells, we tested the transfection ability of CNT-PLGA-fBSA conjugations in different dosages.

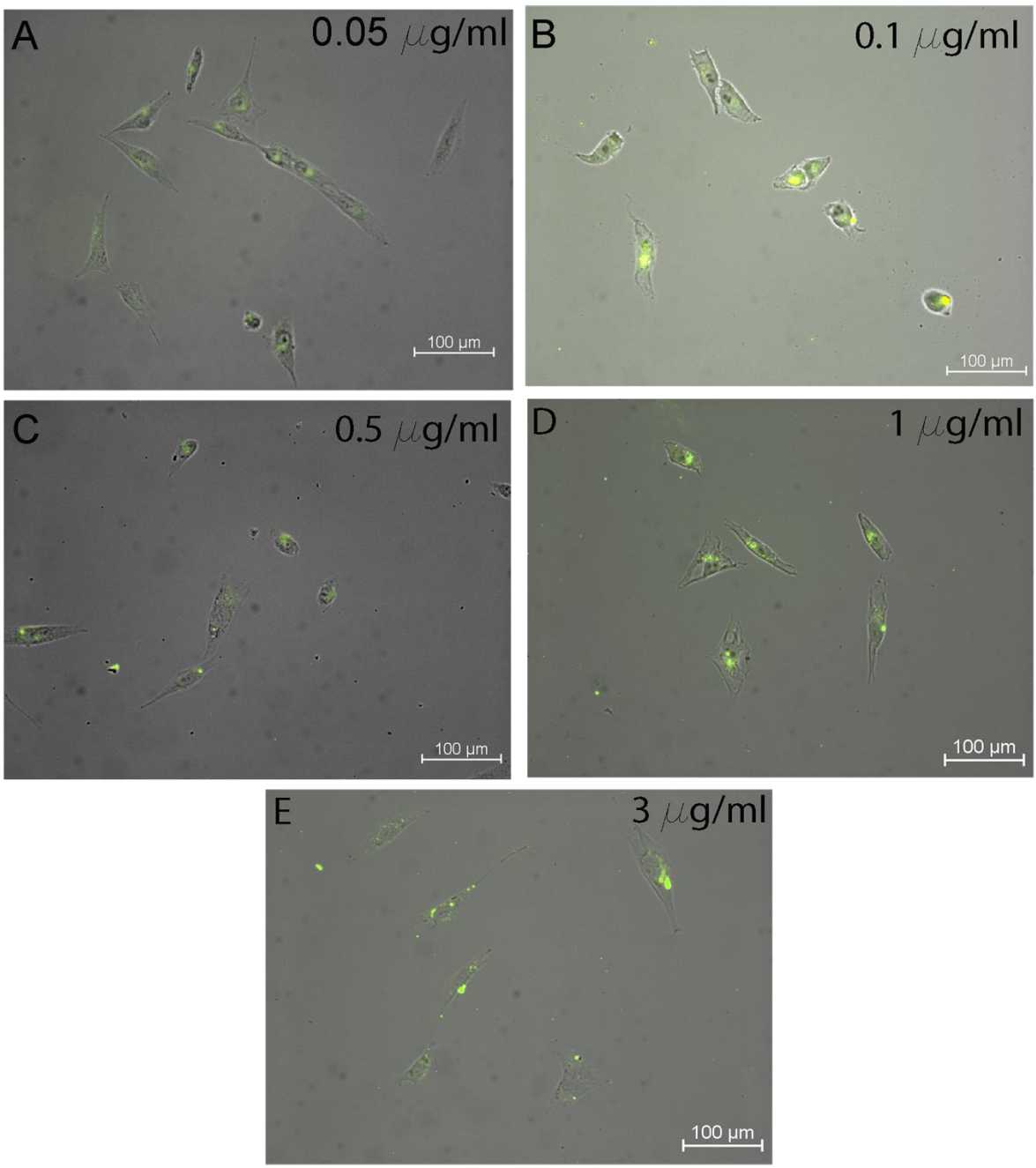

Figure 4. 5 Optic and fluorescent combined images of CNT-PLGA-fBSA delivery into MG-63 osteosarcoma cells. All images are 20 X. The dosage culture with osteosarcoma cells are 0.05 μg×ml^{-1}, 0.1 μg×ml^{-1}, 0.5 μg×ml^{-1}, 1 μg×ml^{-1} and 3 μg×ml^{-1}, respectively. The results showed that CNT-PLGA-fBSA can easily penetrate into cells and transduce osteosarcoma cells. The CNT-PLGA-fBSA conjugates showed a pronounced ability to penetrate cells with a transfection rate close to 100% at all conducted concentrations, ranging from 0.05 to 3 μg/ml.

In order to prevent non-specific background signals, cells were carefully washed to remove any non-penetrated CNT-PLGA-fBSA conjugates. We were able to observe fluorescent signals in cells as shown in Figure 4. 5. The CNT-PLGA-fBSA conjugates showed a pronounced ability to penetrate cells with a transfection rate close to 100% at all conducted concentrations, ranging from 0.05 to 3 μg/ml.

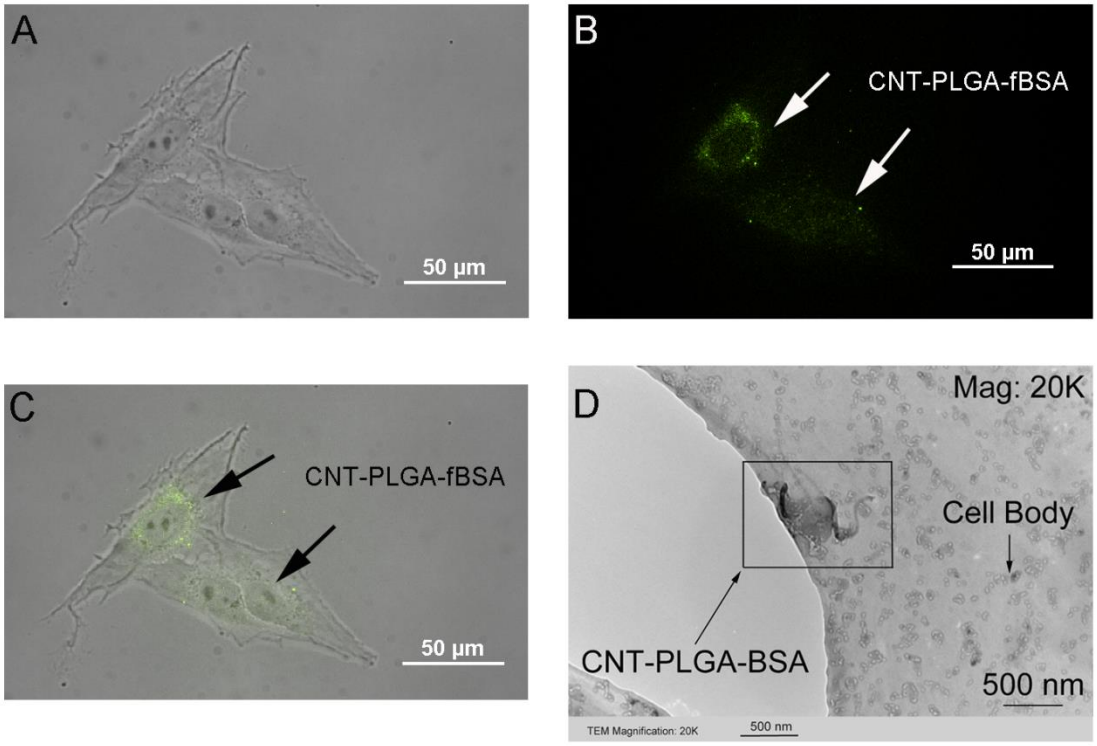

Figure 4. 6 Determination of carbon nanotubes delivered into osteosarcoma cells. The dosage 3 $\mu g \times ml^{-1}$. A is osteosarcoma cells cultured with CNT-PLGA-fBSA. B is image of fluorescent signal within osteosarcoma cells. C is the optic and fluorescent combined image of CNT-PLGA-fBSA image. D is the TEM image of a single CNT-PLGA-BSA penetrating the cell body. The results showed that the conjugates penetrate the cells.

The high magnification images of Figure 4. 6A, Figure 4. 6B, and Figure 4. 6C were able to show higher resolutions around the nuclei which showed higher fluorescent signal, coinciding where large amounts of ribosomes reside. This location of the CNT-PLGA-fBSA conjugate facilitates RNA and transcription factor delivery. TEM was also

used to confirm cell penetration as shown in Figure 4. 6D, where clearly there is a CNT-PLGA-BSA conjugate penetrating into the cytosol, demonstrating the ability of CNTs to transport material across the membrane. We have successfully achieved a transfection rate higher than the 30% or 40% attained by polymers and liposome nanoparticles indicating the promise in non-viral gene delivery vectors.

4.3.4. The efficacy of CNT-PLGA-CP3 in tuning apoptosis

Commonly used drugs for cancer therapies are alkalating agents, anti-metabolites, plant alkaloid and terpenoids, topoisomerase inhibitors, and cytotoxic antibiotics. These chemicals usually have side effects which not only kill cancer cells, but also induce necrosis of normal tissue. In order to prevent the side effects, we chose caspase-3 (CP3) as a potential candidate. CP3 is the key enzyme that is highly involved in the cell apoptosis pathway. Apoptosis is an organized process that signals cells to self-destruct for cell renewal or to control aberrant cell growth. Apoptosis controls the orderly death of damaged cells, whereas necrosis occurs as a result of tissue damage, causing the loss of both damaged and surrounding cells [280]. There are two routes for apoptosis pathway: intrinsic and extrinsic.

Intrinsic apoptotic stimuli, such as DNA damage or endoplasmic reticulum (ER) stress, activate B cell lymphoma 2 (BCL-2), homology 3 (BH3)-only proteins. This activation leads activate BCL-2-associated X protein (BAX) and BCL-2 antagonist or killer (BAK) and mitochondrial outer membrane permeabilization (MOMP). Following MOMP, release of various proteins from the mitochondrial intermembrane space promotes caspase activation and apoptosis. Cytochrome c binds apoptotic protease-

activating factor 1 (APAF1), inducing its oligomerization and thereby forming a structure termed the apoptosome that recruits and activates an initiator caspase: caspase-9. Caspase-9 cleaves and activates executioner caspases: caspase-3 and caspase-7, leading cells to apoptosis [281].

The extrinsic apoptotic pathway is initiated by the ligation of death receptors with their cognate ligands, leading to the recruitment of adaptor molecules such as FAS-associated death domain protein (FADD) and then caspase-8. This results in the dimerization and activation of caspase-8, which can then directly cleave and activate caspase-3 and caspase-7, leading to apoptosis [281]. What's interesting here is that caspase-3 is the downstream and key enzyme responsible in leading cells to apoptosis for both routes. Thus we chose caspase-3 for our study in cancer therapy.

We used MTT assays to test the cell viability as a standard to measure the ability of CNT-PLGA-CP3 to release CP3. The working concentration is set very low in order to eliminate cell necrosis induced by large amount of CNTs. Researchers has demonstrated that functionalized CNTs were found to be less toxic than pristine CNTs [282, 283] and pristine CNTs in low concentrations are also able to exhibit acceptable toxicity levels [284]. So cell death experienced in this experiment is attributed to the contribution of CP3 delivered into cells inducing apoptosis.

Pro-Ject is commercially available liposomes for protein delivery; we use Pro-Ject liposomes as a positive control in comparison to our CNT-PLGA-CP3 conjugation. As shown in Figure 4. 7A, no significant differences were observed in CNT-PLGA-CP3 groups on day 1, however, Pro-Ject groups showed significant difference in comparison. We attribute this to the fact that the degradation of PLGA hasn't fully allowed the release

of significant amounts of CP3 [285]. Pro-Ject liposomes released material with minimal differences in dosage on Day 1. We hypothesize that the average amount of CP3 delivered was significant enough to induce apoptosis even at minimal concentrations.

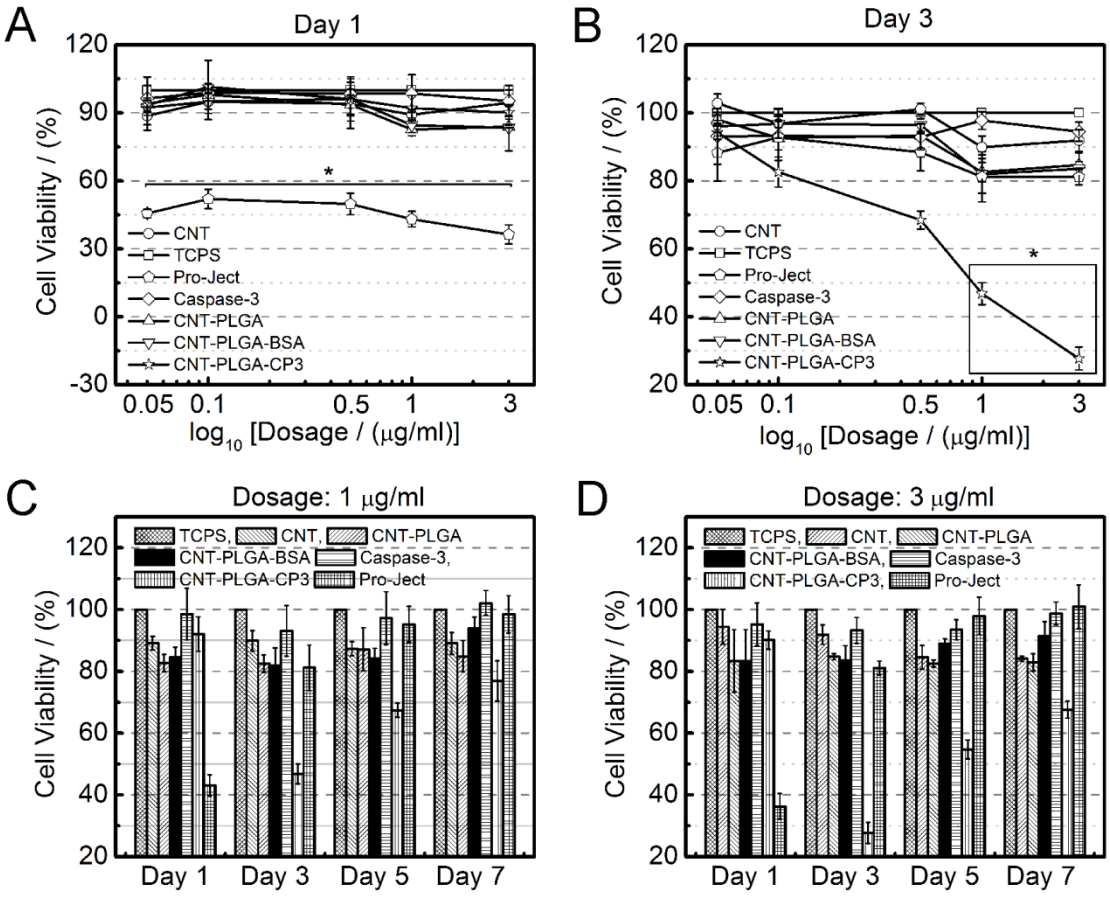

Figure 4. 7 Cell viability on day 1 (A) and day 3 (B) of MG-63 cells under exposure of different dosages of carbon nanoutbes, CNT-PLGA, CNT-PLGA-BSA, caspase-3, Pro-Ject and CNT-PLGA-CP3 treatment. * means significant difference of cell viability under CNT-PLGA-CP3 cojugates exposure and other groupes of same dosage. Results showed that carbon nanotubes have a great ability to penetrate cells and release caspase-3. Our conjugation can release caspase-3 in a week.

Interestingly, the cell viability of all Pro-Ject liposome samples average at approximately 50%. Considering the CP3 was enough to induce apoptosis, the efficiency of Pro-Ject liposome groups was close to 50%. Figure 4. 7B shows the cell viability of

CNT-PLGA-CP3 treated samples were significantly small compared to positive and negative controls on Day 3. Pro-Ject liposome groups treated samples showed minimal differences in this case, indicating there was little to no consistency of material delivery over long periods. Conjugate dosage played an important role in inducing cell apoptosis with no significant differences observed between CNT-PLGA-CP3 in low dosages and controls while CNT-PLGA-CP3 conjugates in high concentration exhibited a significantly low cell viability compared to other controls. We believe the amount of transcription factor reacting with the CNT-PLGA complex is same but the amount of CP3 released was highly dependent on the conjugate dosage.

We also conducted long-term cell viability tests at two high dosages with no additional treatments throughout the experiment. The results shown in Figure 4. 7C and Figure 4. 7D show that cell viability was still suppressed by treating 1 µg/ml CNT-PLGA-CP3 on Day 5 and 3 µg/ml CNT-PLGA-CP3 on Day 7, respectively. Note that cancer cells were able to recover and become fully confluent under Pro-Ject liposome groups between Day 1 and Day 3. We believe CP3 is superior due to the gradual release profile. To further demonstrate this point *in vitro*, we carried out BSA release profile *in vitro*.

In order to detect the BSA release with a UV-Vis spectrometer, we increased the amount of BSA (200 µg compared to 5 µg of caspase-3) reacting with the CNT-PLGA complex. This increased amount of BSA resulted in BSA released at detectable levels through UV-Vis spectrometer. A calibration curve was made to calculate the protein concentration (Figure 4. 8). The protein loaded onto 100 µg of CNT-PLGA was 119±6.73 µg per 200 µg. We observed a gradual release of BSA through the time points

in the 10-day trial (). Throughout the first two days we saw only a slight release of BSA while more than 5 µg of BSA was released after Day 7. This is a possible explanation for the CNT-PLGA-CP3 conjugates showing limited inhibitory effects on Day 1 while the CNT-PLGA-CP3 conjugates showed significantly higher inhibitory effects after Day 3. With only 5 µg of CP3 in the starting reaction, this may help explain the inhibitory effects on cell growth diminishing after Day 7. We also observed an increase in BSA released from Day 8 to Day 10. This is because the large molecular weight PLGA was hydrolyzed to a small fraction, which leads to an increase in protein release. Due to the fact that the CNT-PLGA-CP3 conjugates face a more complicated enzymatic environment, it is extremely difficult to quantitatively monitor the release profile *in situ*. However, this release profile data in combination with our cytotoxicity data give us confidence in the reliability of our results.

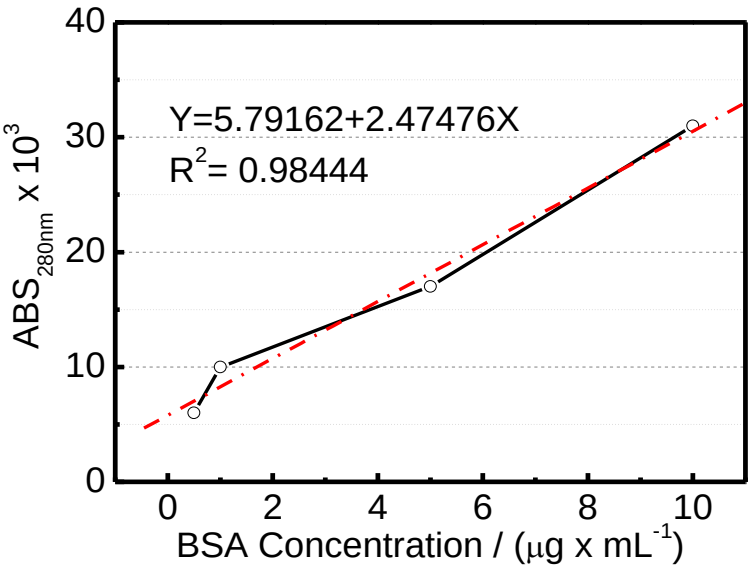

Figure 4. 8 Calibration curve of BSA concentration vs UV aborption at 280 nm.

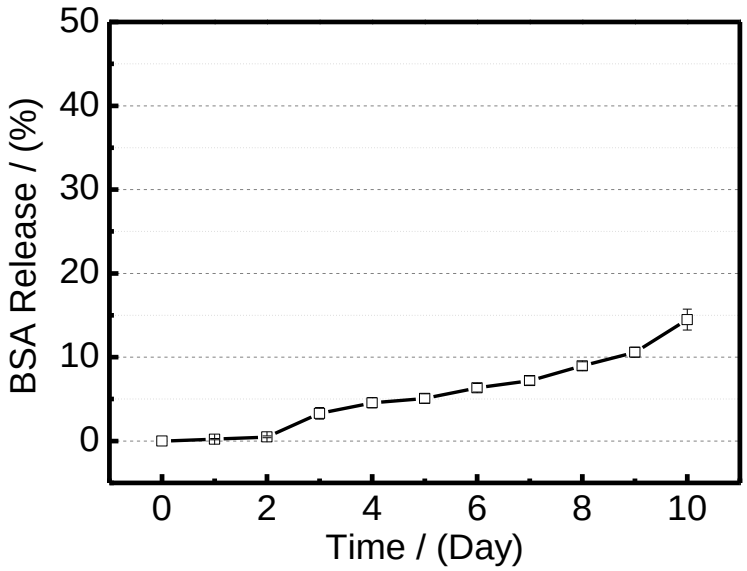

Figure 4. 9. BSA release fraction from the CNT-PLGA-BSA conjugates at predetermined time points. CNT-PLGA-BSA dispersed in PBS was incubated in a water bath (37^{o}C).

4.4. Conclusions

We were able to successfully fabricate a CNT-PLGA system, which is able to deliver biological material including genes, transcriptional factors, and signal molecules into cells. This system has shown a high transfection rate and a reliable, time dependent release profile. Yet another advantage to this system is that the releasing profile can be tuned simply by controlling the molecular weight and ratio of PLGA.

In determining the release profiles of the CNT-PLGA with differing PLGA to PGA and molecular weights, we simplified the experiment using PLGA nanoparticles as an alternative. A calibration curve was made (Figure 4. 10). We observed in general that resveratrol was gradually released from all three groups of PLGA nanoparticles (Figure 4. 11). Note that because the resveratrol was not covalently bound to the PLGA, the

release fraction of resveratrol is higher than that of BSA, which is covalently bound to the CNT-PLGA complex. The amount of resveratrol loaded on to the PLGA nanoparticles are 38%, 36%, and 40%. Interestingly, the 3 groups of PLGA nanoparticles showed different trends of release profiles with the smaller molecular weight PLGA nanoparticles releasing more resveratrol than the higher molecular weight counterparts. Considering the method to covalently bind the protein to the CNT-PLGA, the conjugates would require more time for the same fraction of BSA released.

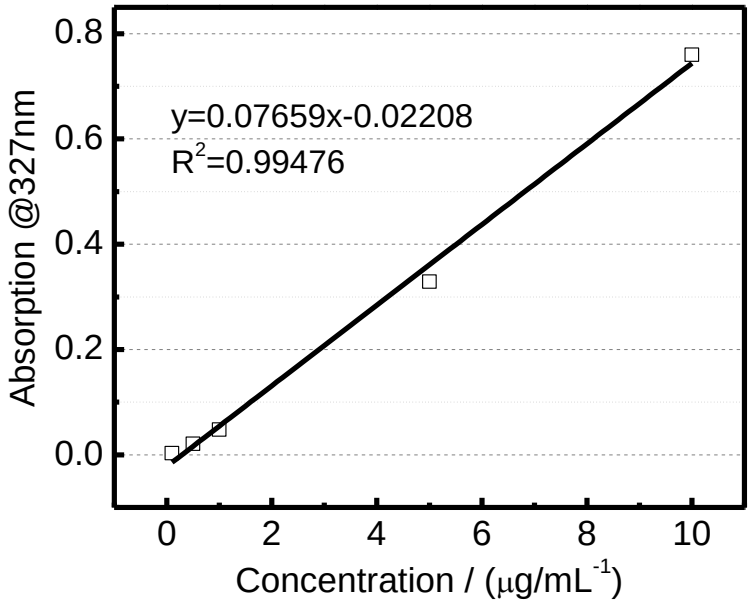

Figure 4. 10. Calibration curve of resveratrol concentration versus UV absorption at 327 nm.

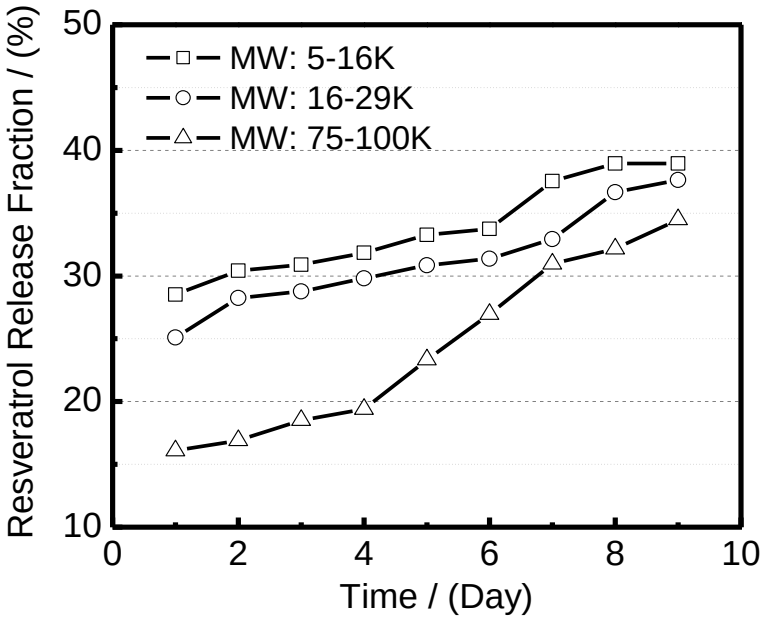

Figure 4. 11 Resveratrol release fraction from the PLGA nanoparticles. PLGA nanoparticles were made from PLGA with differing ratios of PLA to PGA and molecular weight (5,000-16,000/50:50, 16,000-29,000/50:50 and 75,000-100,000/75:25). Resveratrol was released more at the same time point by nanoparticles made by low molecular weight PLGA.

In all aspects, this CNT-PLGA-protein conjugation is a highly efficient and promising as drug delivery system with possible future applications in both treating cancer and directing cellular behavior through intracellular pathways. More attractively, despite the self-fluorescence of CNTs, fluoresce proteins can be conjugated to CNTs for the purpose of imaging hazard distribution, drug bio distribution and disease detection.

The most innovative aspect of our conjugates is that our DDS system based on CNT-PLGA is that we can tune the temporal release profile by controlling the molecular weight and PGA to PLA ratio, which so far has not been established yet. By employing this DDS system, we can incorporate a cocktail of the drugs either for cancer treatment or

stem differentiation, and deliver this cocktail of drugs sequentially by just one shot. This invention would help patients release at significant level.

CHAPTER 5

Summary

CNTs for biomedical engineering has been an emerging area. CNTs are promising candidate in tissue engineering, biomedical imaging and gene delivery. In the previous three chapters, we demonstrated the ability of CNTs as extracellular and intracellular cues to control cellular behaviors.

As extracellular matrix, we developed an aligned CNT substrate to align HUVEC and culture hESCs at single cell level (Chapter2). We functionalized carboxyl CNTs with the ligand proteins and aligned these CNT-ligand conjugates on an Au coated glass substrate by spin coating. With this our newly developed CNT substrate, we can culture hESCs at single cell level, and can control their migrating as demonstrated by HUVEC. This was the great novelty in the Chapter 2. By culturing single hESC, we can take a step forward to different single hESCs to desired phenotype with limited heterogeneity. This would allow us for better understanding differentiation of hESC at single cell level.

We also developed a CNT containing PLGA scaffolds for bone regeneration in Chapter 3. Mechanically strengthened CNT/PLGA scaffolds were fabricated through a dispersion of CNT in PLGA/dichloromethane solution followed by a solvent casting and particulate leaching step. The incorporation of CNTs allowed for tuning the mechanical strength and nano roughness without compromising the porous architecture of scaffolds.

Our results demonstrated that the addition of CNT to PLGA scaffolds led to a significant increase in adhesion, growth and osteogenic differentiation of cells. We were able to confirm the coupling of matrix stiffness and mechanical strength to enhanced osteogenesis in 3D environment by those results. Note that previous reports have just related only one of these two aspects to osteogenesis. Our results first demonstrated mechanical strength and nano roughness were link to osteogenesis together. This finding demonstrated CNTs to be a powerful tool in scaffolds design for stem cell based tissue engineering.

As intracellular cue vesicles, a number of biological cargo has been already delivered intracellularly by a several types of linkers such as PEG or not. We developed a new CNT-PLGA conjugate to delivery biological cargoes into cells in Chapter 5. This system waas able to deliver biological material including genes, transcriptional factors, and signal molecules into cells with a high efficiency. The most innovative aspect of our conjugates was that our DDS system based on CNT-PLGA can tune the temporal release profile by controlling the molecular weight and PGA to PLA ratio, which so far has not been established yet. By employing this DDS system, we can incorporate a cocktail of the drugs either for cancer treatment or stem differentiation, and deliver this cocktail of drugs sequentially by just one shot. This invention would help patients relieved at significant level. More attractively, despite the self-fluorescence of CNTs, fluoresce proteins can be conjugated to CNTs for the purpose of imaging the hazard distribution, drug bio distribution and disease detection.

REFERENCE

[1] Iijima S. Helical Microtubules of Graphitic Carbon. Nature. 1991;354:56-8.

[2] Baughman RH, Zakhidov AA, de Heer WA. Carbon nanotubes - the route toward applications. Science. 2002;297:787-92.

[3] O'Connell M. Carbon nanotubes : properties and applications. Boca Raton, FL: CRC/Taylor & Francis; 2006.

[4] Flahaut E, Bacsa R, Peigney A, Laurent C. Gram-scale CCVD synthesis of double-walled carbon nanotubes. Chem Commun (Camb). 2003:1442-3.

[5] Liu L, Guo GY, Jayanthi CS, Wu SY. Colossal paramagnetic moments in metallic carbon nanotori. Phys Rev Lett. 2002;88:217206.

[6] Nasibulin AG, Pikhitsa PV, Jiang H, Brown DP, Krasheninnikov AV, Anisimov AS, et al. A novel hybrid carbon material. Nat Nanotechnol. 2007;2:156-61.

[7] Abou-Hamad E, Kim Y, Wagberg T, Boesch D, Aloni S, Zettl A, et al. Molecular dynamics and phase transition in one-dimensional crystal of C(60) encapsulated inside single wall carbon nanotubes. ACS Nano. 2009;3:3878-83.

[8] Saito N, Usui Y, Aoki K, Narita N, Shimizu M, Hara K, et al. Carbon nanotubes: biomaterial applications. Chemical Society reviews. 2009;38:1897-903.

[9] Fu CF, Gu LX. Composite Fibers from Poly(vinyl alcohol) and Poly(vinyl alcohol)-Functionalized Multiwalled Carbon Nanotubes. J Appl Polym Sci. 2013;128:1044-53.

[10] Lin TC, Huang BR. Temperature effect on hydrogen response for cracked carbon nanotube/nickel (CNT/Ni) composite film with horizontally aligned carbon nanotubes. Sensor Actuat B-Chem. 2013;185:548-52.

[11] Wang HF, Muren NB, Ordinario D, Gorodetsky AA, Barton JK, Nuckolls C. Transducing methyltransferase activity into electrical signals in a carbon nanotube-DNA device. Chem Sci. 2012;3:62-5.

[12] Cheon JH, Lim J, Seo SM, Woo JM, Kim SH, Kwon Y, et al. Electrical Characteristics of the Concentric-Shape Carbon Nanotube Network Device in pH Buffer Solution. Ieee T Electron Dev. 2010;57:2684-9.

[13] Jeong H, Gweon HM, Kwon BJ, Ahn YH, Park JY. Uncovering operational mechanisms of a single-walled carbon nanotube network device using local probe electrical characterizations. Nanotechnology. 2009;20.

[14] Lee J, Liao A, Pop E, King WP. Electrical and Thermal Coupling to a Single-Wall Carbon Nanotube Device Using an Electrothermal Nanoprobe. Nano Letters. 2009;9:1356-61.

[15] Silambarasan D, Surya VJ, Vasu V, Iyakutti K. One-step process of hydrogen storage in single walled carbon nanotubes-tin oxide nano composite. Int J Hydrogen Energ. 2013;38:4011-6.

[16] Chen L, Xia KS, Huang LZ, Li LW, Pei LB, Fei SX. Facile synthesis and hydrogen storage application of nitrogen-doped carbon nanotubes with bamboo-like structure. Int J Hydrogen Energ. 2013;38:3297-303.

[17] Vozzi G, Corallo C, Daraio C. Pressure-activated microsyringe composite scaffold of poly(L-lactic acid) and carbon nanotubes for bone tissue engineering. J Appl Polym Sci. 2013;129:528-36.

[18] Liao CZ, Li K, Wong HM, Tong WY, Yeung KWK, Tjong SC. Novel polypropylene biocomposites reinforced with carbon nanotubes and hydroxyapatite nanorods for bone replacements. Mat Sci Eng C-Mater. 2013;33:1380-8.

[19] Cheng Q, Rutledge K, Jabbarzadeh E. Carbon nanotube-poly(lactide-co-glycolide) composite scaffolds for bone tissue engineering applications. Ann Biomed Eng. 2013;41:904-16.

[20] Minati L, Antonini V, Dalla Serra M, Speranza G. Multifunctional Branched Gold-Carbon Nanotube Hybrid for Cell Imaging and Drug Delivery. Langmuir. 2012;28:15900-6.

[21] Liu D, Wang ZG, Wang LJ, Cuschieri A. Finite Element Study of Carbon Nanotube Induced Cell Membrane Poration for Drug and Gene Delivery. J Med Imag Health In. 2012;2:132-8.

[22] Liu Z, Winters M, Holodniy M, Dai HJ. siRNA delivery into human T cells and primary cells with carbon-nanotube transporters. Angew Chem Int Edit. 2007;46:2023-7.

[23] Takagi D, Homma Y, Hibino H, Suzuki S, Kobayashi Y. Single-walled carbon nanotube growth from highly activated metal nanoparticles. Nano Letters. 2006;6:2642-5.

[24] Garcia-Cespedes J, Rubio-Roy M, Polo MC, Pascual E, Andujar U, Bertran E. Carbon nanotubes grown by asymmetric bipolar pulsed-DC PECVD. Diam Relat Mater. 2007;16:1131-5.

[25] Coleman JN, Khan U, Blau WJ, Gun'ko YK. Small but strong: A review of the mechanical properties of carbon nanotube-polymer composites. Carbon. 2006;44:1624-52.

[26] Overney G, Zhong W, Tomanek D. Structural Rigidity and Low-Frequency Vibrational-Modes of Long Carbon Tubules. Z Phys D Atom Mol Cl. 1993;27:93-6.

[27] Wong EW, Sheehan PE, Lieber CM. Nanobeam mechanics: Elasticity, strength, and toughness of nanorods and nanotubes. Science. 1997;277:1971-5.

[28] Yu MF, Lourie O, Dyer MJ, Moloni K, Kelly TF, Ruoff RS. Strength and breaking mechanism of multiwalled carbon nanotubes under tensile load. Science. 2000;287:637-40.

[29] Yu MF, Files BS, Arepalli S, Ruoff RS. Tensile loading of ropes of single wall carbon nanotubes and their mechanical properties. Phys Rev Lett. 2000;84:5552-5.

[30] Filleter T, Bernal R, Li S, Espinosa HD. Ultrahigh Strength and Stiffness in Cross-Linked Hierarchical Carbon Nanotube Bundles. Adv Mater. 2011;23:2855-+.

[31] Jiang YY, Zhou W, Kim T, Huang Y, Zuo JM. Measurement of radial deformation of single-wall carbon nanotubes induced by intertube van der Waals forces. Phys Rev B. 2008;77.

[32] Ruoff RS, Tersoff J, Lorents DC, Subramoney S, Chan B. Radial Deformation of Carbon Nanotubes by Van-Der-Waals Forces. Nature. 1993;364:514-6.

[33] Zhao B, Hu H, Mandal SK, Haddon RC. A bone mimic based on the self-assembly of hydroxyapatite on chemically functionalized single-walled carbon nanotubes. Chem Mater. 2005;17:3235-41.

[34] Zanello LP, Zhao B, Hu H, Haddon RC. Bone cell proliferation on carbon nanotubes. Nano Letters. 2006;6:562-7.

[35] Botti S. Physical properties of carbon nanotubes. Kerala, India: Transworld Research Network; 2007.

[36] Sharma A, Tomar M, Gupta V. Room temperature trace level detection of NO2 gas using SnO2 modified carbon nanotubes based sensor. J Mater Chem. 2012;22:23608-16.

[37] Ghaddab B, Sanchez JB, Mavon C, Paillet M, Parret R, Zahab AA, et al. Detection of O-3 and NH3 using hybrid tin dioxide/carbon nanotubes sensors: Influence of materials and processing on sensor's sensitivity. Sensor Actuat B-Chem. 2012;170:67-74.

[38] Vanhove L. The Occurrence of Singularities in the Elastic Frequency Distribution of a Crystal. Phys Rev. 1953;89:1189-93.

[39] Miyauchi Y, Oba M, Maruyama S. Cross-polarized optical absorption of single-walled nanotubes by polarized photoluminescence excitation spectroscopy. Phys Rev B. 2006;74.

[40] Iakoubovskii K, Minami N, Kim Y, Miyashita K, Kazaoui S, Nalini B. Midgap luminescence centers in single-wall carbon nanotubes created by ultraviolet illumination. Appl Phys Lett. 2006;89.

[41] Iakoubovskii K, Minami N, Ueno T, Kazaoui S, Kataura H. Optical characterization of double-wall carbon nanotubes: Evidence for inner tube shielding. J Phys Chem C. 2008;112:11194-8.

[42] Kataura H, Kumazawa Y, Maniwa Y, Umezu I, Suzuki S, Ohtsuka Y, et al. Optical properties of single-wall carbon nanotubes. Synthetic Met. 1999;103:2555-8.

[43] Miyata Y, Yanagi K, Maniwa Y, Kataura H. Optical properties of metallic and semiconducting single-wall carbon nanotubes. Phys Status Solidi B. 2008;245:2233-8.

[44] Ximenes JCM, Melo GC, Melo VMM, Mendes J, Souza AG. Optical properties of single wall carbon nanotubes dispersed in biopolymers. J Phys Chem Solids. 2012;73:232-6.

[45] Mizuno K, Ishii J, Kishida H, Hayamizu Y, Yasuda S, Futaba DN, et al. A black body absorber from vertically aligned single-walled carbon nanotubes. P Natl Acad Sci USA. 2009;106:6044-7.

[46] Souza AG, Chou SG, Samsonidze GG, Dresselhaus G, Dresselhaus MS, An L, et al. Stokes and anti-Stokes Raman spectra of small-diameter isolated carbon nanotubes. Phys Rev B. 2004;69.

[47] Fantini C, Jorio A, Souza M, Strano MS, Dresselhaus MS, Pimenta MA. Optical transition energies for carbon nanotubes from resonant Raman spectroscopy: Environment and temperature effects. Phys Rev Lett. 2004;93.

[48] Thostenson ET, Li CY, Chou TW. Nanocomposites in context. Compos Sci Technol. 2005;65:491-516.

[49] Sinha S, Barjami S, Iannacchione G, Schwab A, Muench G. Off-axis thermal properties of carbon nanotube films. J Nanopart Res. 2005;7:651-7.

[50] Li SH, Feng L, Li HJ, Zhai J, Song YL, Jiang L, et al. Super-hydrophobicity of post-like aligned carbon nanotube films. Chem J Chinese U. 2003;24:340-2.

[51] Aschberger K, Johnston HJ, Stone V, Aitken RJ, Hankin SM, Peters SA, et al. Review of carbon nanotubes toxicity and exposure--appraisal of human health risk assessment based on open literature. Critical reviews in toxicology. 2010;40:759-90.

[52] Liu Z, Tabakman S, Welsher K, Dai HJ. Carbon Nanotubes in Biology and Medicine: In vitro and in vivo Detection, Imaging and Drug Delivery. Nano Res. 2009;2:85-120.

[53] Tournus F, Latil S, Heggie MI, Charlier JC. pi-stacking interaction between carbon nanotubes and organic molecules. Phys Rev B. 2005;72.

[54] Petrov P, Stassin F, Pagnoulle C, Jerome R. Noncovalent functionalization of multi-walled carbon nanotubes by pyrene containing polymers. Chemical communications. 2003:2904-5.

[55] Zimmerli U, Koumoutsakos P. Simulations of electrophoretic RNA transport through transmembrane carbon nanotubes. Biophys J. 2008;94:2546-57.

[56] Ostojic GN, Ireland JR, Hersam MC. Noncovalent functionalization of DNA-wrapped single-walled carbon nanotubes with platinum-based DNA cross-linkers. Langmuir. 2008;24:9784-9.

[57] Simmons TJ, Bult J, Hashim DP, Linhardt RJ, Ajayan PM. Noncovalent functionalization as an alternative to oxidative acid treatment of single wall carbon nanotubes with applications for polymer composites. Acs Nano. 2009;3:865-70.

[58] Xue CH, Zhou RJ, Shi MM, Gao Y, Wu G, Zhang XB, et al. The preparation of highly water-soluble multi-walled carbon nanotubes by irreversible noncovalent functionalization with a pyrene-carrying polymer. Nanotechnology. 2008;19:215604.

[59] Cheng F, Adronov A. Noncovalent functionalization and solubilization of carbon nanotubes by using a conjugated Zn-porphyrin polymer. Chemistry. 2006;12:5053-9.

[60] Chng EL, Pumera M. Nanographite impurities in carbon nanotubes: their influence on the oxidation of insulin, nitric oxide, and extracellular thiols. Chemistry. 2012;18:1401-7.

[61] Yeh JM, Chang KC, Peng CW, Lai MC, Hwang SS, Lin HR, et al. Enhancement in insulation and mechanical properties of PMMA nanocomposite foams infused with multi-walled carbon nanotubes. J Nanosci Nanotechnol. 2011;11:6757-64.

[62] Khandare JJ, Jalota-Badhwar A, Satavalekar SD, Bhansali SG, Aher ND, Kharas F, et al. PEG-conjugated highly dispersive multifunctional magnetic multi-walled carbon nanotubes for cellular imaging. Nanoscale. 2012;4:837-44.

[63] Moghaddam MJ, Yang W, Bojarski B, Gengenbach TR, Gao M, Zareie H, et al. Azide photochemistry for facile modification of graphitic surfaces: preparation of DNA-coated carbon nanotubes for biosensing. Nanotechnology. 2012;23:425503.

[64] Liu C, Zhang Q, Stellacci F, Marzari N, Zheng L, Zhan Z. Carbene-functionalized single-walled carbon nanotubes and their electrical properties. Small. 2011;7:1257-63.

[65] Bayazit MK, Coleman KS. Fluorescent single-walled carbon nanotubes following the 1,3-dipolar cycloaddition of pyridinium ylides. J Am Chem Soc. 2009;131:10670-6.

[66] Lutolf MP, Hubbell JA. Synthetic biomaterials as instructive extracellular microenvironments for morphogenesis in tissue engineering. Nat Biotechnol. 2005;23:47-55.

[67] Conrad ME, Umbreit JN. A concise review: iron absorption--the mucin-mobilferrin-integrin pathway. A competitive pathway for metal absorption. American journal of hematology. 1993;42:67-73.

[68] Discher DE, Janmey P, Wang YL. Tissue cells feel and respond to the stiffness of their substrate. Science. 2005;310:1139-43.

[69] Lo CM, Wang HB, Dembo M, Wang YL. Cell movement is guided by the rigidity of the substrate. Biophys J. 2000;79:144-52.

[70] Lo CM, Wang YL. Guidance of cell movement by substrate rigidity. Mol Biol Cell. 1999;10:259a-a.

[71] Shier D, Butler J, Lewis R. Hole's human anatomy & physiology. 12th ed. Dubuque: McGraw-Hill; 2010.

[72] Goldberg VM, Stevenson S, Feighan J, Davy D. Biology of Grit-Blasted Titanium-Alloy Implants. Clin Orthop Relat R. 1995:122-9.

[73] Feighan JE, Goldberg VM, Davy D, Parr JA, Stevenson S. The Influence of Surface-Blasting on the Incorporation of Titanium-Alloy Implants in a Rabbit Intramedullary Model. Journal of Bone and Joint Surgery-American Volume. 1995;77:1380-95.

[74] D'Lima DD, Lemperle SM, Chen PC, Holmes RE, Colwell CW, Jr. Bone response to implant surface morphology. The Journal of arthroplasty. 1998;13:928-34.

[75] Walboomers XF, Croes HJE, Ginsel LA, Jansen JA. Contact guidance of rat fibroblasts on various implant materials. J Biomed Mater Res. 1999;47:204-12.

[76] Lampin M, WarocquierClerout R, Legris C, Degrange M, SigotLuizard MF. Correlation between substratum roughness and wettability, cell adhesion, and cell migration. J Biomed Mater Res. 1997;36:99-108.

[77] D'Angelo F, Armentano I, Mattioli S, Crispoltoni L, Tiribuzi R, Cerulli GG, et al. Micropatterned Hydrogenated Amorphous Carbon Guides Mesenchymal Stem Cells Towards Neuronal Differentiation. Eur Cells Mater. 2010;20:231-44.

[78] Curtis A, Wilkinson C. New depths in cell behaviour: reactions of cells to nanotopography. Biochem Soc Symp. 1999:15-26.

[79] Blaese RM. The Ada Human Gene-Therapy Clinical Protocol. Hum Gene Ther. 1990;1:327-9.

[80] Anderson WF. Human gene therapy. Nature. 1998;392:25-30.

[81] Sun YS, Finger C, Alvarez-Vallina L, Cichutek K, Buchholz CJ. Chronic gene delivery of interferon-inducible protein 10 through replication-competent retrovirus vectors suppresses tumor growth. Cancer Gene Ther. 2005;12:900-12.

[82] Hoffman RM. Noninvasive imaging for evaluation of the systemic delivery of capsid-modified adenovirus in an orthotopic model of advanced lung cancer. Cancer. 2007;109:1213-.

[83] Marks WJ, Ostrem JL, Verhagen L, Starr PA, Larson PS, Bakay RAE, et al. Safety and tolerability of intraputaminal delivery of CERE-120 (adeno-associated virus serotype 2-neurturin) to patients with idiopathic Parkinson's disease: an open-label, phase I trial. Lancet Neurol. 2008;7:400-8.

[84] Yang XZ, Dou S, Sun TM, Mao CQ, Wang HX, Wang J. Systemic delivery of siRNA with cationic lipid assisted PEG-PLA nanoparticles for cancer therapy. J Control Release. 2011;156:203-11.

[85] Na K, Lee KH, Lee DH, Bae YH. Biodegradable thermo-sensitive nanoparticles from poly(L-lactic acid)/poly(ethylene glycol) alternating multi-block copolymer for potential anti-cancer drug carrier. Eur J Pharm Sci. 2006;27:115-22.

[86] Xu JS, Huang JW, Qin RG, Hinkle GH, Povoski SP, Martin EW, et al. Synthesizing and binding dual-mode poly (lactic-co-glycolic acid) (PLGA) nanobubbles for cancer targeting and imaging. Biomaterials. 2010;31:1716-22.

[87] Kim TH, Jin H, Kim HW, Cho MH, Cho CS. Mannosylated chitosan nanoparticle-based cytokine gene therapy suppressed cancer growth in BALB/c mice bearing CT-26 carcinoma cells. Mol Cancer Ther. 2006;5:1723-32.

[88] Nicklas M, Schatton W, Heinemann S, Hanke T, Kreuter J. Preparation and characterization of marine sponge collagen nanoparticles and employment for the transdermal delivery of 17 beta-estradiol-hemihydrate. Drug Dev Ind Pharm. 2009;35:1035-42.

[89] Ge J, Min SH, Kim DM, Lee DC, Park KC, Yeom YI. Selective gene delivery to cancer cells secreting matrix metalloproteinases using a gelatin/polyethylenimine/DNA complex. Biotechnol Bioproc E. 2012;17:160-7.

[90] Bremmell KE, Tan A, Martin A, Prestidge CA. Tableting lipid-based formulations for oral drug delivery: a case study with silica nanoparticle-lipid-mannitol hybrid microparticles. J Pharm Sci. 2013;102:684-93.

[91] Wang G, Zheng L, Zhao H, Miao J, Sun C, Ren N, et al. In vitro assessment of the differentiation potential of bone marrow-derived mesenchymal stem cells on genipin-chitosan conjugation scaffold with surface hydroxyapatite nanostructure for bone tissue engineering. Tissue engineering Part A. 2011;17:1341-9.

[92] Park JU, Meitl MA, Hur SH, Usrey ML, Strano MS, Kenis PJ, et al. In situ deposition and patterning of single-walled carbon nanotubes by laminar flow and controlled flocculation in microfluidic channels. Angewandte Chemie. 2006;45:581-5.

[93] Kamat PV, Thomas KG, Barazzouk S, Girishkumar G, Vinodgopal K, Meisel D. Self-assembled linear bundles of single wall carbon nanotubes and their alignment and deposition as a film in a dc field. J Am Chem Soc. 2004;126:10757-62.

[94] Jo JW, Jung JW, Lee JU, Jo WH. Fabrication of highly conductive and transparent thin films from single-walled carbon nanotubes using a new non-ionic surfactant via spin coating. Acs Nano. 2010;4:5382-8.

[95] Aziz MA, Yang H. Surfactant and polymer-free electrochemical micropatterning of carboxylated multi-walled carbon nanotubes on indium tin oxide electrodes. Chemical communications. 2008:826-8.

[96] Namgung S, Baik KY, Park J, Hong S. Controlling the growth and differentiation of human mesenchymal stem cells by the arrangement of individual carbon nanotubes. Acs Nano. 2011;5:7383-90.

[97] Abdullah CA, Asanithi P, Brunner EW, Jurewicz I, Bo C, Azad CL, et al. Aligned, isotropic and patterned carbon nanotube substrates that control the growth and alignment of Chinese hamster ovary cells. Nanotechnology. 2011;22:205102.

[98] Kamali R, Binesh AR. A comparison of neural networks and adaptive neuro-fuzzy inference systems for the prediction of water diffusion through carbon nanotubes. Microfluid Nanofluid. 2013;14:575-81.

[99] Liu Z, Chen K, Davis C, Sherlock S, Cao QZ, Chen XY, et al. Drug delivery with carbon nanotubes for in vivo cancer treatment. Cancer Res. 2008;68:6652-60.

[100] White AA, Best SM, Kinloch IA. Hydroxyapatite-carbon nanotube composites for biomedical applications: A review. Int J Appl Ceram Tec. 2007;4:1-13.

[101] Saito N, Usui Y, Aoki K, Narita N, Shimizu M, Ogiwara N, et al. Carbon nanotubes for biomaterials in contact with bone. Curr Med Chem. 2008;15:523-7.

[102] Usui Y, Aoki K, Narita N, Murakami N, Nakamura I, Nakamura K, et al. Carbon nanotubes with high bone-tissue compatibility and bone-formation acceleration effects. Small. 2008;4:240-6.

[103] Saito N, Usui Y, Aoki K, Narita N, Shimizu M, Hara K, et al. Carbon nanotubes: biomaterial applications. Chem Soc Rev. 2009;38:1897-903.

[104] Zinger O, Anselme K, Denzer A, Habersetzer P, Wieland M, Jeanfils J, et al. Time-dependent morphology and adhesion of osteoblastic cells on titanium model surfaces featuring scale-resolved topography. Biomaterials. 2004;25:2695-711.

[105] Su X, Sun K, Cui FZ, Landis WJ. Organization of apatite crystals in human woven bone. Bone. 2003;32:150-62.

[106] Yi CQ, Liu DD, Fong CC, Zhang JC, Yang MS. Gold Nanoparticles Promote Osteogenic Differentiation of Mesenchymal Stem Cells through p38 MAPK Pathway. Acs Nano. 2010;4:6439-48.

[107] Kim MJ, Choi MU, Kim CW. Activation of phospholipase D1 by surface roughness of titanium in MG63 osteoblast-like cell. Biomaterials. 2006;27:5502-11.

[108] Supronowicz PR, Ajayan PM, Ullmann KR, Arulanandam BP, Metzger DW, Bizios R. Novel current-conducting composite substrates for exposing osteoblasts to alternating current stimulation. J Biomed Mater Res. 2002;59:499-506.

[109] Elias KL, Price RL, Webster TJ. Enhanced functions of osteoblasts on nanometer diameter carbon fibers. Biomaterials. 2002;23:3279-87.

[110] Bacakova L, Grausova L, Vacik J, Fraczek A, Blazewicz S, Kromka A, et al. Improved adhesion and growth of human osteoblast-like MG 63 cells on biomaterials modified with carbon nanoparticles. Diam Relat Mater. 2007;16:2133-40.

[111] Abarrategi A, Gutierrez MC, Moreno-Vicente C, Hortiguela MJ, Ramos V, Lopez-Lacomba JL, et al. Multiwall carbon nanotube scaffolds for tissue engineering purposes. Biomaterials. 2008;29:94-102.

[112] Shi XF, Sitharaman B, Pham QP, Liang F, Wu K, Billups WE, et al. Fabrication of porous ultra-short single-walled carbon nanotube nanocomposite scaffolds for bone tissue engineering. Biomaterials. 2007;28:4078-90.

[113] Edwards SL, Church JS, Werkmeister JA, Ramshaw JAM. Tubular micro-scale multiwalled carbon nanotube-based scaffolds for tissue engineering. Biomaterials. 2009;30:1725-31.

[114] Olakowska E, Woszczycka-Korczynska I, Jedrzejowska-Szypulka H, Lewin-Kowalik J. Application of nanotubes and nanofibres in nerve repair. A review. Folia Neuropathol. 2010;48:231-7.

[115] Wu D, Pak ES, Wingard CJ, Murashov AK. Multi-walled carbon nanotubes inhibit regenerative axon growth of dorsal root ganglia neurons of mice. Neurosci Lett. 2012;507:72-7.

[116] Mattson MP, Haddon RC, Rao AM. Molecular functionalization of carbon nanotubes and use as substrates for neuronal growth. J Mol Neurosci. 2000;14:175-82.

[117] Hu H, Ni Y, Montana V, Haddon RC, Parpura V. Chemically Functionalized Carbon Nanotubes as Substrates for Neuronal Growth. Nano Lett. 2004;4:507-11.

[118] Hu H, Ni Y, Mandal SK, Montana V, Zhao B, Haddon RC, et al. Polyethyleneimine functionalized single-walled carbon nanotubes as a substrate for neuronal growth. J Phys Chem B. 2005;109:4285-9.

[119] Chao TI, Xiang S, Chen CS, Chin WC, Nelson AJ, Wang C, et al. Carbon nanotubes promote neuron differentiation from human embryonic stem cells. Biochem Biophys Res Commun. 2009;384:426-30.

[120] Sayes CM, Liang F, Hudson JL, Mendez J, Guo W, Beach JM, et al. Functionalization density dependence of single-walled carbon nanotubes cytotoxicity in vitro. Toxicol Lett. 2006;161:135-42.

[121] Zhao B, Hu H, Niyogi S, Itkis ME, Hamon MA, Bhowmik P, et al. Chromatographic purification and properties of soluble single-walled carbon nanotubes. J Am Chem Soc. 2001;123:11673-7.

[122] Niyogi S, Hamon MA, Hu H, Zhao B, Bhowmik P, Sen R, et al. Chemistry of single-walled carbon nanotubes. Acc Chem Res. 2002;35:1105-13.

[123] Peer D, Karp JM, Hong S, FaroKHzad OC, Margalit R, Langer R. Nanocarriers as an emerging platform for cancer therapy. Nat Nanotechnol. 2007;2:751-60.

[124] Heller DA, Baik S, Eurell TE, Strano MS. Single-walled carbon nanotube spectroscopy in live cells: Towards long-term labels and optical sensors. Adv Mater. 2005;17:2793-+.

[125] Hilder TA, Hill JM. Probability of encapsulation of paclitaxel and doxorubicin into carbon nanotubes. Micro Nano Lett. 2008;3:41-9.

[126] Kumar A, Jena PK, Behera S, Lockey RF, Mohapatra S. Efficient DNA and Peptide Delivery by Functionalized Chitosan-Coated Single-Wall Carbon Nanotubes. J Biomed Nanotechnol. 2005;1:392-6.

[127] Weng XX, Wang MY, Ge J, Yu SN, Liu BH, Zhong J, et al. Carbon nanotubes as a protein toxin transporter for selective HER2-positive breast cancer cell destruction. Mol Biosyst. 2009;5:1224-31.

[128] Pantarotto D, Singh R, McCarthy D, Erhardt M, Briand JP, Prato M, et al. Functionalized carbon nanotubes for plasmid DNA gene delivery. Angew Chem Int Edit. 2004;43:5242-6.

[129] Singh R, Pantarotto D, McCarthy D, Chaloin O, Hoebeke J, Partidos CD, et al. Binding and condensation of plasmid DNA onto functionalized carbon nanotubes:

Toward the construction of nanotube-based gene delivery vectors. J Am Chem Soc. 2005;127:4388-96.

[130] Ladeira MS, Andrade VA, Gomes ERM, Aguiar CJ, Moraes ER, Soares JS, et al. Highly efficient siRNA delivery system into human and murine cells using single-wall carbon nanotubes. Nanotechnology. 2010;21.

[131] Jin H, Heller DA, Strano MS. Single-particle tracking of endocytosis and exocytosis of single-walled carbon nanotubes in NIH-3T3 cells. Nano Letters. 2008;8:1577-85.

[132] Liu Z, Fan AC, Rakhra K, Sherlock S, Goodwin A, Chen X, et al. Supramolecular stacking of doxorubicin on carbon nanotubes for in vivo cancer therapy. Angewandte Chemie. 2009;48:7668-72.

[133] Liu Z, Chen K, Davis C, Sherlock S, Cao Q, Chen X, et al. Drug delivery with carbon nanotubes for in vivo cancer treatment. Cancer Res. 2008;68:6652-60.

[134] Liu Z, Winters M, Holodniy M, Dai H. siRNA delivery into human T cells and primary cells with carbon-nanotube transporters. Angewandte Chemie. 2007;46:2023-7.

[135] Antaris AL, Robinson JT, Yaghi OK, Hong GS, Diao S, Luong R, et al. Ultra-Low Doses of Chirality Sorted (6,5) Carbon Nanotubes for Simultaneous Tumor Imaging and Photothermal Therapy. Acs Nano. 2013;7:3644-52.

[136] Robinson JT, Hong GS, Liang YY, Zhang B, Yaghi OK, Dai HJ. In Vivo Fluorescence Imaging in the Second Near-Infrared Window with Long Circulating Carbon Nanotubes Capable of Ultrahigh Tumor Uptake. J Am Chem Soc. 2012;134:10664-9.

[137] Alidori S, Zeglis BM, Scheinberg DA, Lewis JS, McDevitt MR. Carbon nanotubes constructs as drug delivery systems for tumor targeting and imaging. J Labelled Compd Rad. 2011;54:S61-S.

[138] Ruggiero A, Villa CH, Holland JP, Sprinkle SR, May C, Lewis JS, et al. Imaging and treating tumor vasculature with targeted radiolabeled carbon nanotubes. Int J Nanomed. 2010;5:783-802.

[139] Shi XY, Wang SH, Shen MW. Tumor targeting and imaging using multifunctional dendrimer-modified multiwalled carbon nanotubes. Abstr Pap Am Chem S. 2009;237.

[140] Xiang LZ, Yuan Y, Xing D, Ou ZM, Yang SH, Zhou FF. Photoacoustic molecular imaging with antibody-functionalized single-walled carbon nanotubes for early diagnosis of tumor. J Biomed Opt. 2009;14.

[141] Aschberger K, Johnston HJ, Stone V, Aitken RJ, Hankin SM, Peters SAK, et al. Review of carbon nanotubes toxicity and exposure-Appraisal of human health risk assessment based on open literature. Crit Rev Toxicol. 2010;40:759-90.

[142] Johnston HJ, Hutchison GR, Christensen FM, Peters S, Hankin S, Aschberger K, et al. A critical review of the biological mechanisms underlying the in vivo and in vitro toxicity of carbon nanotubes: The contribution of physico-chemical characteristics. Nanotoxicology. 2010;4:207-46.

[143] Ding L, Stilwell J, Zhang T, Elboudwarej O, Jiang H, Selegue JP, et al. Molecular characterization of the cytotoxic mechanism of multiwall carbon nanotubes and nano-onions on human skin fibroblast. Nano Lett. 2005;5:2448-64.

[144] Liu D, Yi C, Zhang D, Zhang J, Yang M. Inhibition of proliferation and differentiation of mesenchymal stem cells by carboxylated carbon nanotubes. Acs Nano. 2010;4:2185-95.

[145] Sun Z, Liu Z, Meng J, Meng J, Duan J, Xie S, et al. Carbon nanotubes enhance cytotoxicity mediated by human lymphocytes in vitro. Plos One. 2011;6:e21073.

[146] Poland CA, Duffin R, Kinloch I, Maynard A, Wallace WA, Seaton A, et al. Carbon nanotubes introduced into the abdominal cavity of mice show asbestos-like pathogenicity in a pilot study. Nat Nanotechnol. 2008;3:423-8.

[147] Lutolf MP, Gilbert PM, Blau HM. Designing materials to direct stem-cell fate. Nature. 2009;462:433-41.

[148] Song W, Lu HX, Kawazoe N, Chen GP. Adipogenic Differentiation of Individual Mesenchymal Stem Cell on Different Geometric Micropatterns. Langmuir. 2011;27:6155-62.

[149] Chen CS, Alonso JL, Ostuni E, Whitesides GM, Ingber DE. Cell shape provides global control of focal adhesion assembly. Biochem Bioph Res Co. 2003;307:355-61.

[150] McBeath R, Pirone DM, Nelson CM, Bhadriraju K, Chen CS. Cell shape, cytoskeletal tension, and RhoA regulate stem cell lineage commitment. Developmental cell. 2004;6:483-95.

[151] Zhu BS, Lu QH, Yin J, Hu J, Wang ZG. Alignment of osteoblast-like cells and cell-produced collagen matrix induced by nanogrooves. Tissue Eng. 2005;11:825-34.

[152] Chen CS, Tan J, Tien J. Mechanotransduction at cell-matrix and cell-cell contacts. Annu Rev Biomed Eng. 2004;6:275-302.

[153] Sridharan I, Kim T, Wang R. Adapting collagen/CNT matrix in directing hESC differentiation. Biochem Bioph Res Co. 2009;381:508-12.

[154] Jones ENB, Mallapragada SK. Directed growth and differentiation of stem cells towards neural cell fates using soluble and surface-mediated cues. J Biomat Sci-Polym E. 2007;18:999-1015.

[155] Engler AJ, Sen S, Sweeney HL, Discher DE. Matrix elasticity directs stem cell lineage specification. Cell. 2006;126:677-89.

[156] Forte G, Carotenuro F, Pagliari F, Pagliari S, Cossa P, Fiaccavento R, et al. Criticality of the biological and physical stimuli array inducing resident cardiac stem cell determination. Stem Cells. 2008;26:2093-103.

[157] Otero JJ, Fu WM, Kan LX, Cuadra AE, Kessler JA. beta-catenin signaling is required for neural differentiation of embryonic stem cells. Development. 2004;131:3545-57.

[158] Thomas CH, Collier JH, Sfeir CS, Healy KE. Engineering gene expression and protein synthesis by modulation of nuclear shape. P Natl Acad Sci USA. 2002;99:1972-7.

[159] Lee MR, Kwon KW, Jung H, Kim HN, Suh KY, Kim K, et al. Direct differentiation of human embryonic stem cells into selective neurons on nanoscale ridge/groove pattern arrays. Biomaterials. 2010;31:4360-6.

[160] Xie JW, Willerth SM, Li XR, Macewan MR, Rader A, Sakiyama-Elbert SE, et al. The differentiation of embryonic stem cells seeded on electrospun nanofibers into neural lineages. Biomaterials. 2009;30:354-62.

[161] Lee LH, Peerani R, Ungrin M, Joshi C, Kumacheva E, Zandstra PW. Micropatterning of human embryonic stem cells dissects the mesoderm and endoderm lineages. Stem Cell Res. 2009;2:155-62.

[162] Dai HJ, Wong EW, Lieber CM. Probing electrical transport in nanomaterials: Conductivity of individual carbon nanotubes. Science. 1996;272:523-6.

[163] Shokrieh MM, Rafiee R. A review of the mechanical properties of isolated carbon nanotubes and carbon nanotube composites. Mech Compos Mater. 2010;46:155-72.

[164] Cheng Q, Rutledge K, Jabbarzadeh E. Carbon Nanotube–Poly(lactide-co-glycolide) Composite Scaffolds for Bone Tissue Engineering Applications. Ann Biomed Eng. 2013.

[165] Ishii M, Hamilton B, Poolton N. Imaging of charge trapping in distorted carbon nanotubes by x-ray excited scanning probe microscopy. J Appl Phys. 2008;104.

[166] Borka D, Lukic V, Timko J, Jovanovic VB. Using proton beams as a diagnostic tool in carbon nanotubes. Nucl Instrum Meth B. 2012;279:169-72.

[167] Ryoo SR, Kim YK, Kim MH, Min DH. Behaviors of NIH-3T3 Fibroblasts on Graphene/Carbon Nanotubes: Proliferation, Focal Adhesion, and Gene Transfection Studies. ACS Nano. 2010;4:6587-98.

[168] Zhang XK, Wang XF, Lu QH, Fu CL. Influence of carbon nanotube scaffolds on human cervical carcinoma HeLa cell viability and focal adhesion kinase expression. Carbon. 2008;46:453-60.

[169] Cheng Q, Rutledge K, Jabbarzadeh E. Carbon Nanotube-Poly(lactide-co-glycolide) Composite Scaffolds for Bone Tissue Engineering Applications. Ann Biomed Eng. 2013.

[170] McCarron PA, Marouf WM, Donnelly RF, Scott C. Enhanced surface attachment of protein-type targeting ligands to poly(lactide-co-glycolide) nanoparticles using variable expression of polymeric acid functionality. J Biomed Mater Res A. 2008;87A:873-84.

[171] Liu Z, Tabakman SM, Chen Z, Dai HJ. Preparation of carbon nanotube bioconjugates for biomedical applications. Nat Protoc. 2009;4:1372-82.

[172] Saha K, Mei Y, Reisterer CM, Pyzocha NK, Yang J, Muffat J, et al. Surface-engineered substrates for improved human pluripotent stem cell culture under fully defined conditions. P Natl Acad Sci USA. 2011;108:18714-9.

[173] Gunawan RC, Silvestre J, Gaskins HR, Kenis PJA, Leckband DE. Cell migration and polarity on microfabricated gradients of extracellular matrix proteins. Langmuir. 2006;22:4250-8.

[174] Lagunas A, Comelles J, Martinez E, Prats-Alfonso E, Acosta GA, Albericio F, et al. Cell adhesion and focal contact formation on linear RGD molecular gradients: study of non-linear concentration dependence effects. Nanomed-Nanotechnol. 2012;8:432-9.

[175] Rosca ID, Watari F, Uo M, Akaska T. Oxidation of multiwalled carbon nanotubes by nitric acid. Carbon. 2005;43:3124-31.

[176] Niyogi S, Hamon MA, Hu H, Zhao B, Bhowmik P, Sen R, et al. Chemistry of single-walled carbon nanotubes. Accounts Chem Res. 2002;35:1105-13.

[177] Zhao B, Hu H, Yu AP, Perea D, Haddon RC. Synthesis and characterization of water soluble single-walled carbon nanotube graft copolymers. J Am Chem Soc. 2005;127:8197-203.

[178] Chen Z, Tabakman SM, Goodwin AP, Kattah MG, Daranciang D, Wang XR, et al. Protein microarrays with carbon nanotubes as multicolor Raman labels. Nat Biotechnol. 2008;26:1285-92.

[179] Liu Z, Fan AC, Rakhra K, Sherlock S, Goodwin A, Chen XY, et al. Supramolecular Stacking of Doxorubicin on Carbon Nanotubes for In Vivo Cancer Therapy. Angew Chem Int Edit. 2009;48:7668-72.

[180] Chen J, Liu HY, Weimer WA, Halls MD, Waldeck DH, Walker GC. Noncovalent engineering of carbon nanotube surfaces by rigid, functional conjugated polymers. J Am Chem Soc. 2002;124:9034-5.

[181] Moon HK, Il Chang C, Lee DK, Choi HC. Effect of Nucleases on the Cellular Internalization of Fluorescent Labeled DNA-Functionalized Single-Walled Carbon Nanotubes. Nano Res. 2008;1:351-60.

[182] Fournier RL. Basic transport phenomena in biomedical engineering. 2nd ed. New York: Taylor & Francis; 2007.

[183] Chen JY, Chen SY, Zhao XR, Kuznetsova LV, Wong SS, Ojima I. Functionalized Single-Walled Carbon Nanotubes as Rationally Designed Vehicles for Tumor-Targeted Drug Delivery. J Am Chem Soc. 2008;130:16778-85.

[184] Wang JX, Ye R, Wei YH, Wang HH, Xu XJ, Zhang F, et al. The effects of electrospun TSF nanofiber diameter and alignment on neuronal differentiation of human embryonic stem cells. J Biomed Mater Res A. 2012;100A:632-45.

[185] Guan JJ, Wang F, Li ZQ, Chen J, Guo XL, Liao J, et al. The stimulation of the cardiac differentiation of mesenchymal stem cells in tissue constructs that mimic myocardium structure and biomechanics. Biomaterials. 2011;32:5568-80.

[186] Pijnappels DA, Schalij MJ, Ramkisoensing AA, van Tuyn J, de Vries AAF, van der Laarse A, et al. Forced alignment of mesenchymal stem cells undergoing cardiomyogenic differentiation affects functional integration with cardiomyocyte cultures. Circ Res. 2008;103:167-76.

[187] Wang PY, Yu JS, Lin JH, Tsai WB. Modulation of alignment, elongation and contraction of cardiomyocytes through a combination of nanotopography and rigidity of substrates. Acta Biomater. 2011;7:3285-93.

[188] Huang CY, Fu XL, Liu J, Qi YM, Li SH, Wang HJ. The involvement of integrin beta 1 signaling in the migration and myofibroblastic differentiation of skin fibroblasts on anisotropic collagen-containing nanofibers. Biomaterials. 2012;33:1791-800.

[189] Ng CP, Swartz MA. Mechanisms of interstitial flow-induced remodeling of fibroblast-collagen cultures. Ann Biomed Eng. 2006;34:446-54.

[190] Curran JM, Stokes R, Irvine E, Graham D, Amro NA, Sanedrin RG, et al. Introducing dip pen nanolithography as a tool for controlling stem cell behaviour: unlocking the potential of the next generation of smart materials in regenerative medicine. Lab Chip. 2010;10:1662-70.

[191] You MH, Kwak MK, Kim DH, Kim K, Levchenko A, Kim DY, et al. Synergistically Enhanced Osteogenic Differentiation of Human Mesenchymal Stem

Cells by Culture on Nanostructured Surfaces with Induction Media. Biomacromolecules. 2010;11:1856-62.

[192] Dror Y, Salalha W, Khalfin RL, Cohen Y, Yarin AL, Zussman E. Carbon nanotubes embedded in oriented polymer nanofibers by electrospinning. Langmuir. 2003;19:7012-20.

[193] Opatkiewicz J, LeMieux MC, Bao ZN. Nanotubes on Display: How Carbon Nanotubes Can Be Integrated into Electronic Displays. ACS Nano. 2010;4:2975-8.

[194] Lin DW, Bettinger CJ, Ferreira JP, Wang CL, Bao ZN. A Cell-Compatible Conductive Film from a Carbon Nanotube Network Adsorbed on Poly-L-lysine. ACS Nano. 2011;5:10026-32.

[195] Chen CS, Mrksich M, Huang S, Whitesides GM, Ingber DE. Geometric control of cell life and death. Science. 1997;276:1425-8.

[196] Burdick JA, Vunjak-Novakovic G. Engineered microenvironments for controlled stem cell differentiation. Tissue Eng Part A. 2009;15:205-19.

[197] Kingham EJ, Tsimbouri M, Gadegaard N, Dalby MJ, Oreffo ROC. Nanotopography induced osteogenic differentiation of human stem cells. Bone. 2011;48:S108-S9.

[198] Vartanian KB, Kirkpatrick SJ, Hanson SR, Hinds MT. Endothelial cell cytoskeletal alignment independent of fluid shear stress on micropatterned surfaces. Biochem Bioph Res Co. 2008;371:787-92.

[199] Gruschwitz R, Friedrichs J, Valtink M, Franz CM, Muller DJ, Funk RHW, et al. Alignment and Cell-Matrix Interactions of Human Corneal Endothelial Cells on

Nanostructured Collagen Type I Matrices. Investigative ophthalmology & visual science. 2010;51:6303-10.

[200] Namgung S, Baik KY, Park J, Hong S. Controlling the Growth and Differentiation of Human Mesenchymal Stem Cells by the Arrangement of Individual Carbon Nanotubes. Acs Nano. 2011;5:7383-90.

[201] Wang JHC, Goldschmidt-Clermont P, Wille J, Yin FCP. Specificity of endothelial cell reorientation in response to cyclic mechanical stretching. J Biomech. 2001;34:1563-72.

[202] Butcher JT, Penrod AM, Garcia AJ, Nerem RM. Unique morphology and focal adhesion development of valvular endothelial cells in static and fluid flow environments. Arterioscl Throm Vas. 2004;24:1429-34.

[203] Uttayarat P, Chen M, Li M, Allen FD, Composto RJ, Lelkes PI. Microtopography and flow modulate the direction of endothelial cell migration. Am J Physiol-Heart C. 2008;294:H1027-H35.

[204] Goldfinger LE, Tzima E, Stockton R, Kiosses WB, Kinbara K, Tkachenko E, et al. Localized alpha 4 integrin phosphorylation directs shear stress-induced endothelial cell alignment. Circ Res. 2008;103:177-85.

[205] Cai KY, Dong HD, Chen C, Yang L, Jandt KD, Deng LH. Inkjet printing of laminin gradient to investigate endothelial cellular alignment. Colloid Surface B. 2009;72:230-5.

[206] Lai ES, Huang NF, Cooke JP, Fuller GG. Aligned nanofibrillar collagen regulates endothelial organization and migration. Regen Med. 2012;7:649-61.

[207] Uttayarat P, Perets A, Li MY, Pimton P, Stachelek SJ, Alferiev I, et al. Micropatterning of three-dimensional electrospun polyurethane vascular grafts. Acta Biomater. 2010;6:4229-37.

[208] Schimmenti LA, Yan HC, Madri JA, Albelda SM. Platelet endothelial cell adhesion molecule, PECAM-1, modulates cell migration. J Cell Physiol. 1992;153:417-28.

[209] Xu CH, Inokuma MS, Denham J, Golds K, Kundu P, Gold JD, et al. Feeder-free growth of undifferentiated human embryonic stem cells. Nat Biotechnol. 2001;19:971-4.

[210] Sjogren-Jansson E, Zetterstrom M, Moya K, Lindqvist J, Strehl R, Eriksson PS. Large-scale propagation of four undifferentiated human embryonic stem cell lines in a feeder-free culture system. Dev Dynam. 2005;233:1304-14.

[211] Cowan CA, Klimanskaya I, McMahon J, Atienza J, Witmyer J, Zucker JP, et al. Derivation of embryonic stem-cell lines from human blastocysts. New Engl J Med. 2004;350:1353-6.

[212] Rosler ES, Fisk GJ, Ares X, Irving J, Miura T, Rao MS, et al. Long-term culture of human embryonic stem cells in feeder-free conditions. Dev Dynam. 2004;229:259-74.

[213] Carpenter MK, Rosler ES, Fisk GJ, Brandenberger R, Ares X, Miura T, et al. Properties of four human embryonic stem cell lines maintained in a feeder-free culture system. Dev Dynam. 2004;229:243-58.

[214] Hasegawa K, Fujioka T, Nakamura Y, Nakatsuji N, Suemori H. A method for the selection of human embryonic stem cell sublines with high replating efficiency after single-cell dissociation. Stem cells. 2006;24:2649-60.

[215] Draper JS, Smith K, Gokhale P, Moore HD, Maltby E, Johnson J, et al. Recurrent gain of chromosomes 17q and 12 in cultured human embryonic stem cells. Nat Biotechnol. 2004;22:53-4.

[216] Herszfeld D, Wolvetang E, Langton-Bunker E, Chung TL, Filipczyk AA, Houssami S, et al. CD30 is a survival factor and a biomarker for transformed human pluripotent stem cells. Nat Biotechnol. 2006;24:351-7.

[217] Burridge PW, Thompson S, Millrod MA, Weinberg S, Yuan XA, Peters A, et al. A Universal System for Highly Efficient Cardiac Differentiation of Human Induced Pluripotent Stem Cells That Eliminates Interline Variability. PLoS One. 2011;6.

[218] Hudson J, Titmarsh D, Hidalgo A, Wolvetang E, Cooper-White J. Primitive Cardiac Cells from Human Embryonic Stem Cells. Stem Cells Dev. 2012;21:1513-23.

[219] Laurencin CT, Ambrosio AMA, Borden MD, Cooper JA. Tissue engineering: Orthopedic applications. Annual Review of Biomedical Engineering. 1999;1:19-46.

[220] Kessler P, Thorwarth M, Bloch-Birkholz A, Nkenke E, Neukam FW. Harvesting of bone from the iliac crest--comparison of the anterior and posterior sites. Br J Oral Maxillofac Surg. 2005;43:51-6.

[221] Silber JS, Anderson DG, Daffner SD, Brislin BT, Leland JM, Hilibrand AS, et al. Donor site morbidity after anterior iliac crest bone harvest for single-level anterior cervical discectomy and fusion. Spine (Phila Pa 1976). 2003;28:134-9.

[222] Zimmermann CE, Borner BI, Hasse A, Sieg P. Donor site morbidity after microvascular fibula transfer. Clin Oral Investig. 2001;5:214-9.

[223] Nakajima T, Iizuka H, Tsutsumi S, Kayakabe M, Takagishi K. Evaluation of posterolateral spinal fusion using mesenchymal stem cells: differences with or without osteogenic differentiation. Spine (Phila Pa 1976). 2007;32:2432-6.

[224] Kretlow JD, Mikos AG. Review: mineralization of synthetic polymer scaffolds for bone tissue engineering. Tissue Eng. 2007;13:927-38.

[225] Langer R, Tirrell DA. Designing materials for biology and medicine. Nature. 2004;428:487-92.

[226] Jadlowiec JA, Celil AB, Hollinger JO. Bone tissue engineering: recent advances and promising therapeutic agents. Expert Opin Biol Ther. 2003;3:409-23.

[227] Murphy WL, Mooney DJ. Molecular-scale biomimicry. Nat Biotechnol. 2002;20:30-1.

[228] Karageorgiou V, Kaplan D. Porosity of 3D biomaterial scaffolds and osteogenesis. Biomaterials. 2005;26:5474-91.

[229] Gloria A, De Santis R, Ambrosio L. Polymer-based composite scaffolds for tissue engineering. J Appl Biomater Biomech.8:57-67.

[230] Rezwan K, Chen QZ, Blaker JJ, Boccaccini AR. Biodegradable and bioactive porous polymer/inorganic composite scaffolds for bone tissue engineering. Biomaterials. 2006;27:3413-31.

[231] Liu X, Ma PX. Polymeric scaffolds for bone tissue engineering. Ann Biomed Eng. 2004;32:477-86.

[232] Schliephake H, Weich HA, Dullin C, Gruber R, Frahse S. Mandibular bone repair by implantation of rhBMP-2 in a slow release carrier of polylactic acid--an experimental study in rats. Biomaterials. 2008;29:103-10.

[233] Larsson S, Bauer TW. Use of injectable calcium phosphate cement for fracture fixation: a review. Clin Orthop Relat Res. 2002:23-32.

[234] Balasundaram G, Sato M, Webster TJ. Using hydroxyapatite nanoparticles and decreased crystallinity to promote osteoblast adhesion similar to functionalizing with RGD. Biomaterials. 2006;27:2798-805.

[235] Habraken WJ, Wolke JG, Mikos AG, Jansen JA. Injectable PLGA microsphere/calcium phosphate cements: physical properties and degradation characteristics. J Biomater Sci Polym Ed. 2006;17:1057-74.

[236] Khan YM, Katti DS, Laurencin CT. Novel polymer-synthesized ceramic composite-based system for bone repair: an in vitro evaluation. J Biomed Mater Res A. 2004;69:728-37.

[237] Saito E, Kang H, Taboas JM, Diggs A, Flanagan CL, Hollister SJ. Experimental and computational characterization of designed and fabricated 50:50 PLGA porous scaffolds for human trabecular bone applications. J Mater Sci Mater Med.21:2371-83.

[238] Spalazzi JP, Dagher E, Doty SB, Guo XE, Rodeo SA, Lu HH. In vivo evaluation of a multiphased scaffold designed for orthopaedic interface tissue engineering and soft tissue-to-bone integration. J Biomed Mater Res A. 2008;86:1-12.

[239] Webster TJ, Ejiofor JU. Increased osteoblast adhesion on nanophase metals: Ti, Ti6Al4V, and CoCrMo. Biomaterials. 2004;25:4731-9.

[240] Boyan BD, Hummert TW, Dean DD, Schwartz Z. Role of material surfaces in regulating bone and cartilage cell response. Biomaterials. 1996;17:137-46.

[241] Khang D, Choi J, Im YM, Kim YJ, Jang JH, Kang SS, et al. Role of subnano-, nano- and submicron-surface features on osteoblast differentiation of bone marrow mesenchymal stem cells. Biomaterials. 2012;33:5997-6007.

[242] Akasaka T, Yokoyama A, Matsuoka M, Hashimoto T, Watari F. Thin films of single-walled carbon nanotubes promote human osteoblastic cells (Saos-2) proliferation in low serum concentrations. Mat Sci Eng C-Mater. 2010;30:391-9.

[243] Rho JY, Kuhn-Spearing L, Zioupos P. Mechanical properties and the hierarchical structure of bone. Med Eng Phys. 1998;20:92-102.

[244] Tseng IH, Lin HC, Tsai MH, Chen DS. Thermal conductivity and morphology of silver-filled multiwalled carbon nanotubes/polyimide nanocomposite films. J Appl Polym Sci. 2012;126:E182-E7.

[245] Kim SS, Sun Park M, Jeon O, Yong Choi C, Kim BS. Poly(lactide-co-glycolide)/hydroxyapatite composite scaffolds for bone tissue engineering. Biomaterials. 2006;27:1399-409.

[246] Wick P, Manser P, Limbach LK, Dettlaff-Weglikowska U, Krumeich F, Roth S, et al. The degree and kind of agglomeration affect carbon nanotube cytotoxicity. Toxicol Lett. 2007;168:121-31.

[247] Narimissa E, Gupta R, Bhaskaran M, Sriram S. Influence of nano-graphite platelet concentration on onset of crystalline degradation in polylactide composites. Polym Degrad Stabil. 2012;97:829-32.

[248] Saotome T, Kokubo K, Shirakawa S, Oshima T, Hahn HT. Polymer nanocomposites reinforced with C-60 fullerene: effect of hydroxylation. J Compos Mater. 2011;45:2595-601.

[249] McNally T, Potschke P, Halley P, Murphy M, Martin D, Bell SEJ, et al. Polyethylene multiwalled carbon nanotube composites. Polymer. 2005;46:8222-32.

[250] Bikiaris D. Microstructure and Properties of Polypropylene/Carbon Nanotube Nanocomposites. Materials. 2010;3:2884-946.

[251] Pooyan P, Tannenbaum R, Garmestani H. Mechanical behavior of a cellulose-reinforced scaffold in vascular tissue engineering. J Mech Behav Biomed Mater. 2012;7:50-9.

[252] Favier V, Canova GR, Shrivastava SC, Cavaille JY. Mechanical percolation in cellulose whisker nanocomposites. Polym Eng Sci. 1997;37:1732-9.

[253] Donaldson K, Stone V, Tran CL, Kreyling W, Borm PJA. Nanotoxicology. Occup Environ Med. 2004;61:727-8.

[254] Donaldson K, Aitken R, Tran L, Stone V, Duffin R, Forrest G, et al. Carbon nanotubes: a review of their properties in relation to pulmonary toxicology and workplace safety. Toxicological sciences : an official journal of the Society of Toxicology. 2006;92:5-22.

[255] Jensen AW, Wilson SR, Schuster DI. Biological applications of fullerenes. Bioorganic & medicinal chemistry. 1996;4:767-79.

[256] Mikael PE, Nukavarapu SP. Functionalized Carbon Nanotube Composite Scaffolds for Bone Tissue Engineering: Prospects and Progress. Journal of Biomaterials and Tissue Engineering. 2011;1:76-85.

[257] Singh R, Pantarotto D, Lacerda L, Pastorin G, Klumpp C, Prato M, et al. Tissue biodistribution and blood clearance rates of intravenously administered carbon nanotube radiotracers. Proc Natl Acad Sci U S A. 2006;103:3357-62.

[258] Meng SY, Zhang Z, Rouabhia M. Accelerated osteoblast mineralization on a conductive substrate by multiple electrical stimulation. J Bone Miner Metab. 2011;29:535-44.

[259] Martinelli V, Cellot G, Toma FM, Long CS, Caldwell JH, Zentilin L, et al. Carbon Nanotubes Promote Growth and Spontaneous Electrical Activity in Cultured Cardiac Myocytes. Nano Letters. 2012;12:1831-8.

[260] Stewart BW, Kleihues P, International Agency for Research on Cancer. World cancer report. Lyon: IARC Press; 2003.

[261] Matsumura Y, Maeda H. A New Concept for Macromolecular Therapeutics in Cancer-Chemotherapy - Mechanism of Tumoritropic Accumulation of Proteins and the Antitumor Agent Smancs. Cancer Res. 1986;46:6387-92.

[262] Gul-Uludag H, Xu P, Marquez-Curtis LA, Xing J, Janowska-Wieczorek A, Chen J. Cationic liposome-mediated CXCR4 gene delivery into hematopoietic stem/progenitor cells: implications for clinical transplantation and gene therapy. Stem Cells Dev. 2012;21:1587-96.

[263] Kim SK, Day RW, Cahoon JF, Kempa TJ, Song KD, Park HG, et al. Tuning Light Absorption in Core/Shell Silicon Nanowire Photovoltaic Devices through Morphological Design. Nano Lett. 2012;12:4971-6.

[264] Goldberger J, He R, Zhang Y, Lee S, Yan H, Choi HJ, et al. Single-crystal gallium nitride nanotubes. Nature. 2003;422:599-602.

[265] Chopra NG, Luyken RJ, Cherrey K, Crespi VH, Cohen ML, Louie SG, et al. Boron-Nitride Nanotubes. Science. 1995;269:966-7.

[266] Mor GK, Varghese OK, Paulose M, Shankar K, Grimes CA. A review on highly ordered, vertically oriented TiO2 nanotube arrays: Fabrication, material properties, and solar energy applications. Sol Energ Mat Sol C. 2006;90:2011-75.

[267] Wang ZL. Zinc oxide nanostructures: growth, properties and applications. J Phys-Condens Mat. 2004;16:R829-R58.

[268] Iijima S, Ichihashi T. Single-Shell Carbon Nanotubes of 1-Nm Diameter. Nature. 1993;363:603-5.

[269] Singh R, Pantarotto D, McCarthy D, Chaloin O, Hoebeke J, Partidos CD, et al. Binding and condensation of plasmid DNA onto functionalized carbon nanotubes: toward the construction of nanotube-based gene delivery vectors. J Am Chem Soc. 2005;127:4388-96.

[270] Liu Y, Yu ZL, Zhang YM, Guo DS, Liu YP. Supramolecular architectures of beta-cyclodextrin-modified chitosan and pyrene derivatives mediated by carbon nanotubes and their DNA condensation. J Am Chem Soc. 2008;130:10431-9.

[271] Zheng M, Jagota A, Semke ED, Diner BA, Mclean RS, Lustig SR, et al. DNA-assisted dispersion and separation of carbon nanotubes. Nat Mater. 2003;2:338-42.

[272] Cheng FY, Su CH, Wu PC, Yeh CS. Multifunctional polymeric nanoparticles for combined chemotherapeutic and near-infrared photothermal cancer therapy in vitro and in vivo. Chemical communications. 2010;46:3167-9.

[273] Wu Y, Phillips JA, Liu H, Yang R, Tan W. Carbon nanotubes protect DNA strands during cellular delivery. Acs Nano. 2008;2:2023-8.

[274] Zhang ZH, Yang XY, Zhang Y, Zeng B, Wang ZJ, Zhu TH, et al. Delivery of telomerase reverse transcriptase small interfering RNA in complex with positively

charged single-walled carbon nanotubes suppresses tumor growth. Clin Cancer Res. 2006;12:4933-9.

[275] Karajanagi SS, Yang HC, Asuri P, Sellitto E, Dordick JS, Kane RS. Protein-assisted solubilization of single-walled carbon nanotubes. Langmuir. 2006;22:1392-5.

[276] Yoshimura SH, Khan S, Maruyama H, Nakayama Y, Takeyasu K. Fluorescence Labeling of Carbon Nanotubes and Visualization of a Nanotube-Protein Hybrid under Fluorescence Microscope. Biomacromolecules. 2011;12:1200-4.

[277] Diao XH, Chen HY, Zhang GL, Zhang FB, Fan XB. Magnetic Carbon Nanotubes for Protein Separation. J Nanomater. 2012.

[278] Ebbesen TW. Carbon nanotubes : preparation and properties. Boca Raton: CRC Press; 1997.

[279] Lacerda L, Raffa S, Prato M, Bianco A, Kostarelos K. Cell-penetrating CNTs for delivery of therapeutics. Nano Today. 2007;2:38-43.

[280] Hedrick SM, Ch'en IL, Alves BN. Intertwined pathways of programmed cell death in immunity. Immunological reviews. 2010;236:41-53.

[281] Tait SW, Green DR. Mitochondria and cell death: outer membrane permeabilization and beyond. Nature reviews Molecular cell biology. 2010;11:621-32.

[282] Chen X, Tam UC, Czlapinski JL, Lee GS, Rabuka D, Zettl A, et al. Interfacing carbon nanotubes with living cells. J Am Chem Soc. 2006;128:6292-3.

[283] Sayes CM, Wahi R, Kurian PA, Liu Y, West JL, Ausman KD, et al. Correlating nanoscale titania structure with toxicity: a cytotoxicity and inflammatory response

study with human dermal fibroblasts and human lung epithelial cells. Toxicological sciences : an official journal of the Society of Toxicology. 2006;92:174-85.

[284] Lacerda L, Bianco A, Prato M, Kostarelos K. Carbon nanotubes as nanomedicines: from toxicology to pharmacology. Advanced drug delivery reviews. 2006;58:1460-70.

[285] Anderson JM, Shive MS. Biodegradation and biocompatibility of PLA and PLGA microspheres. Adv Drug Deliver Rev. 1997;28:5-24.